# SYNTHESIS AND CHARACTERIZATION OF NANOCRYSTALLINE DIAMOND FROM MECHANICALLY ALLOYED SUPERSATURATED SOLID SOLUTION OF NI-$C_{gr}$

**Ph.D. Thesis**

**NITIKA KUNDAN**
**ID No. 2015RMT9056**


**DEPARTMENT OF METALLURGICAL AND MATERIALS ENGINEERING**
**MALAVIYA NATIONAL INSTITUTE OF TECHNOLOGY JAIPUR**
**July 2019**

# Synthesis and Characterization of Nanocrystalline Diamond from Mechanically Alloyed Supersaturated Solid Solution of Ni-$C_{gr}$

*Submitted in*

*fulfilment of the requirements for the degree of*

***Doctor of Philosophy***

by

**NITIKA KUNDAN**

ID: **2015RMT9056**

Under the supervision of

**Dr Anup Kumar Keshri**
Co-supervisor (External)
IIT Patna

**Prof. P. R. Soni**
Supervisor
MNIT Jaipur


**DEPARTMENT OF METALLURGICAL AND MATERIALS ENGINEERING**

**MALAVIYA NATIONAL INSTITUTE OF TECHNOLOGY JAIPUR**

**JULY 2019**

# DEDICATION

I wish to dedicate this thesis to my loving parents,

*Sh. Jodh Raj Kundan and Smt. Shakuntla Kundan*

# DECLARATION

I**, Nitika Kundan**, declare that this thesis titled, "**Synthesis and Characterization of Nanocrystalline Diamond from Mechanically Alloyed Supersaturated Solid Solution of Ni-$C_{gr}$**" and the work presented in it are my own. I confirm that:

- This work was done wholly or mainly while in candidature for a research degree at this university.
- Where any part of this thesis has previously been submitted for a degree or any other qualification at this university or any other institution, this has been clearly stated.
- Where I have consulted the published work of other, this is always clearly attributed.
- Where I have quoted from the work of others, the source is always given with the exception of such quotations; this thesis is entirely my own work.
- I have acknowledged all main sources of help.
- Where the thesis is based on work done by myself, jointly with other, I have made clear exactly what was done by others and what I have contributed myself.

**Date:** **Nitika Kundan**

**Place:** (2015RMT9056)

# CERTIFICATE

This is to certify that the thesis entitled **"Synthesis and Characterization of Nanocrystalline Diamond from Mechanically Alloyed Supersaturated Solid Solution of Ni-$C_{gr}$"** being submitted by **Ms. Nitika Kundan (2015RMT9056)** is a bonafide research work carried out under my supervision and guidance in fulfillment of the requirement for the award of the degree of **Doctor of Philosophy** in the Department of **Metallurgical and Materials Engineering,** Malaviya National Institute of Technology, Jaipur, India. The matter embodied in this thesis is original and has not been submitted to any other University or Institute for the award of any other degree.


**Dr Anup Kumar Keshri**
Asst. Professor & Co-supervisor (External)
Department of Metallurgical & Materials Engineering
IIT Patna

**Dr P. R. Soni**
Professor & Supervisor
Department of Metallurgical & Materials Engineering
MNIT Jaipur


**Date:**

**Place: Jaipur**

# Acknowledgement

I would like to express my sincere gratitude to my supervisor **Prof. P. R. Soni**, Professor, Department of Metallurgical and Materials Engineering, MNIT Jaipur for giving me this opportunity and providing precious guidance, valuable discussions, constant supervision, moral support and encouragement for working with integrity and efficiency during the course of time. It was my pleasure to work with such a grounded person like him. I am indebted to **Mrs Pramila Soni** for her unconditional support and encouragement.

I also want to express my deep gratitude to my external joint supervisor **Dr Anup Kumar Keshari,** Department of Metallurgical and Materials Engineering, IIT Patna wholeheartedly for providing moral support, facilities and a comfortable environment.

I further extend my thanks **to Dr S. R. Bakshi (IIT Madras)** for providing Spark Plasma Sintering facility required to complete my research work and all staff members of **Materials Research Centre (MNIT Jaipur)** for providing characterization facilities.

I must thank **Dr S.K. Gupta**, **Dr Vijay N. N.** and **Dr A. K. Pradhan** for being in my DREC committee and for their patience and support in overcoming numerous obstacles I have been facing through my research.

I thank Malaviya National Institute of Technology (MNIT) Jaipur for supporting my research by providing institute assistantship so that work could be completed without any financial constraint. I am thankful to **Dr V.K. Sharma,** H.O.D. in Metallurgical and Materials Engineering Department, and **Dr R. K. Dhuchaniya,** DPGC for providing me with a positive and supportive environment during my research work. I would like to thanks all other faculty members and staff of the Department of Metallurgical and Materials Engineering, MNIT Jaipur for their help and support.

I express my deep appreciation to my fellow doctoral students **Mr Ankit Goyal, Mrs Versha Goyal, Mr Mukesh Suthar, Mr Biswajit Parida, Mr Mrigesh Verma, Mr**

**Ravindra Singh, Mr Sandeep Dhaka, Mr Ravindra S. Shekhawat and Mr Mukesh Kumar** for their feedback, cooperation, support and of course friendship.

I express my wholehearted appreciation and respect for my beloved parents for their unconditional love and support throughout my Ph.D. work. I would like to thank my aunts **Mrs Rita Rani and Mrs Aruna** for providing me mental and moral support and to stand by me whenever required throughout my research journey; my brothers **Mr. Shubham Kundan** who always stands beside me in every up and down and **Late Mr. Abhi Kundan** who was always there to cheer me up in my tough days; and also to my sisters **Mrs. Priyanka** for providing me support by understanding each and every day without getting tired and **Tabbu Kundan** for being there for much needed emotional support and pushing me harder when I lose hope and feel lost and she was always for me through my thick and thin during my PhD duration; and also to **Nityam** and **Samayra** for bearing with me for less attention towards them. I gratefully thanks **Rubia, Sarv Priya, Mona, Seema, Varun, Shariq, Vibha Uttam, Monika Sheoran Rao, Rupali Baghel, Jyoti Yadav, Priya Pal, Ritika Bhatt, Prachi, Pallavi, Shalu, Vartika** and **Monika** for being my second family and providing that homely atmosphere away from home which helps me to focus and concentrate more on my research work and for giving such memorable time during my stay in MNIT Jaipur. I would like to offer my heartfelt thanks to all others whose name I couldn't mention here. At last, I would like to thank the almighty God who gave me inner strength to pursue this marathon task.

To sum up my experience of Ph.D., I have made many mistakes and have faced many failures but I have learned to never give up and move on which enabled me to evolve into a better version of myself.

**Nitika Kundan**

# Abstract

Diamond is a fascinating material with extraordinary properties such as extremely high hardness, high electronic saturation velocity, high carrier mobility, the best thermal conductivity, very high optical refractive index and biocompatibility. Diamonds finds use in many different applications including gemstone, heat sink, abrasive, and inserts and/or wear-resistant coatings for cutting tools. As nanostructured materials have been found to have many fascinating properties, in the recent past greater interest has arisen in synthesis and study of the properties of diamonds having crystal grains less than 100nm, the so-called nanocrystalline diamonds

The aim of the present investigation was to synthesize nanocrystalline diamond using mechanical alloying (MA) and spark plasma sintering (SPS) techniques. In this study, supersaturated solid solutions (SSSSs) of Ni-x wt.% $C_{gr}$ (x= 5, 10, 15) were prepared from the elemental powder mixtures by mechanically alloying in an attrition mill for 15 h in an inert atmosphere. The SSSSs prepared were degassed for 2 h in the vacuum of $10^{-2}$ torr at 200 $^{\circ}$C and characterized by SEM and XRD techniques. The changes in crystallite size, lattice strain, lattice parameter and dislocation density in the SSSS were estimated. To estimate the consolidation temperature DSC was performed and accordingly, the SSSSs were consolidated under a pressure of 10 MPa at 1000 $^{\circ}$C by hot pressing as well as by spark plasma sintering. Raman spectroscopy revealed the formation of diamonds in the hot pressed as well as in SPSed samples. Interestingly in the SPSed samples, the formation of SWCNTs also took place. The ratio of $I_D/I_G$ was used to assess the yield of the diamond phase. Synthesized diamond powder was extracted by dissolving the matrix in boiling acidic solution. Carbonaceous material from the diamond surfaces was removed by heating the powder at 250 $^{o}$C in an oxidative atmosphere. The diamond powders thus obtained were characterized for their surface morphology by FE-SEM. In order to know the particle size and particle size distribution, the powders were also characterized by nanoparticle analyzer (Malvern Zetasizer ZSP). The average particle size of the diamond agglomerates was found to be 3.8 μm and 2.5 μm, in the case of HP and SPS samples, respectively. TEM

micrographs have shown sub-micron and nano-size crystallites in the diamond powder particles synthesized via hot pressing and SPS, respectively. The fourier transform infrared (FTIR) spectra of the MA and diamond powders were determined on KBr pellets. The FTIR spectrum shows the formation of type IaA and Ib diamonds by HP and SPS, respectively.

# TABLE OF CONTENTS

# List of Figures

# List of Tables

# List of Abbreviations

| | |
|---|---|
| **MA** | Mechanical alloying |
| **HP** | Hot pressing |
| **SSSS** | Supersaturated solid solution |
| **$C_{gr}$** | Graphite |
| **ND** | Nanodiamond |
| **DLC** | Diamond-like carbon |
| **CNTs** | Carbon nanotubes |
| **SWCNT** | Single walled carbon nanotube |
| **MWCNT** | Multi walled carbon nanotube |
| **RBM** | Radial breathing mode |
| **SPS** | Spark plasma sintering |
| **SEM** | Scanning electron microscopy |
| **XRD** | X-ray diffraction |
| **TEM** | Transmission electron microscopy |
| **XPS** | X-ray photoelectron microscopy |
| **DSC** | Differential scanning calorimetry |
| **SPSed** | Spark plasma sintered |

| | |
|---|---|
| **FTIR** | Fourier transform infrared |
| **HPHT** | High pressure high temperature |
| **CVD** | Chemical vapor deposition |

# 1. Introduction

Diamond is a fascinating material. Probably more so than any other gemstone, diamond attracts much attention in the history and cultural heritage of the human race [1]. Diamond is composed of $sp^3$ hybridized carbon atoms coordinated by tetrahedral bonds. The strength of the C–C bonds and the 3-dimensional structure of the tetrahedral bonding arrangement are responsible for diamond's renowned material hardness [2-4]. It also has a broad span of transparency and extortionate thermal conductivity [5, 6]. Because diamond exhibits these extraordinary properties which make it not only a precious gem but also give a reason for its various technical applications that had emerged recently.

The extraction of the diamond is estimated to be around 1.2 billion carats globally, but diamond increasing demand is much higher than its production which leads to the artificial formation of diamond on a large scale. The production of synthetic diamond is approximately 4.3 billion carats, 4 times higher than natural diamond [7]. Diamond has major applications in drilling, sawing, and grinding of hard materials [8]. Diamond in the form of films also finds applications in surgical blades [9, 10], optical components [11-13], high pressure anvil [14, 15], and heat sensors for electronic chips and power devices [16], etc.

Nature itself carried out the earliest diamond synthesis several billion years ago. The oldest diamonds are to be about 3.2 billion years old, which is almost three-quarters of the Earth's age [17]. The process of natural diamond synthesis is not clear yet, but it is vaguely outlined. Although diamonds may be rare on earth, they may be found all over the universe [18]. Nano-sized diamond particles have been recovered from plunging meteorites.

Diamonds are basically categorized into two groups: i) natural, ii) synthetic. Natural diamond is formed due to the huge amount of hydrostatic pressure acting upon carbonaceous material within Earth mantle whereas synthetic diamond is prepared by three methods; high pressure high temperature (HPHT) [19], chemical vapour deposition (CVD) [20], and detonation synthesis [21]. In the HPHT method,

conditions similar to those of growth of diamond in earth mental are created. In this method, the liquid metal having dissolved carbon atoms, along with the tiny diamond seeds, is equi-axially pressurized in the growth cell. The metals used in this technique are from the group of transition elements, e.g. Ni, Fe, Co and their alloys, which act as a catalyst. Role of catalysts here is to minimize the transformation energy needed to convert graphite into diamond. In the CVD method, diamond growth takes place due to the decomposition of hydrocarbon gas mixture at low temperature and pressure [22] whereas, during the detonation synthesis process, nano-diamonds are formed by the detonation of carbon-based explosives in a metal chamber. Most of the scientists have used the idea of CVD for making the nano-diamonds and diamond-like carbon (DLC) [23] as it is the most convenient way for their preparation. As nanostructured materials have been found to have many fascinating properties, in the recent past greater interest has arisen in synthesis and study of the properties of diamonds having crystal grains less than 100nm, the so-called nanocrystalline diamonds

Nickel-carbon composites are attracting the interest of various researchers because of their diverse applications, such as shielding gaskets [24], hydrogenation [25], hydrogen storage [26], and synthesis of carbon nanotubes [27]. Various processes like powder metallurgy (PM), chemical vapour deposition (CVD), electroplating, sputtering etc., are in use for fabrication of metal-carbon composites [28]. But due to the vast difference in densities of nickel (8.9 $g/cm^3$) and carbon (2.25 $g/cm^3$), the promising technique for the formation of metal/carbon composites is powder metallurgy (PM); more precisely mechanical alloying.

Mechanical alloying (MA) is a solid-state powder processing technique involving repeated cold welding, fracturing, and re-welding of powder particles in a high-energy ball mill to produce a homogeneous material [29-31]. MA technique has attracted the interest of various researchers for the synthesis of nanostructured materials as well as fine dispersions in metallic matrices. The formation of a supersaturated solid solution by mechanical alloying has been observed in various systems like Fe-C, Al-C, Cu-C, Fe-Li, Fe-Al-C, Cu-Nb to form supersaturated solid solutions (SSSSs) [32-37], where the solid solubility could be extended to tens to a hundred times. Nevertheless, the MA of nickel-carbon systems poses specific

obstacles, such as amorphization of carbon phase [38] and the formation of carbides [39]. Using MA processing for dispersion of graphite in nickel, the formation of nanocrystalline nickel carbide, which is relatively unstable, have been reported [40, 41]. In addition to the self-lubricating property of the graphite, dispersoids of graphite also offer reinforcement potential to nanostructured nickel [42].

Spark plasma sintering (SPS) is a very promising consolidation technique which provides very fine microstructure and enhanced mechanical properties. The SPS is based on three stages: plasma heating, Joule heating and plastic deformation. In the initial state, powder particles are locally and momentarily heated to high temperature (5000–10000 ºC) due to electrical discharges, and thereafter the joule heating starts. SPS has shorter dwell time which minimizes the grain growth. The sintered specimens achieve very high densification and superior properties in comparison to conventionally sintered ones [43, 44].

After getting the awareness of MA and SPS techniques, the aim of the present investigation was decided to synthesize nanocrystalline diamond using MA technique to prepare SSSS of graphite in nickel matrix and subsequent consolidation of the SSSS by SPS technique.

# 2. Literature Survey

## 2.1 Nanocrystalline Materials

A polycrystalline material with grains below 100 nm size is known as nanocrystalline materials. These materials have special properties by the virtue of their small grain size, as by grains being small there is higher volume fraction of atoms at grain boundaries. Nanocrystalline or nanostructured materials have attracted the attention of the research community as a result of the extraordinary physical and chemical properties. When compared to normal coarse-grained materials, nanocrystalline materials have far better properties. The enhanced property are improved strength, hardness and toughness, improved thermal conductivity, reduced elastic modulus, higher electrical resistivity, lowered thermal conductivity, improved soft magnetic properties. There are many production routes for making nanocrystalline materials like inert gas condensation, mechanical alloying, plasma deposition, spray conversion processing and many more [29, 45-48].

Improved diffusivity in nanocrystalline materials imposes a significant effect on mechanical properties of material like creep and superplasticity. Nanocrystalline materials have the ability of doping impurities for the formation of synthesis of alloy phases in immiscible metals at temperatures lower than that required for other materials.

Hardness follows an inverse trend with grain size i.e. with decreasing grain size hardness increases. But this relationship has a limit after which a decrease in grain size leads to a decrease in hardness, this phenomenon is known as inverse Hall-Petch relationship. This reversal point or critical grain size varies from material to material. For a few materials, the hardness increase is linear with $d^{-1/2}$ and with further decrease in grain size the hardness change is flat. The Hall-Petch slope for nanograined materials are quite smaller of the order of nanometers as than compared to materials with normal grain size [30].

Nanocrystalline materials have two great possibilities of usage for production of nanoglass and nanocomposites. Glassy particles of nanometer size are produced and then these are compacted to form a bulk material. Glassy materials have far superior properties than the crystalline material, thus it can be expected that nanoglass have enhanced properties that that of the nanocrystalline materials. Nanocomposites are materials with the dispersion of nanoparticles inside grains and/or along the grain boundaries. Nanocomposites have many superior properties and other advantages as compared to conventional composites [29].

## 2.2 Carbon and its Allotropes

Carbon ranks fourth in the universal abundance of the elements, after the three gas elements: hydrogen, helium, and oxygen [49]. Carbon is the most abundant solid element in nature and in earth's crust, it is the most $15^{th}$ most found element. Fig.2.1 shows the carbon distribution as follows [50]:

i) Earth crust consists of 2700 ppm of carbon
ii) Oceanic crusts consist of 200 ppm of carbon
iii) Our atmosphere consists of 400 ppm of carbon
iv) Hydrosphere is composed of 30 ppm of carbon content

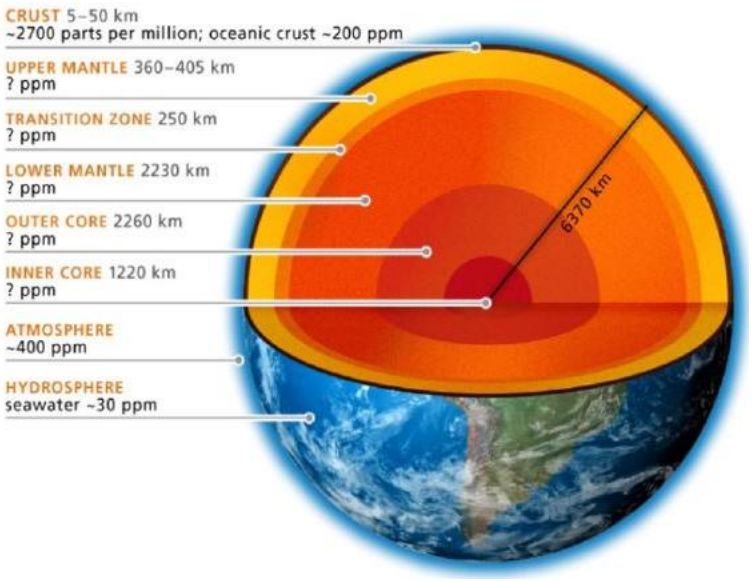


Fig 2.1: Earth's carbon concentration

Carbon is a prime element present in biological life forms as small as cells in the form of DNA and protein. This is one of the major initiator of life on earth. The bonding nature of carbon provides it with vivid physical and chemical properties. Carbon is a nonmetallic element from the $14^{th}$ group in the periodic table. With the ground state electron configuration of $1s^2 2s^2 2p^2$ it has four electrons available in its valence shell which are available for making covalent bond. Carbon's oxidation state varies from 4 to -4 with an electronegativity value of 2.55 on Pauling scale. Carbon is in the solid state at room temperature and gets converted to sublime state at 3642 °C. Carbon has the highest sublimation point amongst all the elements in the periodic table. [51].

***Carbon hybridization***

Carbon form bonds by mixing different orbitals, namely s- and p-orbitals with other atoms. Carbon is capable of forming $sp^3$, $sp^2$ and sp bonds [49] as shown in Fig. 2.2.

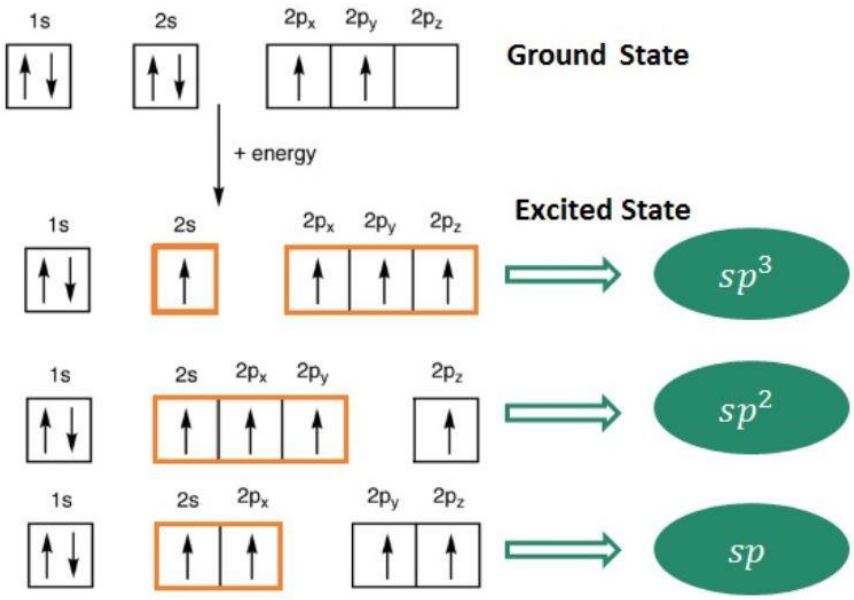


Fig. 2.2: Schematic of hybridization in carbon

A carbon atom consists of six electrons occupying the following electron configuration: $(1s)^2$ $(2s)^2$ $(2p)^2$. In the ground state, there are two unpaired electrons in the outer shell (p orbits), which may bind only two additional molecules. Diamond, methane, ethane shows this type of hybridization. The characteristic angle between the hybrid orbitals in $sp^3$ -configuration is 109.5 degree (Fig. 2.3 (a)).

When a carbon atom is bound to three atoms (two single bonds, one double bond), it is $sp^2$ hybridized and angles between the bond is $120^o$ which forms flat trigonal or triangular arrangement (Fig. 2.3 (b)). The best example of this type of hybridization is graphite.

Carbon bound to two other atoms to form its sp hybridization. For sp hybridization, carbon either forms one triple bond+one single bond (e.g. acetylene) or two double bonds (e.g. carbon dioxide). This type of hybridization forms a linear arrangement with a bond of $180^o$ between carbon bonds (Fig. 2.3 (c)).

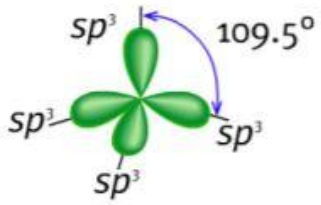


(a) $sp^3$

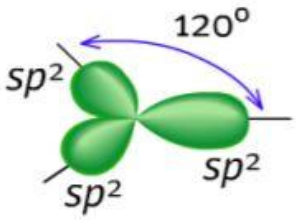


(b) $sp^2$

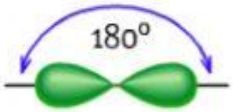


(c) sp

Fig. 2.3: Carbon hybrid orbitals

**Allotropes of carbon**

When a chemical element can be present in two or more physical state naturally, this property of a material/element is called allotropy. Carbon is found in various allotropic forms with varying properties. These allotropes of carbon can be subdivided into two basic groups of crystalline and amorphous allotropes. Some allotropic forms of carbon are shown in Fig. 2.4 [52, 53].

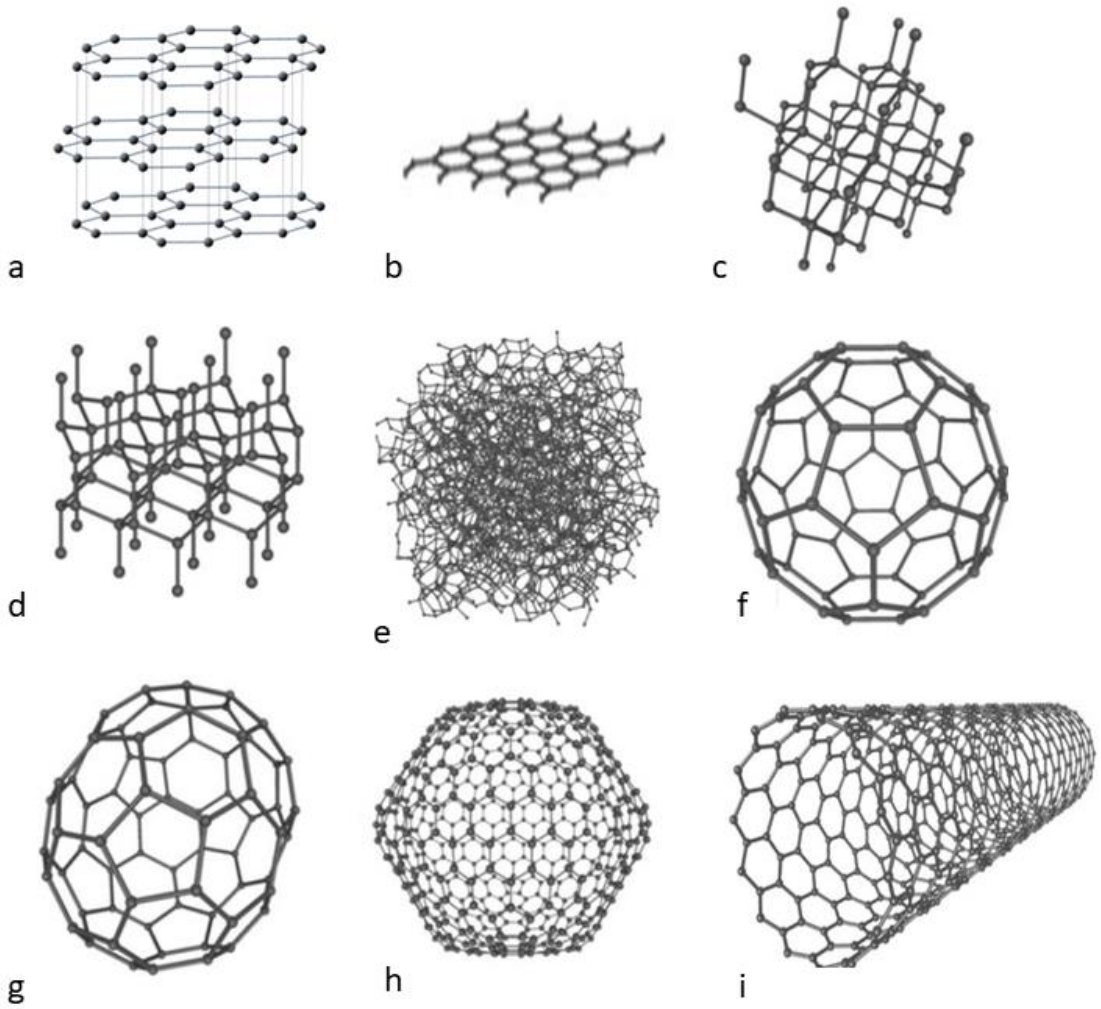


Fig. 2.4: Allotropes of carbon (a) graphite, (b) graphene, (c) diamond (d) lonsdaleite (e) amorphous carbon, (f) $C_{60}$, (g) $C_{70}$, (h) $C_{540}$, and (i) single-walled carbon nanotube

***Graphite***

Graphite is one of the allotropic forms of carbon. Graphite's properties differ from diamond as graphite is conductor of electricity and behaves like semi-metal. From all the forms of carbon, graphite is the most stable form in standard conditions. Graphite is used in thermochemistry as the standard state for defining the heat of formation of carbon compounds. Graphite is found in three states naturally [54]:

i) Crystalline flake graphite

ii) Amorphous graphite

iii) Lump or vein graphite

Graphite has a planar structure with layers, each layer is of carbon atoms arranged in hexagonal lattice formation. In this lattice formation distance between each carbon atom is 0.142 nm and the planes are 0.335 nm apart [55]. Atoms of a layer are bonded by covalent bond between them and layers have van der walls bond keeping them together [56, 57]. Two different arrangements of graphite known as alpha which is a hexagonal arrangement and beta with rhombohedral arrangements of atom have almost similar properties even though having different stacking arrangement. Alpha graphite can be present in flat or buckled form [58]. Beta graphite or rhombohedral graphite have carbon atom arrangement like an extended stacking fault in the hexagonal graphite lattice. Interconversion of graphite in both forms is possible. Alpha graphite can be converted to beta by mechanical treatment and reversal is possible by heating beta graphite to a temperature above 1300 °C [59]. Graphite is a good conductor of electricity because of the presence of the delocalized electron between the carbon layers, and because of the freedom of movement of electron between the layers, electricity passes between these carbon layers in graphite. Graphite also has lubricating properties and makes them suitable as dry lubricants [60, 61]. Graphite also finds its application in the form of heat-resistant materials as it can easily withstand temperatures up to 3000 °C [62].

***Graphene***

Graphene is a single layer of graphite. Graphene is basically an allotrope of carbon with a uniplanar $sp^2$ bonded carbon atoms which are closely packed with honeycomb crystal lattice. This is a base for all the other allotropic forms of carbon like graphite, carbon nanotubes and fullerenes. This also shows distinctively high electrical, thermal and physical properties. The properties are so great that graphene is the strongest material known discovered yet with a tensile strength of 130 GPa. Graphene acts as semi-metal or zero-gap semiconductor with high electron mobility at

normal conditions. Because of such attractive properties of graphene, it has attracted attention of research community [63, 64].

***Diamond***

Diamond is the most popular allotrope of carbon. In this carbon atoms are arranging in a modified face centred cubic arrangement [65]. Extraordinary physical properties of diamond are by the virtue of its carbon arrangement with strong covalent bond between atoms. In diamond, every atom of carbon is bonded with covalent bond with four other carbon atoms forming a tetrahedron [66]. Each such tetrahedron joins in three dimensions in a six atom carbon ring in chair conformation, which allows the arrangement with zero bond angle strain. Such a stable arrangement of carbon atoms with covalent bonds and hexagonal rings makes diamonds extremely strong substance [3, 4].

Diamond exhibits extraordinarily hardness (highest known) and great thermal conductivity. Also, such a rigid lattice configuration prevents contamination. Diamond surface is repellent to water but it is lipophilic that means it can be wetted by oil. It also shows limited reactivity with chemical reagents like strong acids and bases. Diamond finds uses in cutting, drilling, grinding and jewellery and few in semiconductor industry [1, 67-70].

***Lonsdaleite***

Variation of diamond in a hexagonal form is known as lonsdaleite. This is believed to be formed from graphite in meteorites on the impact with earth. The immense heat and the impact stresses transform this graphite to diamond but it happens suddenly so the hexagonal lattice structure of graphite is unchanged. Similar diamonds with hexagonal structures are being formed in laboratory by applying heat and pressure in a static press by explosives [71]. It is also reported that it can be formed via thermal decomposition of polymer, polyhydridoocarbyne under standard pressure of inert atmosphere and temperature around 110 °C [72].

***Amorphous carbon***

Amorphous carbon is a form of carbon which does not have the crystalline structure. When such amorphous carbon is produced there is minute presence of carbonaceous materials in crystalline form resembling graphite or diamond. Fraction of hybridization of $sp^2$ and $sp^3$ affects the properties of the amorphous carbon [73, 74]. In the case of graphite, only $sp^2$ hybridization is present whereas for diamond only $sp^3$ hybridization is present. A material which has greater number of $sp^3$ hybridized bond is known as tetrahedral amorphous carbon because of its tetrahedral shape or because diamond-like carbon (DLC) as its properties resemble those of diamond.

***Fullerene***

A fullerene is a molecule formed from only carbon atoms to form the shape of a hollow sphere, ellipsoid, or tube. Fullerenes are also known as "buckyballs". The various types of fullerene are given in Fig. 2.5.

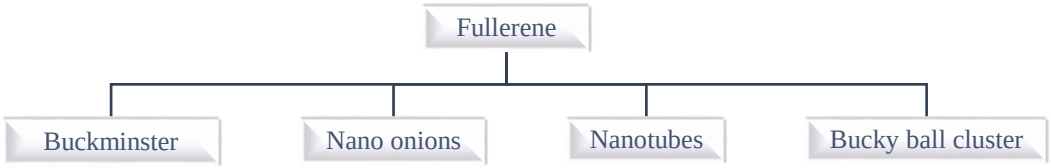


Fig. 2.5: Types of fullerene

*Buckminsterfullerene ($C_{60}$)*

Buckminsterfullerene is closed spherical structure of carbon $C_{60}$ with hexagonal and pentagonal rings. The suffix behind the carbon represents as the number of carbon atoms present in structure in which each carbon atom is having $sp^2$ hybridisation. This structure has around 20 hexagonal and 12 pentagonal rings. The name Buckminsterfullerene is given to $C_{60}$ after the American architect Richard

Buckminster Fuller who designed geodesic domes in the 1960s. Other than $C_{60}$ probable structures of fullerene are $C_{20}$, $C_{26}$, $C_{28}$, $C_{32}$, $C_{50}$, and $C_{70}$ [75, 76].

*Carbon nanotubes (CNTs)*

Carbon nano tubes are part of fullerene group. Its name is given due to its cylindrical structure. CNT can be referred to as rolled graphene sheets which form up cylindrical shape with single atom thickness. There are two types of CNT which are singe walled and multi walled CNT (shown in Fig. 2.6).

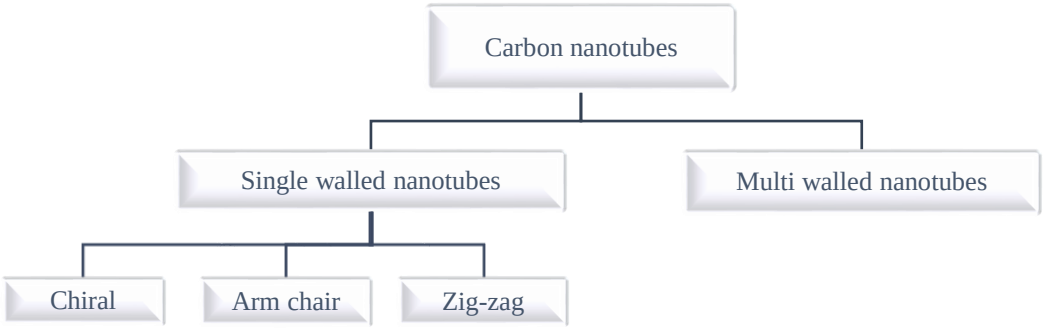


Fig. 2.6: Classification of carbon nanotubes

Single sheet of graphene rolls up to form a single walled nanotube. Fig. 2.7 shows formation process schematics of SWCNT [77].

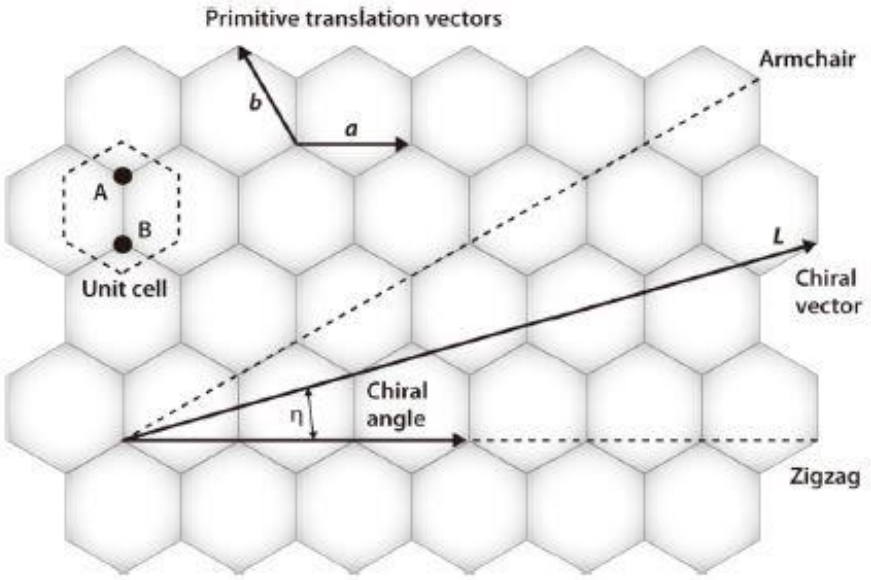


Fig. 2.7: Graphene sheet indicating the formation of different types of SWCNTs

If graphene sheets are rolled up concentrically, they form multi-walled nanotubes as shown in Fig. 2.8. There are two possibilities for the formation of MWCNT by rolling of graphene [78, 79]. In one possibility multiple SWCNTs are arranged coaxially arranged to form MWCNT. In other possibility graphene sheet is rolled in multiple turns. The typical separation between two layers is around 3.4 Å.

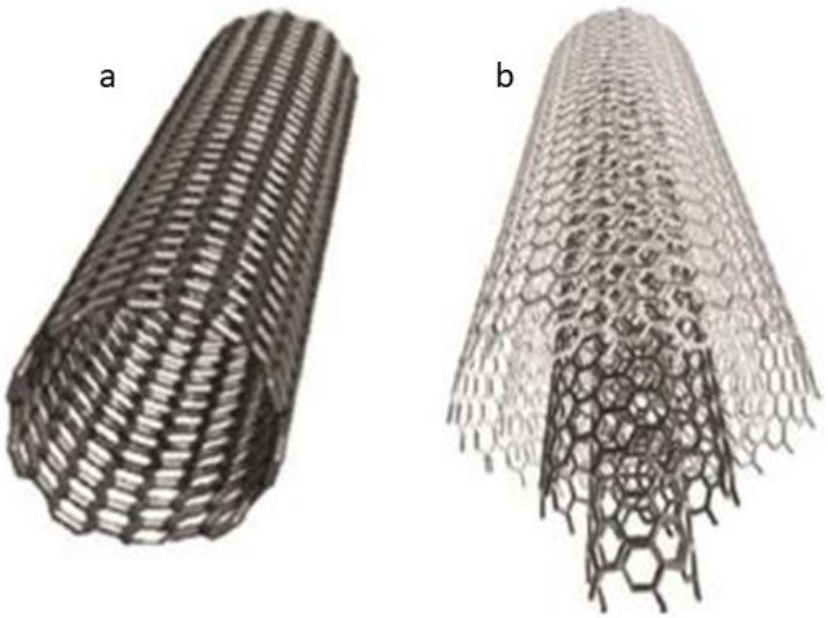


Fig.2.8: Carbon nanotubes: (a) single-walled nanotube (b) multi-walled nanotube

*Nanobuds*

Nanobuds are relatively recent discovery of carbon's allotropic form. This is a mashup of fullerene and CNT in which fullerene is attached to CNT on the outer surface by covalent bond (refer Fig. 2.9) [80]. This material has property advantages of both CNT and fullerenes. As an example, they have properties which makes them great field emitters.

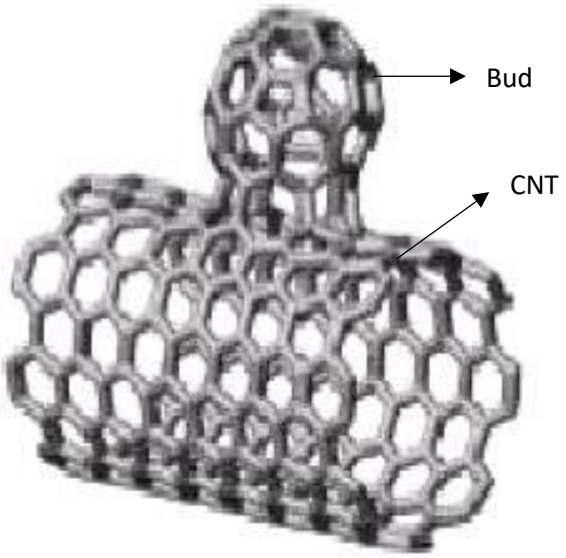


Fig. 2.9. A carbon nanobud

*Carbon onions*

Carbon onion is a structure which is similar to fullerenes with multiple concentric fullerenes arrangement forming a layered structure like an onion (Fig. 2.10) [81]. Carbon onions are many times referred to as carbon nano onions (CNOs) or onion-like carbon [82]. Vladimir Kuznetsov et.al have produced carbon onions in large quantities (gram quantities) by vacuum annealing of a nanodiamond precursor [83, 84].

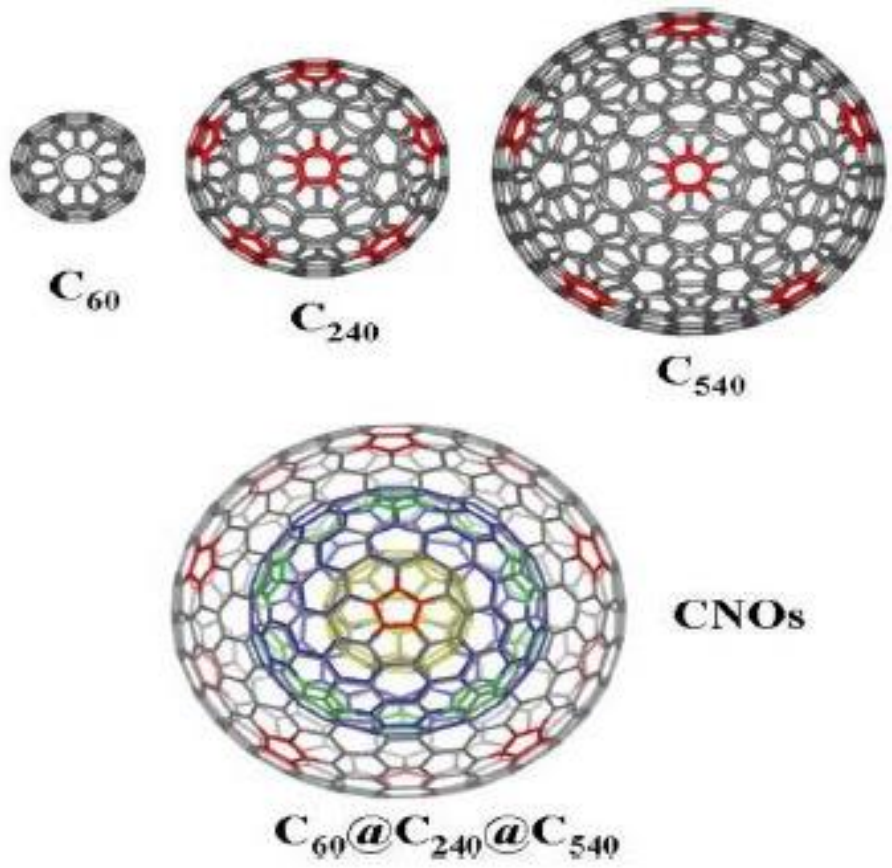


Fig 2.10: Carbon nano-onions

*Buckyball clusters*

When multiple buckyballs gets together, combinely they are called as buckyball cluster. The shape of each buckyball is not modified, but they bond with each other by surface to surface bonding [85]. Tens to hundreds of buckyballs bonds to form a super-bucky ball cluster (Fig. 2.11).

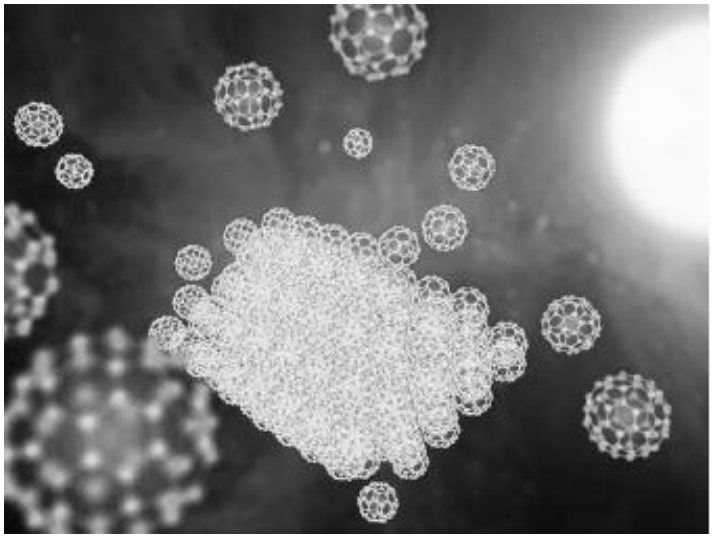

Fig. 2.11: Buckyball cluster

## Applications

In the coming days carbon allotropes will find such extensive usage that it won't be a matter of surprise if one finds them in goods which are essential for day to day life. Fig 2.12 shows few of the usage areas of carbon nanomaterials as in present age. All nanomaterials are not suitable for bio usage but carbon nanomaterials such as diamonds, CNTs possesses very well biocompatibility. Carbon nanomaterials like C60 and CNTs are the basis of the energy conversion devices. Also, carbon nanomaterials can be effectively used in electrical application because of their good conductivity.

Biomedical devices have vast presence of CNTs. CNTs provide a more efficient drug delivery and thus they can be effectively used for vaccine delivery systems and they have proved themselves as successful systems. Biosensors made from SWCNTs are used to detect biomolecules IgG and Streptavidin [86]. Whereas sensors with MWCNTs as useful for detecting glucose, such sensors are built with platinum transducers [86].

Field effect transistors (FETs) have been made from SWCNTs and MWCNTs. There are sensors developed in form of CNT FET which detects proteins [87] and carbohydrates [86]. It is possible to store hydrogen at room temperature by usage of CNTs [88]. CNTs have important role in heterogeneous catalysis application as the support processing of noble metal catalysts which have good mechanical properties, large surface area and resistivity to harsh environments [89]. Plenty of research outcomes are present on applications of CNTs in field of fuel cells and electro catalysis. Such kind of usage provides as power source for next-generation electrical devices and vehicles [90]. CNTs also find utility as a structural reinforcement material in composites which is used for sporting goods like tennis racket. This is possible because of their high tensile strength around 150 GPa [91].

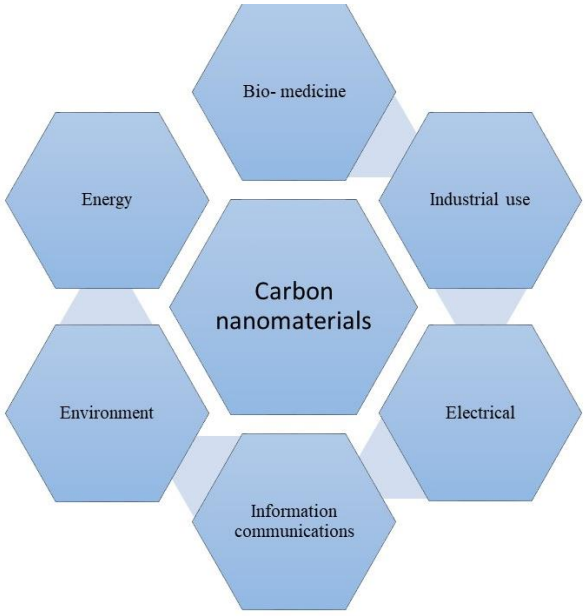


Fig. 2.12: Application of carbon nanomaterials

Carbon onions also finds applications in energy storage devices like super capacitors because of the possibility of high surface area of carbon electrode [92]. Multiwalled carbon onions are used for biological applications especially for skin treatment as they are reported to show improved cell growth and maintenance ability.

Carbon dots are used for bio imaging with no toxic effect when their surface is passivated [93]. It is possible to detect $Cu^{2+}$ and $Hg^{2+}$ ions using optical sensing because of the fluorescence quenching. Carbon dots also finds their usage in light emitting devices which emits white light and plausibly used for liquid crystal display and also in next generation lighting systems [94].

Carbon spheres find wide range of applications from nanoscale electronic devices to neuro-protective agents. High anodes of lithium ion batteries can be formed by combination of carbon sphere and tin [95]. Carbon spheres are templet for production of many other compounds. Templet based method gives an array of mesoporous carbon spheres which are useful in super capacitors. These show 93% capacitance retention even after 5000 cycles [96]. Carbon spheres with surface modification are brain theranostic agents as they show properties like super-paramagnism and luminescence with no cytotoxicity and are also tested for nucleus resembling brain cells. Carbon fibres find extensive usage in sports accessories and automobiles because they are material with highest strength with least density and also they are flexible enough to be moulded into components of various shapes. Some example of usage is in BMW i8 which is equipped with multiple carbon fibre body components [97], in professional bicycles, golf clubs, surfboards, also military protective goods like helmets, Kevlar, etc. It is also used as reinforcing material in composites and also act as micro electrodes [98].

Nanoscale carbon has potential to change the world in terms of technology, strength, and precision which leads to mankind towards touching new heights and new depths.

## 2.3 Diamond

Diamond is a meta-stable allotrope of carbon and the stereochemistry draws the carbon atoms arranged in a face-centered cubic crystal structure. The diamond structure is somehow similar to a face-centered cubic (FCC) lattice, having two atoms at each lattice point: (0, 0, 0) and (¼, ¼, ¼), where the coordinates are fractions along the cube sides. This is equivalent to two interpenetrating FCC lattices, offset from one another along a body diagonal by 1/4 of its length.

The lonsdaleite label is attributed to diamond due to its unique adaptability of (2H) hexagonal crystal structure. The shocks generated due to impact of meteorites are believed to cause conversion of graphite to this remarkably rare polymorph, first discovered in 1967 [99]. Such an impact is also speculated to have formed a new, super-hard crystalline polymorph of carbon [100].

Diamond is composed of only $sp^3$ hybridization of carbon. It is arranged in the crystal structure similar to that of face-centered cubic (fcc) (Fig 2.13), which is widely known as the diamond lattice. Diamond cubic structure have the lattice constant 'a' of 3.567 Å between each carbon atoms. Each carbon atom is attached to four other neighbouring carbon atoms via $sp^3$ bonds and bond length between C-C atoms is 1.54 Å and the bond angle is 109.5˚ (Fig. 2.14). A unit cell has eight atom for each lattice and there is no absorption of infrared rays in the one-phonon region. The diamond atomic density is $1.77\times10^{23}/cm^3$ and its specific gravity is 3.52±0.01 (density: 3.5-3.53 g/cm3) [101-103].

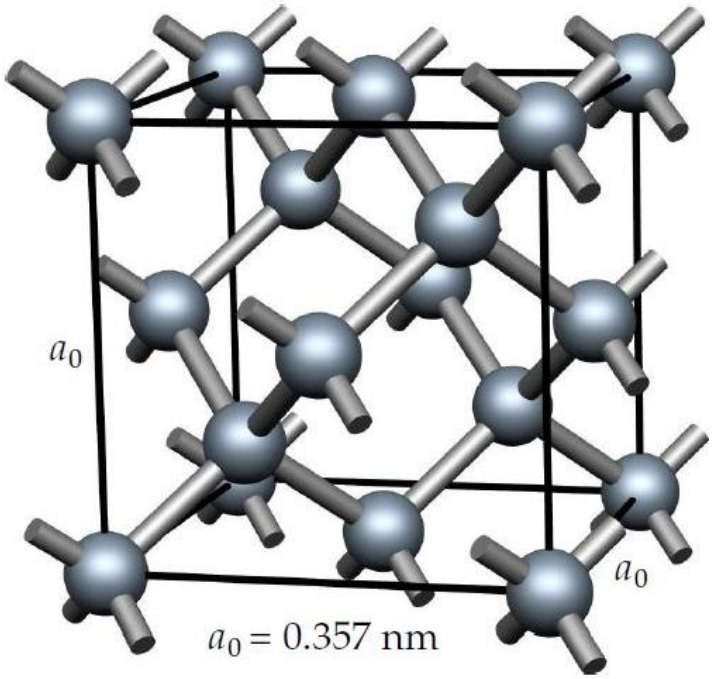


Fig. 2.13: Conventional unit cell of diamond

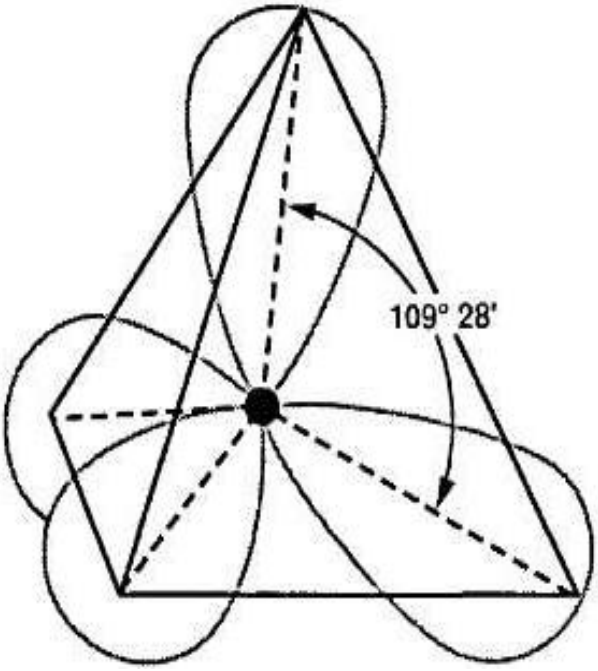


Fig. 2.14: Tetrahedral structure of diamond

The naturally occurring diamonds contain pure carbon rendering them white colour. However, the presence of impurities, like those of different elements (Nitrogen, Boron) imparts specific colours to the allotrope such as blue, brown, yellow etc.

**Properties of diamond**

The main physical properties of diamond are given in Table 2.1 [103].

Table 2.1: Physical properties of diamond

| Property | Natural Diamond |
|---|---|
| Density, g/cm$^3$ | 3.515 |
| Thermal conductivity at 25°C, W/m.K | 2200 |
| Bandgap, eV | 5.45 |
| Index of refraction at 10 μm | 2.40 |
| Electrical resistivity, Ωcm | $10^{16}$ |
| Dielectric constant (45 MHz – 20 GHz) | 5.70 |
| Vickers Hardness, Kg/mm$^2$ | 5700 - 10400 |
| Coefficient of friction (varies with humidity) | 0.05 – 0.15 |

*Electrical*

Diamond is also known as wide bandgap semiconductor with a bandgap (Eg) of 5.47 eV (at standard conditions) and tetrahedral $sp^3$ structure of carbon atoms bonded by covalent bonds. Figure 2.15 shows the resistivity variation in Ia, Ib and IIb type of diamonds. Resistivity of 1016~1018 Ω.m [104, 105] for Ia and Ib forms and IIb having totally contrastingly lower resistivity of 1~105 Ω.m and its boron dopants have $E_g$ of 0.35~0.38 eV above the valence band which is shown in figure 2.10 [106, 107].

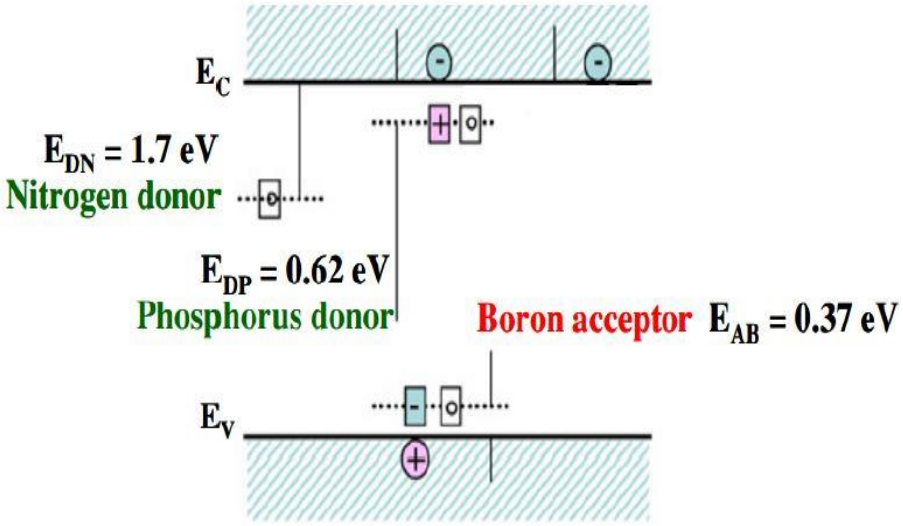


Fig. 2.15: Bandgap structure of diamond and impurities doping in diamond

*Optical*

Diamonds have capability of transmitting ultraviolet light from a light source ranging from visible to infrared regions and it is also a special material with wide far infrared transmission range and excellent ability to withstand thermal shock. As a result of such optical properties, diamonds are used as microwave shield window [108]. Table 2.2 lists out the optical and electronic properties of diamond [101, 109-114].

Table 2.2: Optical and electronic properties of diamond

| Property | Value |
|---|---|
| Refractive index | |
| (546.1 nm) | 2.424 |
| (589 nm) | 2.419 |
| (591 nm) | 2.41 |
| (visible light range) | ~ 2.40–2.46 |
| Dielectric constant | |
| (300 K, 1–10 kHz) | 5.70 |
| (25 °C, 1 MHz) | 5.5–5.7 |
| Dielectric strength | 1000 kV $mm^{-1}$ |
| Dissipation factor | 0.0002 |
| Electronic bandgap (indirect) | |
| (0 K) | 5.48 eV |
| (300 K) | 5.50 eV |
| | 5.47 eV |
| Direct bandgap | 7.3 eV |
| Electron mobility (300 K) | 1800 $cm^2$ $V^{-1}$ $s^{-1}$ |
| Hole mobility (300 K) | 1200 $cm^2$ $V^{-1}$ $s^{-1}$ |
| Relative permittivity | 5.570 |

*Chemical*

Glassy carbon (GC), carbon fibre or carbon nanotubes (CNTs) are exceptional choice for carbon electrode as they have large surface to area ratio, economical availability and broad potential window. Other than this conductive film of boron doped diamond is an alternative material for manufacturing of carbon electrodes. The electrochemistry properties have been reviewed by Pleskov, Fujishima, and Nebel et al [115, 116].

*Mechanical*

As it is very difficult to dislocate bonds between carbon atoms in diamonds, they are the hardest material and is considered as 10 on Moh's scale. Table 2.3 summarizes distinct properties of diamonds [117-119].

Summarising all this gives us diamonds as materials i) with very wide bandgap and phenomenal breakdown voltage greater than 100 V, ii) they have excellent thermal conductivity which is superior in the naturally occurring materials and iii) have chemical inertness with a very wide potential response window. Meanwhile, the refractive index of diamond is as high as 2.4 in the visible light.

Table 2.3: Mechanical and thermal properties of diamond

| Properties | Values | Units |
|---|---|---|
| Hardness | 10,000 | $kg/mm^2$ |
| Strength (tensile) | >1.2 | GPa |
| Strength (compressive) | >110 | GPa |
| Lowest Compressibility | $8.3\times10^{-13}$ | $m^2.N^{-1}$ |
| Young's Modulus | 1,050-1,220 | GPa |
| Thermal Conductivity | 20.9 | W/cm.K |
| Poisson's Ratio | 0.2-0.1 | N/A |
| Debye Temperature | 2,200-1,860 | K |
| Melting Temperature | 3,820 | K |
| Dielectric Constant | 5.7 | N/A |
| Thermo Expansion Coefficient | $1\times10^{-6}$ | /K (@300K) |
| Friction coefficient | 0.1 | N/A |

### 2.3.1 Classification

Diamonds are classified in two categories on the basis of (i) occurrence (natural or synthetic) (ii) type of impurity (type I or type 2), as shown in Fig.2.16.

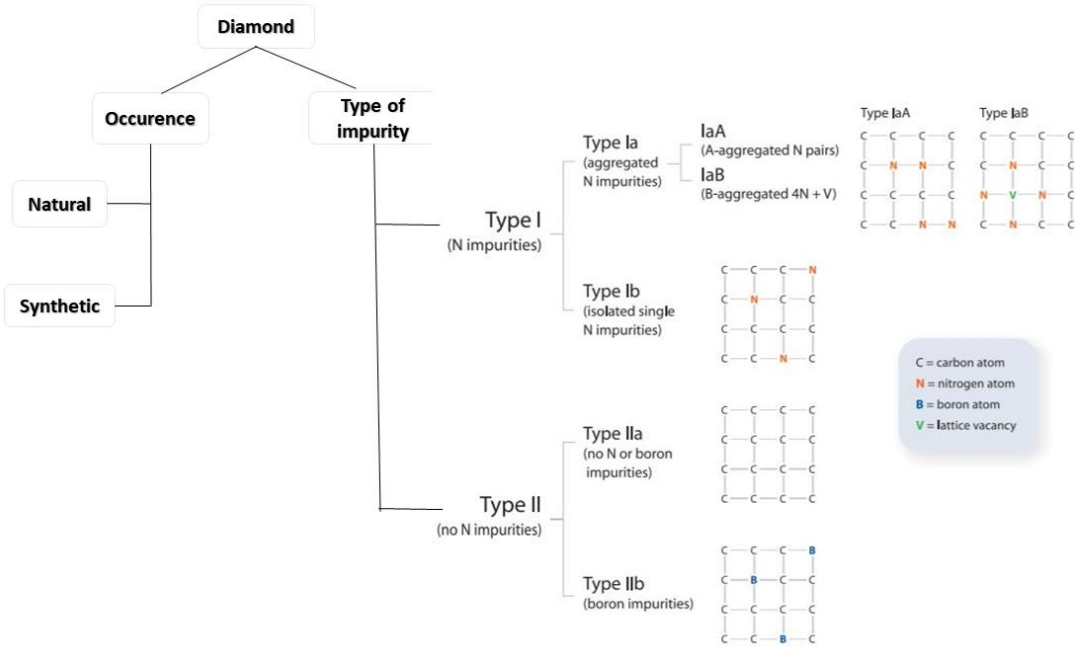


Fig. 2.16: Classification of diamond

***Classification based on occurrence***

*Natural*

Diamond is basically 99% of carbon$^{12}$ and 1% of carbon$^{13}$. Natural diamonds are formed under high temperature and pressure which are found at depth of around 140 - 190 kilometres in earth's crust. Pressure is approximately 45 to 60 kilobars and temperatures rages from 900 to 1300 °C in natural conditions of diamond formation. Such kind of conditions are present naturally in two conditions one in lithospheric mantle which is below continental plates and other is site of meteorite impact. Diamonds from the depth of earth are surfaced by volcanic eruption with magma which cools down and forms rocks known as kimberlites and lamproites. Such a process results in additional contamination by boron and nitrogen which give colours to diamonds (blue and yellow respectively) [120].

*Synthetic*

There are different processes which are used for synthesis of synthetic diamonds like high pressure high temperature (HPHT), chemical vapour deposition (CVD), and detonation synthesis [19-21]. Commercially available diamonds are majorly yellow in colour.

***Classification based on impurities***

*Type I: S*ignificant concentrations of nitrogen impurities [121, 122].

*Type Ia:* aggregates of nitrogen as substitutional atoms which can go as high as 0.3 % of material (3000 ppm).

- Type IaA: Atoms of nitrogen are present in the nearest neighbour substitutional pairs (the `A' aggregate) and this material does not show any tendency of fluorescence.
- Type IaB: Presence of nitrogen is in form of groups of four atoms which surrounds vacancy (the `B' aggregate) and samples shows moderate to strong blue fluorescence.
- Type IaAB: other than A and B centres, groups of three nitrogen substitutions around a vacancy (`N3' centres) are present. The B centres result in possibility of blue fluorescence, but the high concentrations of N3 centres lead to strong absorption of visible blue light, which results as the yellow colouration of the diamond.

*Type Ib:* Nitrogen is present as in form of isolated substitutional impurities. Absorption of light tends toward the blue end of the spectrum, which gives deep yellow colour to the material. Nitrogen concentration is around 500 ppm in Type Ib diamonds with a noticeable yellow colouration starting from the concertation of 50 ppm of nitrogen.

*Type II:* Ultra low amounts of nitrogen almost in the undetectable range [122].

*Type IIa:* These are majorly colourless with almost nil electrical conductivity. These have no clear nitrogen-related features in the infrared (IR) absorption spectrum in the range 400.1332 $cm^{-1}$ (the single phonon region).

*Type IIb:* Substitutional boron acceptors are uncompensated due to the lack of nitrogen donors, and the material, therefore, displays a significant *p*-type semi-conductivity. The boron impurities also cause absorption of light toward the red end of the visible spectrum and therefore lend a slight blue colour to the diamond.

## 2.3.2. Synthesis

High pressure high temperature (HPHT), chemical vapour deposition (CVD), and detonation synthesis are the main techniques used for the synthesis of diamond.

***High pressure high temperature (HPHT)***

High temperature high pressure (HPHT) is a diamond synthesis process which was devised in 1950s. This is simple imitation of natural diamond formation phenomenon which occurs at a depth of around 200 km in earth's crust [19]. Figure 2.17 shows a schematic of this process. In this process graphite or glassy carbon [123] is kept in a ceramic hydraulic press where it is compressed to a pressure of few GPa with simultaneous heating to couple of thousands of degree kelvin for several hours. This processing results in conversion of graphite to a single crystal diamond. This conversion is many times hindered by the presence of impurities.

The procedure begins with the liquid metal having dissolved carbon atoms, along with the tiny diamond seeds. These are equi-axially pressurized in the growth cell. Basically the transition group metals like Ni, Fe, Co and their alloys are used in this technique. These act as catalysts which minimize the transformation energy needed to convert graphite into diamond. The combination of high pressure and high temperature causes carbon atoms to deposit on the surface of seeds as diamond [124, 125].

The resultant HPHT crystals are typically a few micrometres in size, although the size of the diamonds is in fact only limited by the ability to sustain the same pressure and temperature conditions. Naturally, the diamond formation is spread across millions (or indeed billions) of years and thereby, most HPHT diamonds are far too erroneous and inaccurate for their use as gemstones. Nevertheless, they find their potential usage in many industrial applications, such as fabrication of saw blades for cutting asphalt and marble, and to coat the drill bits used in oil and gas drilling.

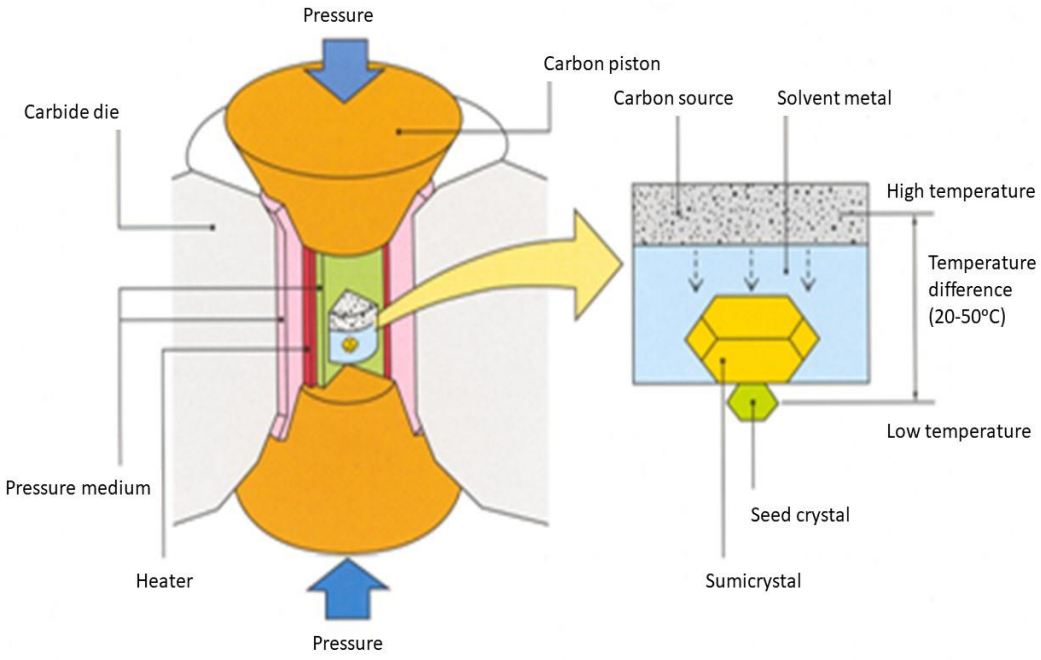


Fig. 2.17: HPHT setup for synthetic diamond

***Chemical vapour deposition (CVD)***

In the CVD method, diamond growth takes place due to decomposition of hydrocarbon gas mixture at low temperature (800-1000 $^{\circ}$C) and pressure typically under 27 kPa (Fig. 2.18). Here the typical growth of diamond is from methane. The growth of diamond normally requires a precursor gas to be diluted in hydrogen. A typical concentration of methane in the gas mixture is 0.5 to 2%. The CVD methods require a substrate preparation prior to deposition to generate diamond nuclei which subsequently grow. The growth pre-treatment process like mechanical abrading, ultrasonic seeding or ionic bombardment is used to prepare such nucleation on the

surface of substrates [20]. Diamond growth by chemical vapour deposition (CVD), growth from low-pressure gases was first reported in the 1950s. But the rate of growth in these early techniques was very low. This was caused by the deposition of graphite which finally leads to a mixture of $sp^3/sp^2$ phases. The breakthrough in CVD diamond was the discovery by Angus who found that the presence of nascent hydrogen in the gas mixture leads to preferential etching of graphite which means that diamond growth was favoured [126].

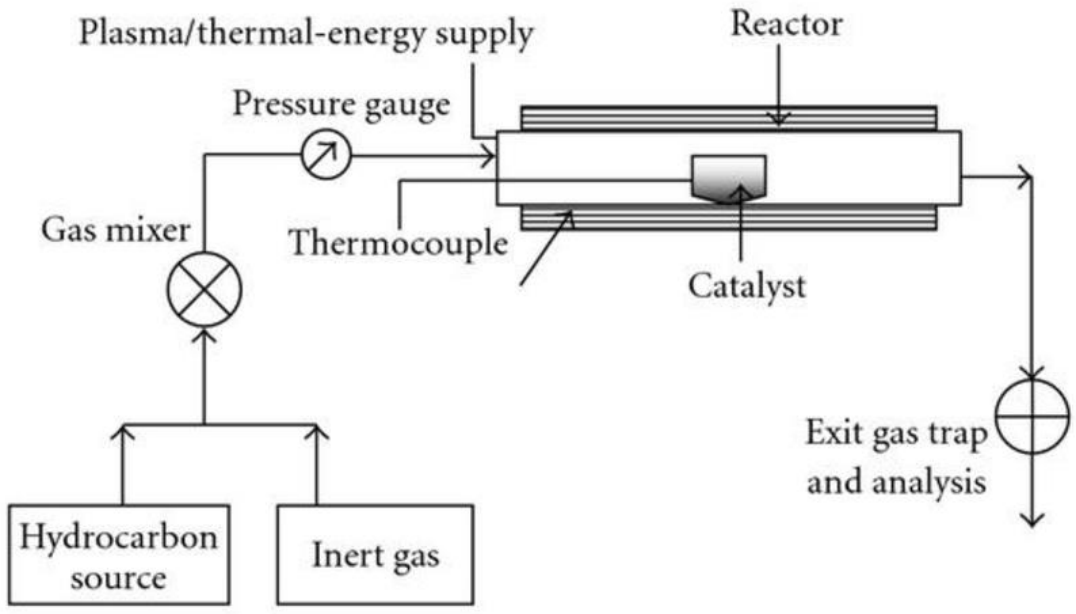


Fig 2.18: Schematic of the CVD process for the diamond synthesis

***Detonation synthesis***

In the detonation synthesis process, nano-diamonds are formed by detonation of carbon-based explosives in a metal chamber (Fig. 2.19). This explosion provides sufficient temperature and pressure for carbon of explosive to get converted to diamond [21]. Detonation process seems very profit making process but a large number of explosives are required for making 5-10 gms of artificial diamond [127]. The average size of the detonation diamond was determined to have 4-5nm. However, due to lack of interest in the nanotechnology at that time and the

application of nano-diamond remained underexploited. A thorough purification is needed to obtain graphite free diamond.

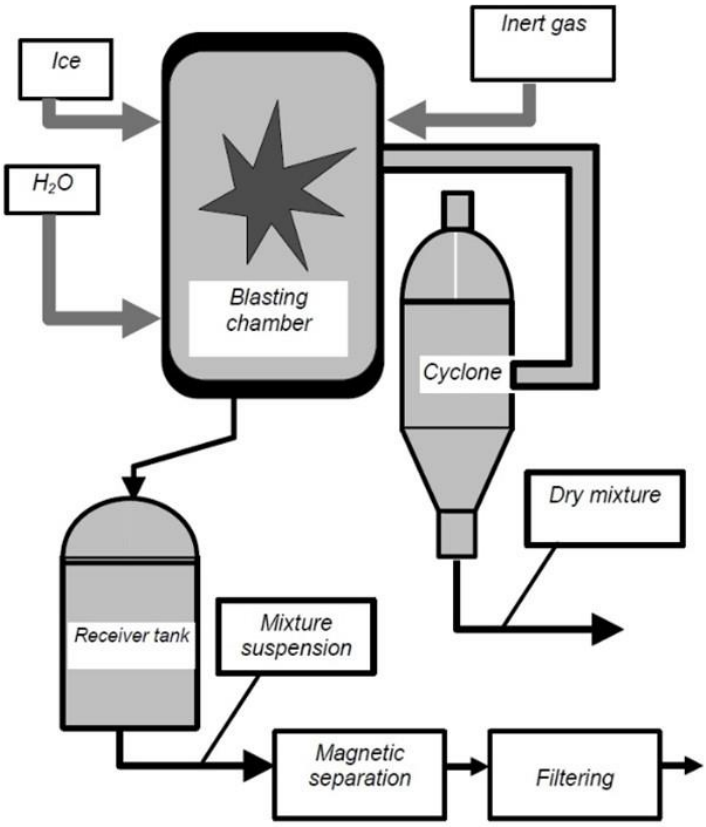


Fig 2.19: Detonation nanodiamond

Mirzaei et. al [128] successfully prepared nano-sized diamond structures by directly transforming SWCNTs as carbon, without application of any catalyst, to diamond by means of SPS process. The direct conversion of SWCNT to diamond took place at a temperature of 1700$^{o}$ C under 100 MPa pressure. The NDs prepared are of polyhedron shaped with an average diameter of 10nm.

Zhang et. al [129] investigated the formation of diamond from MWCNTs, $C_{60}$ and graphite (with and without the application of catalysts) by using SPS technique. In case of a catalyst, cubic and n-type diamond had obtained by MWCNTs; cubic diamonds were obtained from $C_{60}$ but no diamond formation was observed in case of graphite at 1500$^{o}$ C and 80 MPa pressure for 20 min. But in case of a catalyst,

temperature and pressure requirement for diamond formation get reduced to 1200$^{o}$ C-1300$^{o}$ C, and pressure to 50-70 MPa. Moreover, transformation of graphite to diamond was also observed. The size of diamond particles obtained ranges between 1-3µm.

### 2.3.3. Mechanism of diamond formation

The main flaw of the early diamond makers was to eliminate the heating factor as pressure itself is sufficient for conversion of graphite to diamond. Bridgman discovered that the formed diamond reverts back to graphite upon cooling.

$$C_{graphite} \longleftrightarrow C_{diamond}$$

It is very well known that by application of heat the electrons in the atoms are excited which leads to electron compromise and eventually disturbing its atomic bond. Pressure itself is sufficient for squashing the material and distorting the atomic lattice, but if the bonds are in disturbed state, atoms are not able to maintain its distorted configuration.

It is already known that graphite is $sp^2$ hybridized and diamond is $sp^3$ hybridized so when heated, the covalent bond gets disturbed and may break it in graphite configuration. At standard conditions graphite have the most stable crystalline state of carbon.

A hydrothermal synthesis of diamond was devised by Zhao et. al. in which mixture of glassy carbon with nickel powder, diamond seeds and water at high temperature (800 $^{o}$C) at 1.4 Kbar [130]. Nakano et. al. has produced nano diamonds using a mixture of interstellar organic material with water at 200-400 $^{o}$C [131]. Spear was successful in making diamonds of hexagonal form by shock loading, this is also known as Lonsdaleite which is 3C packing of cubic diamond [132].

Fig 2.20 shows the phase transformation diagram of graphite. In the diagram the phase transformation is illustrated with respect to the temperature and pressure

which is requisite for transforming graphite ($C_{gr}$) to diamond using different processes [133].

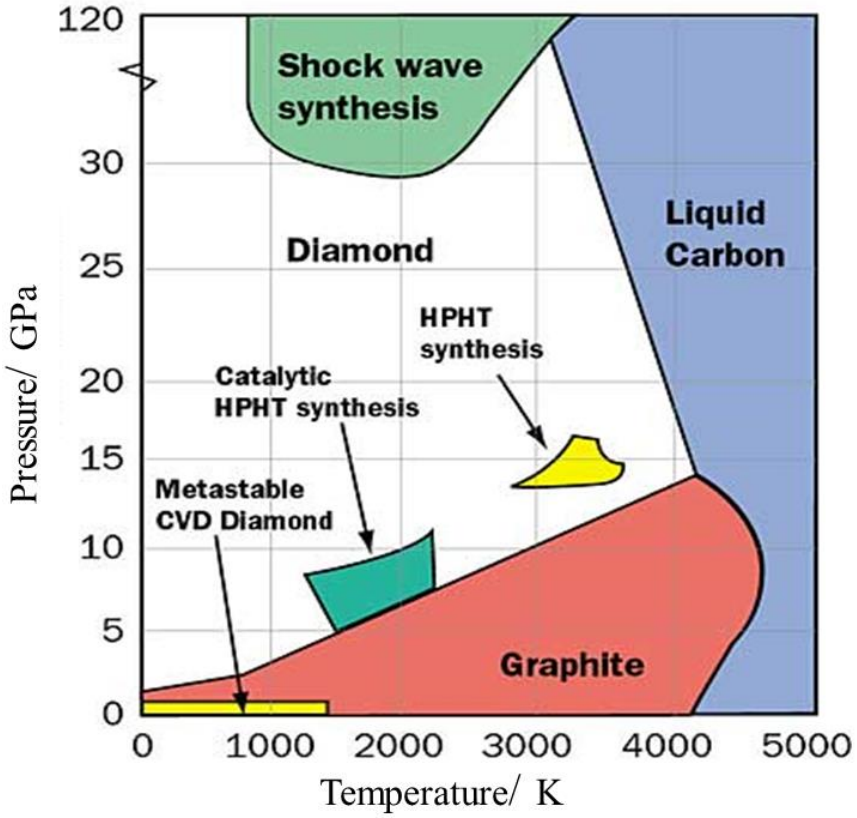


Fig 2. 20: Phase transformation diagram of graphite into a diamond by a different process.

An overview of thermodynamic field stability is as follows

i. The graphite to diamond transformation line runs from 1.7GPa/0 K to the point at 12GPa/5000 K where triple-phase is present as graphite/diamond/liquid.
ii. Graphite's melting line runs from 0.11GPa/5000 K extending up to the graphite/liquid/vapour point at 12GPa/5000 K.
iii. Melting point of diamond is above the graphite/liquid/vapour triple point at 12GPa/5000 K.

Transformation energy required for phase transformation can be easily deduced from the energy diagram shown in Fig 2.21. The energy diagram shows the

conversion of graphite to diamond. Conventionally the material which has lower potential energy is considered as stable material and this is the reason why graphite is positioned below in this diagram. Carbon atoms have very large binding energy within the atoms. Thus, the lower barrier energy required for transformation of graphite to diamond is above the energy region of transition state which shows involvement of higher energy structure in the reaction. During this transformation, the bond between carbon atoms gets stretched and the atoms starts to rearrange themselves in plane arrangement of diamond. There will be some buckling in the planes due to the elongated bonds between the non-bonded planes of carbon atoms in diamond. As a result, the stabilization afforded by four single C=C bonds at each C atom has begun to be gain, but the resonance stabilization of diamond has been fully realized. As a result, the C=C bonds in the transition state on average are weaker than the bonds of either diamond or graphite (Fig. 2.22).

Activation energy is the difference of energy between the starting state of material and the transition state. The activation energy also depends on the reaction direction; the activation energy for transformation of graphite to diamond in lower that that of the activation energy of graphite to diamond. A reaction will happen slowly if the activation energy of the reaction is high.

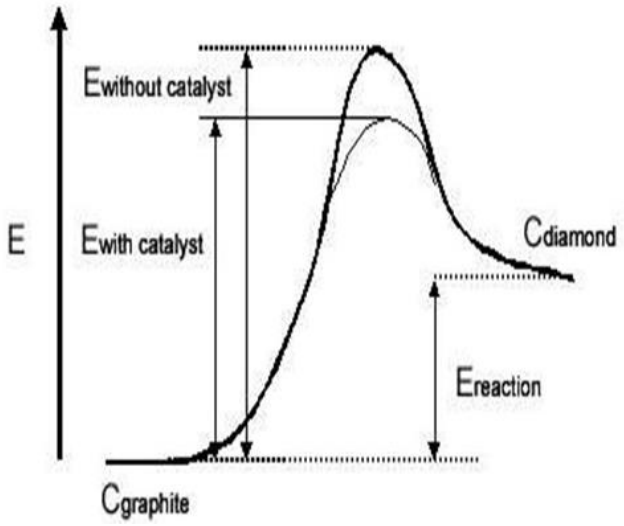


Fig 2.21: Role of catalyst in activation energy

Rate of reaction is the speed at which the atoms gains enough energy to cross the energy barrier. Thus, higher the energy barrier slower will be the process of reaction. Also, the rate of reaction can be improved by raising the temperature or

giving additional kinetic energy to the atoms as it will give additional energy required for climbing the energy barrier. Huge amount of energy is needed as in form of high temperature for conversion of diamond to a transition state for graphite formation.

Activation energy for transformation of graphite to diamond is lowered by the addition of catalytic metals and also reduces the reaction kinetics. But the thermodynamics of the reaction are unaffected by the presence of catalyst. It is a requisite for catalytic metals to have unpaired electrons which is required for the chemical bonding but they should not be highly reactive to prevent formation of carbides.

The transition metals with intermediate reactivity like Fe, Ni, Co, Mn, and Cr can be used to catalyse the conversion of graphite to diamond at low pressure and at temperatures above 700 °C. Such catalytic reaction can go in both directions. A catalyst is called effective when it catalyses formation of diamond from graphite under the suitable condition of high pressure and also conversion of diamonds to graphite under the low-pressure conditions. So, the graphite which comes in direct contact of such catalytic materials at elevated temperature its lattice structure tends to deform into diamond or amorphous carbon. There are protruding surfaces on graphite which was in contact with catalyst and got changed into diamond or other non-diamond carbon. These can be separated easily after the transformation due to the weak bonds binding between transformed product and graphite.

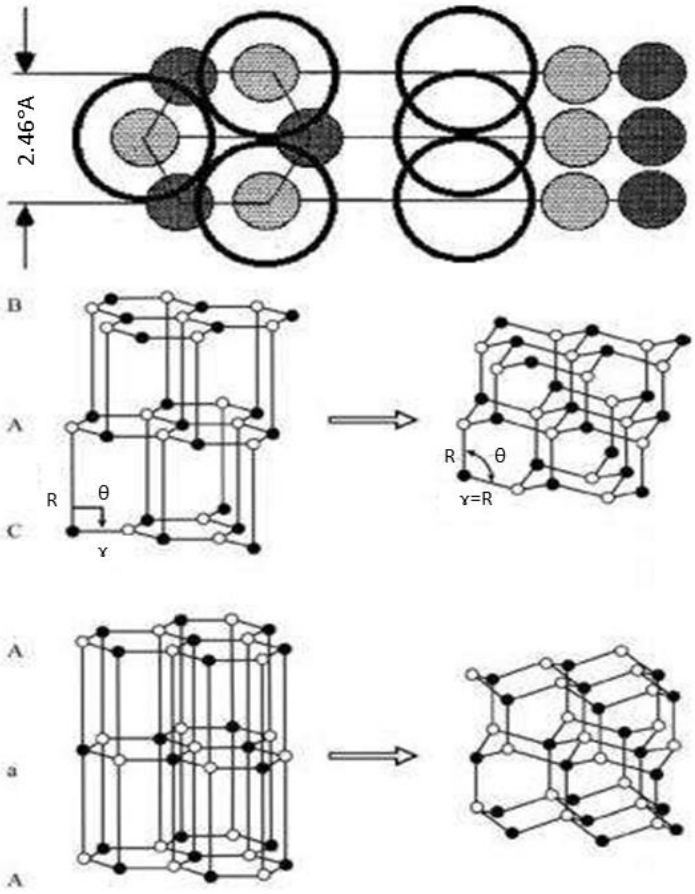


Fig. 2.22: Stretching of chains of graphite during diamond formation

## 2.4 Mechanical Alloying

Mechanical alloying is a process which is easily adaptable and because of such adaptability it still finds its usage in research areas. Mechanical alloying was developed in 1960s by ODS for manufacturing superalloys and later in 1980s the same method was adapted for making alloy phase like solid solution, quasicrystalline, crystalline and amorphous state. Mechanical alloying is still utilized for analysis of and manufacturing of such state of material. The mechanism of reaction by displacement was given in 1989 which originated a stream concentrating on the production of pure metals, alloys and varying compounds directly from the metal ore or scrap. From past few year studies on the formation of nanocomposites using mechanical alloying route gained major interest.

Processing steps of mechanical alloying is simple starting from pure metal powder mixing in required quantities inside vial along with grinding media (commonly steel balls are used) and then this is subjected to milling for specific period of time. The milling time is the time required for achieving the uniform composition. Mechanical alloying inevitably a solid state alloying process in which a repeated cycle of a set of incidences is done, these incidences are welding of particles, fracture of such welded particle by the impact force and rewelding of the particles. All these steps take place inside a high energy ball mill. By the text, it may sound like mechanical alloying is a very simple process but in reality, it is complex process with many variables which plays their role in getting the final state of product. These parameters include type of high energy mill, the container or vial used for milling, the speed at which milling is carried out, milling duration, grinding medium, the ratio of grinding media to powder, the atmosphere of milling, process control agent and milling environment/temperature. Post milling process the powders are consolidated into shape of component and then further treatment is done to get the final microstructure and properties required in the component [30].

### 2.4.1 Process variables

The parameters which affect the outcome of mechanical milling are:

- Type of mill
- Milling container/vial
- Milling speed
- Milling duration
- Type, size, and size distribution of the grinding medium
- Ball-to-powder weight ratio
- The extent of filling the vial
- Milling atmosphere and
- Temperature of milling

***Type of mill***

Numerous types of high energy ball mills are available for doing mechanical alloying. Every mill has its distinct milling capacity, milling speed, temperature controllability and level of contamination. A ball is selected based on the required final state of powders after mechanical alloying and also the properties initial feed powder. Usually it is preferred to use attritor or Fritsch Pulverisette for bulk powder production. There are many customised mills which are used to get the desired powder properties [134].

*Attrition mill:*

Attrition mill is basically a closed cylinder oriented vertically which has impellers mounted inside the cylinder on agitator shaft in a pattern that every next impeller is perpendicular to the previous impeller blade. Impellers are the one which pushes the balls into motion leading to collision between balls, impellers and agitator shaft and resulting in particle size reduction due to this entrapment of powder in such collision site. Rotational motion of impeller is done by using a high-power motor. In this the container or tank is stationary and the powder is feed to it with defined amount of balls, Then the tank is closed and the mixture is agitated a speeds around 250 rpm causing shearing and impact forces on the powders [134]. Attritor is multiple times faster than the conventional ball mills

***Milling container***

Container material is also a crucial factor in the milling process as the container's inner wall is constantly under impact by grinding media leading to wear of container giving contamination to the powder. These contaminations may modify the property of the resultant powder and many a times it is harmful. This is prominent in the case where the material of container is way more different than the powder. Even when the material of container is similar to the powder then also it has some negative effect by varying the composition of the produced powder. The most common materials for making the milling container are hardened steel, tool steel, tungsten

carbide coated steel, bearing steel etc. There are also some special materials developed for special application, some of these materials are titanium, copper, yttria-stabilized zirconia, sapphire, hard porcelain, $Si_3N_4$ and Cu-Be [135].

***Milling speed***

Higher rotation speeds lead to higher energy transfer to the powder via grinding media. Such increase of speed also has some negative effect like increase in the temperature inside the container. In few cases this is desirable situation as it tends to improve the homogenization and alloying effect in powder. But this kind of situation of temperature rise is a non-desirable outcome as increased temperatures helps transformation and decomposition of supersaturated solid solution giving metastable phase formation during milling. There are many study results present which says that higher milling speeds forms nanocrystalline materials as the increased temperature enhances dynamic recrystallization in powder. Temperatures generated in mills varies with varying the type of mill, milling container size and materials.

***Milling duration***

One other crucial parameter is milling duration or the time period of milling. Milling duration is intertwined with other parameters type of mill, speed of milling, ball to powder weight ratio and the temperature at which milling is done. Optimum milling duration is experimentally determined for a particular set of parameters used for powder composition. Also with increase in milling duration the contamination is also increased which may negatively affect the properties of powder by formation of undesirable phases by the contamination [136]. This is the reason powders are milled for specific durations only and not more than that.

***Grinding medium***

In the same as that of grinding container, materials of grinding media have very broad spectrum of materials to select from. Some of such extensive choices are tempered steel, tool steel, tungsten steel, tungsten carbide etc. Majorly balls with higher density as that of powder is desirable as it gives higher impact force. Also,

there some special material available for grinding medium similar to the materials available for grinding container like yttria stabilized zirconia, zirconia, agate, titanium, niobium, silicon nitride etc. It is always advised to use same material for grinding container and grinding medium. This reduces cross contamination during the milling process [137].

Size of grinding medium is also one important affecting parameter. It is preferred that balls of larger size are used as they have the extra mass which enhances the impact energy transferred to the powder particles. There are many literatures which has analyses effect of size of milling media on the final particle conditions. One such example is of balls used for milling of titanium and aluminium powder. When 15 mm balls were used it gave solid solution of aluminium in titanium but when balls of 20 and 25 mm diameter are used they resulted in mixing of titanium and aluminium and lacks the alloying even when the milling was done for a prolonged duration [138]. In another study it was stated that amorphous phase formation happens faster when balls of 4.76 mm diameter were used compared to the usage of ball of 1.9 mm diameter [139]. In yet another investigation on Ni-C and Co- C system was done. The steel balls of 9.5 mm were used and the BPR was kept 1:100. For the Ni-C system, after 500 hours MA in the compositions of $Ni_{1-x}$ $C_x$ (x = 0.10 and 0.15), the supersaturated solid solution of fcc Ni was formed. Supersaturated fcc phase decomposed into metastable carbide of $Ni_3C$ at about 600 K. In the case of Co-C system, a supersaturation of about 6 at. C in fcc Co and the formation of $Co_3C$ carbide were also obtained [40]. It is evident that ball of smaller diameter generates more intense frictional action promoting amorphous phase formation. Also the soft milling condition that is balls of smaller diameter and a lower ball to powder weight ratio helps the amorphization.

Balls of same diameters are usually used for investigations but there are many literatures available which reports usage of balls of different size for fairly resembling study. Such investigations have shown that it is always better to use balls of different size as they provide higher collision energy [140]. It is found that at the primary stages of milling powder coat up the grinding balls and also gets cold welded to the surface of balls. Such a coating is advantageous as it reduces contamination of powder as a result of reduced wear. But the thickness of such coaptation desired to be kept

minimum as it prevents formation of heterogeneous product [141]. The only drawback of such powder coating is that it is very difficult to withdraw which ultimately reduces the yield of the milling process. For usage of balls of varying diameter, it is reported that cold welding of such powder coating is reduced. But even though no results have shown the improvement of yield in such a milling condition. It is possible that the balls of different size have a shearing action in between themselves which repeatedly reduces the attached powder on the balls.

Usage had shown that balls of same diameter in a contoured or flat bottom vial have shown formation for tracks of ball movement. As when balls of same size are used, they follow a well define trajectory that the collision with end surface. Thus, it is always advised to use balls of smaller and bigger diameter together to help the randomization of ball motion in a mill.

***Ball-to-powder weight ratio***

Ratio of weight of ball and weight of powder used in a mill is called as ball to powder weight ratio (BPR) or charge ration. This is also an important parameter affecting the outcomes of a milling process. The usual variation range of BPR is from 1:1 to 200:1 [142]. Ration of 10:1 is usually used for milling in a small capacity mill. But for mills of higher production capacity this ration ranges from 50:1 to 100:1 [143].

During the milling process BPR is a prime factor deciding the milling duration requirement. Relation of BPR is inverse with the milling time [144]. When BPR is increased for a specific amount of powder, the number of impact size increases and thus the energy input is increased which leads in quicker alloying. But with such increased energy input the temperature rise also happens which might change the powder's state. It is possible that amorphous phases getting converted to crystalline phases if the temperature increases significantly [134].

***The extent of filling the vial***

It is necessary to provide space for ball movement inside vial as the impact by ball is the driving parameter of alloying. Container which is not filled very low than the optimum level the production rate reduces significantly and in contrary if the vial is filled way higher than the optimal level there is lower space for movement of grinding media which reduces the impact energy. Thus proper filling of vial is also crucial and is typically around 50% volume of the vial.

***Milling atmosphere***

Powders have sensitivity for contamination by the atmospheric condition. Thus, milling is always done in containers with protective inert atmosphere or which are evacuated. Oxidation of the powder can be controlled by providing atmosphere with high purity argon gas as a protective gas. Nitrogen had also shown promising results in prevention of oxidation of powder but its fails when the powder are of reactive material like titanium and its alloys [145].

Glove boxes with protective atmosphere are used extensively for charging and discharging of powders from the vial/milling container. Glove boxes are many a time evacuated first and then purged with argon gas. There are researches which has used entire ball mill setup inside an evacuated glove box [145].

Customized atmospheres are used suiting a specific milled powder. Some of such examples are milling of nitrides under nitrogen or ammonia atmosphere [146,147]. Milling of hydrides using hydrogen as milling atmosphere [148]. Nitrides and oxides are generally found in the milling products when milling is done in presence of air, especially when powders are reactive. So, it is very important to use inert atmosphere during the milling process of reactive powder.

The nature of the final product is affected by the milling atmosphere. Some researchers have found that when Cr-Fe powder mixtures is milled in different milling atmosphere the composition was different for every milling atmosphere [149]. When

an argon atmosphere was used for milling of powder than there was no amorphous phase observed, and the X-ray diffraction was showing Cr peaks. But when the milling of powder was conducted in the air which has argon or nitrogen than the resultant milled powder was completely amorphous. Similar studies were done for Ni-Nb system and observed that the kinetics of amorphization can be enhanced by using oxygen as a milling atmosphere [150].

***Temperature of milling***

Milling temperature is also one factor which have decisive role in finalization of composition of milled powder. Temperature shows prominent effect on the different kind of alloy systems like intermetallic, solid solution, amorphous or nanostructured material, due to the diffusion process happening in the alloy system during milling. Very less literature is present which reports the effect of temperature on the outcome. One method of reducing temperature during milling is by adding liquid nitrogen to the milling container during the milling process. And if the temperature needs to be raised it can be easily done by using electrical heating around the container [151].

## 2.4.2. Process control agents

During milling of powder of ductile material, they tend to get cold welded with each other. Alloying can only happen when there is balance between cold welding and fracturing of particles. To reduce cold welding in such ductile material process control agents (PCA) are added to the powder mixture. PCA can be in solid, liquid of gaseous form. Usually PCA which are organic compounds act like surface activating agents. They are absorbed on to the powder surface and reducing the surface tension in solid material which limits cold welding of particles.

There are various kinds of PCSs used with usage around 1-5 wt.% of the entire powder mix. Common PCAs are stearic acid, methanol, ethanol and hexane. These compounds tend to decompose during the milling process forming compounds by interaction with powder and these are then combined to form dispersoids in the

powder particles. Therefore carbohydrates which have carbon, oxygen and hydrogen like hydrocarbons containing carbon and hydrogen adds oxygen and hydrogen to the powder particles which forms oxides and carbides in the matrix. Such dispersoids works as strengthening materials for the matrix and helps enhancing strength and hardness. These kind of dispersoids are not found to dangerous it, they help in improving hardness and strength of matrix [152]. Hydrogen gets evaporated during heating of powder or might get entrapped in metal lattice during sintering process. Even though the fact is that hydrogen gas serves as a surfactant and does not generally involve in the alloying process [153], even some studies has shown that in titanium-rich alloys that hydrogen acts as a catalyst for amorphous phase formation It has also been concluded that PCAs have an effect on the final phase formation by altering the solid solubility levels [156], changing the glass-forming range, and modifying the contamination levels [155].

The type of a PCA which can be utilized for milling depends on the type of the powder being milled and the desired purity in the final product. The final powder particle size and yield of the powder depending on the quantity and nature of PCA used in milling. The effectiveness of a PCA can be judged by the powder yield. If the powder yield isn't high, which means either the quantity of PCA used isn't sufficient, or most likely it's not the appropriate PCA.

### 2.3.3. Mechanisms in mechanical alloying

The MA technique is being used mainly for three types of processing: alloying, metastable phase formation and activation of chemical reactions [30].

#### a) Alloying

The alloying happens in five stages. Within the first stage, once the particles begin obtaining comminuted, the malleable components are deformed into long lamellae by the impact of the balls whereas the more friable components are comminuted. This is often followed by growth within the number of lamellae because

of cold welding; these composite lamellae within the coarser particles have a multilayered, oriented (plate-like) structure. The next stage is related to the reduction within the aspect ratio of the lamellae and the plate-like coarse particles changing into equiaxed. In the fourth stage, the welding orientation within the composite particles becomes random and convoluted. The ultimate stage is characterized by a narrow particle size distribution and therefore the composition changing into uniform. At this stage, the individual lamellae cannot be resolved in an optical microscope. A saturation level of hardness of the particle is attained and therefore the particles are within the heavily cold worked state.

### b) Metastable phase formation

#### *Amorphization*

MA has also been used as a promising methodology for the fabrication of amorphous and nanocrystalline material. Many theories are recommended for the mechanism of the amorphization phase formation by MA. These include liquid quenching (LQ) model and solid-state amorphization reaction (SSAR) model [30].

#### *Nanocrystallization*

The process of the nanocrystallization can be understood within the following manner. In general, plastic deformation precedes by slip and twinning at low and moderate strain rates, whereas at high strain rates, the formation of shear bands that consist of a dense network of dislocations becomes the dominant deformation mechanism. Within the early stage of ball-milling, as dislocation density increases strain at an atomic level also increases. At a certain dislocation density, the crystal disintegrates into subgrains that are at first separated by low-angle grain boundaries with offset angles of less than 20°. Throughout processing, firstly the deformation takes place in the unstrained region of the materials creating shear bands. The nanograin size in the material is obtained by diminishing the size of the subgrain existing in these bands. Once the nanograins are obtained, which cannot be further deformed, fully randomly oriented nanograins are obtained in material, as the milling progresses.

Many researchers recommend that nanocrystalline grains are relatively dislocation free [157]. Further refinement is not possible when a completely nanocrystalline structure is achieved. In the case of small crystallites to avoid the plastic deformation, high amount of stress required for this dislocation movement. Hence, further deformation and energy storage can only be accomplished by a glide along the grain boundary, which ends up which results in random rotation of the subgrains.

***Supersaturated solid solution by MA***

Equilibrium solid solubility limits can be extended by non -equilibrium processing techniques such as rapid solidification and the MA process. The supersaturated solution formation indicates the elevation of free energy caused by the stored energy as defects but also the mixing of immiscible materials in the range of nano- order. There is a number of examples of this effect in literature. Schwarz et al. [158] found that the solubility limit of Ti in fcc Ni increases to 28 at.% on MA. This may be compared with the equilibrium solubility limit of only a few percents. In the Ni - Nb system [153] a considerable enhancement in solid solubility by MA was observed by Lee et al. The terminal Ni fcc solid solution and the Nb bcc solid solution were found to have approx. 10 at.% Nb and 10 at.% Ni, respectively. In equilibrium conditions, these values are 4.2 at.% Nb and 3.5 at.% Ni. Ishihara et al. successfully formed SSSS of Fe-Li by MA and the maximum solubility obtaines was 15.3 at.% after milling for 10 h. There was formation of oxides in the process which, as an impurity, enhances the MA process [32]. Lei et al. studied the Cu-10 wt.% Nb system and claimed formation of SSSS with solubility of 9.6 wt. % Nb in Cu matrix when MA for 100 h in planetary ball mill. The solid solubility of Nb in Cu content was found to increase to 5.6 wt. % after 40 h milling but it increases further to 9.1 wt. % for 70h milling and finally no further increase in solid solubility was observed after 100 h of milling [33]. Rochman et al. studied Fe-C system and extended the solid solubility of C in Fe to 1.3 wt. %, at 253 K when MA for 20 h, much greater than the solid solubility at equilibrium conditions [34]. Another set of investigation was done by Liu et al. indicated that high energy ball mill could extend the solid solubility of C

in Cu to 4 wt. % after 24 h milling. The increase in solid solubility is a result of reduction in grain size and increment in lattice strains during milling process [35]. Wu et al. [36] successfully formed SSSS of C in Al up to 23 at.% which was far greater than their equilibrium solubility, whereas amorphization took place in the span of 28-50 at. % C when milling was carried for 220 h. Minamino et al. studied properties and microstructure of bulk nanocrystalline in Fe-Al-C system prepared by MA. During the process, the SSSS in α-Fe was observed having crystal grains of 10nm [37]. Tanaka et al. studied the Ni-C and Co-C system [40]. In Co-C system, a supersaturation of about 6 at.% C in fcc Co for the Co-C sample of x = 0.10 after 1000 hours MA and of x = 0.15 after 500 hours MA while in Ni-C system, after 1000 hours MA, the carbon contents were estimated to be about 9 and about 12 at. pct for x = 0.10 and 0.15, respectively. The supersaturated solid solution of fcc Ni was obtained. Supersaturated fcc phase decomposed into metastable carbide of $Ni_3C$ at about 600 K. [40]. But as per the nickel-carbon equilibrium phase diagram (Fig. 2.23), the solid solubility of carbon in the nickel system is negligible at room temperature [159]. The Ni-C phase diagram does not show any stable carbide phase. The maximum concentration of carbon dissolved in nickel at eutectic point, i.e. 1326.5 $^{o}$C, is 0.56 wt.%.

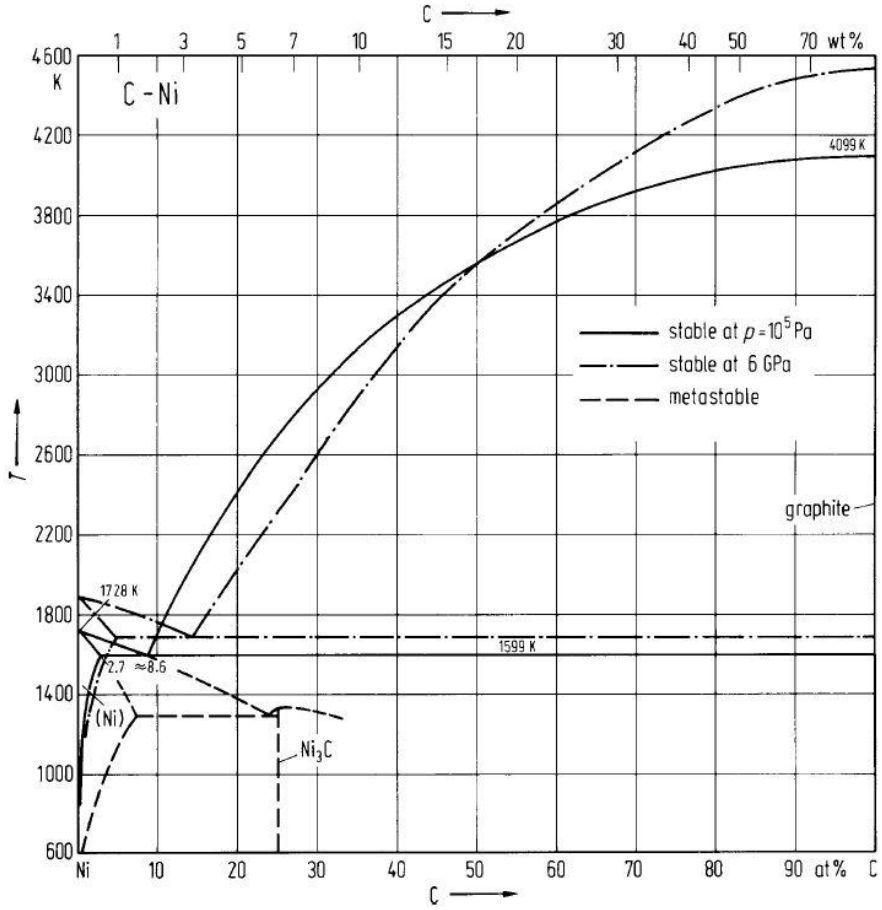


Fig. 2.23: Ni-C equilibrium phase diagram

Thus, the supersaturated solution formation indicates the elevation of free energy caused by the stored energy as defects but also the mixing of immiscible materials in the range of nano- order.

### c) Activation of chemical reactions

Mechanical alloying considerably increase solid-state reaction rates by dynamically maintaining high reaction interface areas and at the same time providing the conditions for fast diffusion [160]. During MA, plastic deformation, welding, and fracturing of powder particles occur endlessly. Plastic deformation and fracture of powder particles produce atomically clean surfaces. Particle welding can occur when such surfaces are impacted throughout subsequent collision and reactions can proceed across these new, internal interfaces. Therefore the chemical composition of powder particles changes throughout milling.

## 2.5. Hot Consolidation Techniques

Consolidation of milled powders is an important step for reliable and reproducible physical/mechanical properties of the fabricated materials for most industrial applications. Consolidation of ball-milled powders into bulk, full density compacts with retaining grain size is a major task [161].

The principal goal of the compaction process is to apply pressure and make a bond among the particles due to cohesion forces. This is usually termed as *green strength.*

The compaction processes have the following effects:

i) Reduces the voids within the milled powders and enhances the density of the consolidated powder.
ii) Creates adhesion and bonding in the powder particles.
iii) Facilitates the plastic deformation of particles to confirm the final desired shape of the material.
iv) Enhances the contact area among the particles and facilitates the subsequent sintering process.

Hot consolidation methods are applied to obtain fully dense metal powder compacts with controlled microstructures at high temperatures. Hot consolidation has to be done under conditions in which the powder before it is consolidated to near theoretical density, is to be protected from reaction with air, and makes the operation more complex and costly. The improved properties which may be due to microstructural features which can be obtained in certain materials when they are produced by hot consolidation of metal powders rather than by conventional means [30]. The various techniques used for hot consolidation of powders are as follows:

i) Uniaxial pressing
ii) Isostatic pressing

iii) Extrusion

iv) Forging

v) Roll pressing

### 2.5.1. Uniaxial pressing

Hot pressing can be performed in a rigid die using uniaxial pressurization as shown in Fig. 2.24. The die is usually made from graphite to allow external electrical heating. Other common die materials include refractory metals and their alloys used at low stresses. Vacuum is often selected for the process environment to minimize contamination of the compact. This also eliminates the problem of oxide layer formation, traditionally associated with hot die pressing. This also reduces wear of the die and increases its life. As the powder has to be heated to the hot pressing temperature, held at this temperature and then cooled back to room temperature in a vacuum [162, 163]. Temperature is a critical factor and small grain sizes aid densification. During hot pressing, the total amount of deformation of the compact is relatively limited in contrast to the hot extrusion and hot forging, but complete densification is generally achieved.

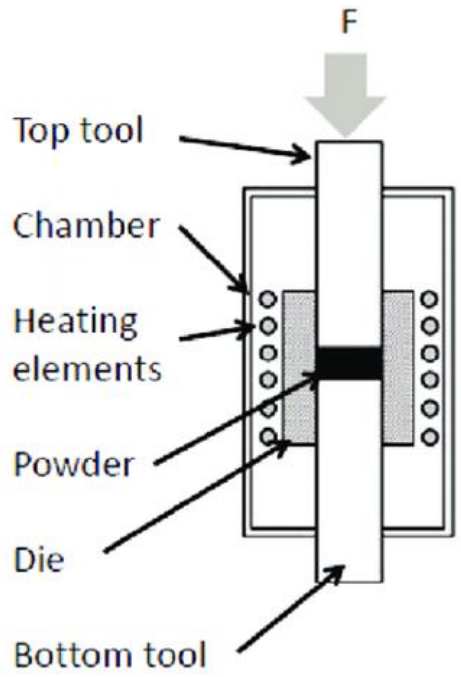


Fig. 2.24: Schematic of hot pressing

## 2.5.2. Isostatic pressing

In hot isostatic pressing (HIP), shapes close to that of the final shape of the product, 'near net shape' can be produced. Production by HIP is economically justified not only because of the improved microstructure and properties of the component but also because the amount of raw material needed in the HIP is less than that required for casting which has to be forged and machined [164].

Flexible dies are used in the HIP with isotropic pressurization. The primary control parameters are pressure, temperature and time. Fig.2.25 shows a schematic of the HIP process.

For loose powder, a gas-tight container is used to shape the powder. Cans made of stainless steel or mildsteel are used as a container in this method. Pressure medium used is a gas (nitrogen or argon). The applied pressure is commonly between 100 MPa to 300 MPa. The part shrinks and densifies, forming sound high strength structure. The method may be used without a mold. In this case, the part is first compacted by the cold isotactic pressing method, and then it is sintered in order to close the interconnecting porosity. The sintered (but still porous) part is then pressed isostatically at high temperature without any can (mold). Titanium alloys, high speed steels, super-alloys, hard alloys and various ceramics are produced by the HIP [165- 168].

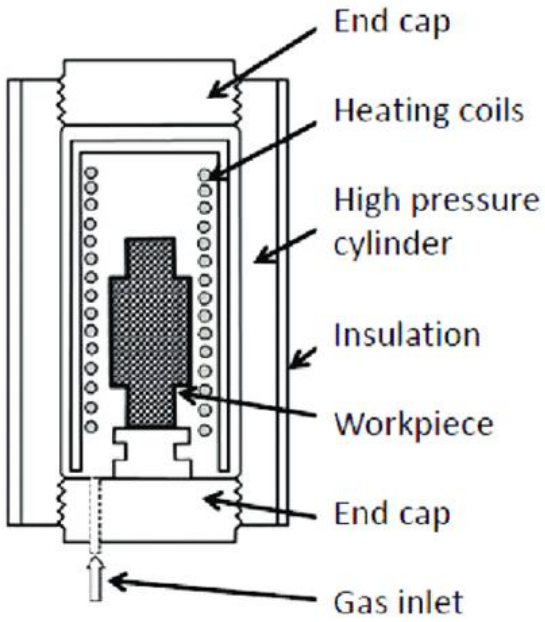


Fig 2.25: Schematic of hot isostatic pressing

### 2.5.3. Extrusion

Extrusion of metal powder at elevated temperature is another method to achieve full density. It combines hot compaction and hot mechanical working, yielding a fully dense product. In extrusion, large hydrostatic compressive forces occur and a unidirectional force makes the compact flow through the die. Frictional forces produce a shear component which results in a characteristic shear pattern in the extruded metal. The energy expended in shear represents almost half of the total energy needed for the extrusion. The total amount of deformation in extrusion is much larger than in any other single metal working step.

Temperature is the main process control variable. Too high a temperature can damage the product microstructure and shorten the life of the extrusion tooling. Alternatively, too low a temperature makes extrusion difficult because of the higher stresses involved. Typically, extrusion is performed at temperatures over two-thirds of the absolute melting temperature for the material. The force to initiate extrusion flow is higher than the force to maintain flow and increases with smaller particle sizes [169].

The extrusion force F required to achieve a dense compact can be given by the equation (1) below;

$$F = C.\ A.\ \ln(R) \qquad \text{…….. (1)}$$

where A is the cross-sectional area of the feed material, R is the reduction ratio and *C* is the extrusion constant, which provides a measure of the difficulty in achieving deformation and flow of the powder.

Extrusion is employed to consolidate MA powders, rapidly solidified powders, composite powders, and ODS alloy powders.

### 2.5.4. Forging

Metal powders, especially spherical powders which have a high tap density, can be forged directly when encapsulated in a steel can [170]. Hot forging requires lower loads and easy flow of material occurs. In upset forging, there is always the chance of occurrence of surface cracks due to excessive tensile stresses. This method is not widely used.

### 2.5.5. Roll pressing

Conventional rolling technology is used to densify a porous feed material. Loose powder is gravity fed into the gap between two rolls which generates the green sheet. This is the case of cold pressing but in case of hot roll pressing, there are heating coils inside the rolls for heating the rolls. For a given final density, the necessary roll force is independent of the initial powder density [171]. The final product is limited in geometry and powder rolling is generally restricted to forming sheet products. Fig. 2.26 represents the schematic of the roll pressing sequence.

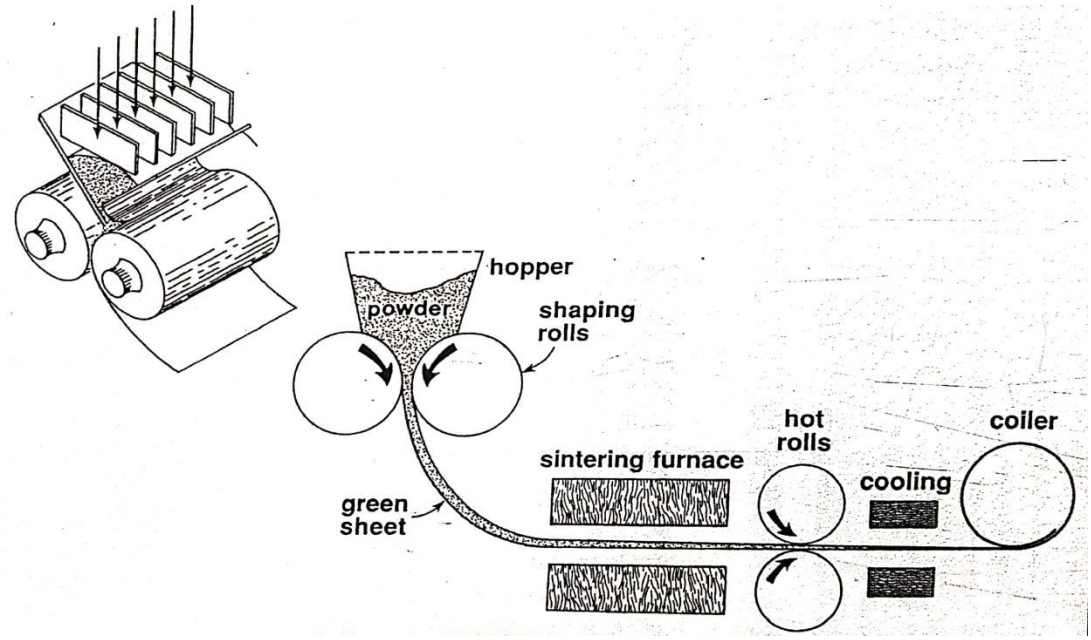


Fig. 2.26: Schematic of roll pressing sequence.

## 2.5.6 Spark plasma sintering

### 2.5.6.1 Introduction

There many innovative sintering processes followed by researchers worldwide. One such technique is spark plasma sintering (SPS). This has three main important sintering conditions: 1) pulsed direct current, 2) vacuum as atmosphere and 3) uniaxially acting force [172].

SPS have three basic mechanism stages of sintering which is plasma heating, Joule heating and lastly plastic deformation. During plasma heating, because of current flowing through the powders, give high heating rate and achieve high temperatures easily. As the powders are at high temperatures neck formation results due to melting and fusion of powder surfaces. Due to necking current flow path changes from the surface to through the particles resulting in an increase in temperature and also grain size by diffusion. The uniaxial force acting during SPS makes the sintered component denser. Grain size in a spark plasma sintered component is lower than that of in a conventionally sintered as the soaking time is relatively low. Thus, one can say that grain growth is directly related to the soaking period during sintering operation and the density of component is inversely related to

the holding/soaking time. So, lower soaking time gives lower grain growth and higher density [173].

SPS is a versatile process and can be used for sintering of metals, ceramics and in even many cases for composites. SPS have temperature and pressure acting on component simultaneously which give a superior product property as that of conventionally thermo-mechanically treated. Conventional thermomechanical processes don't have that great control over the grain size, whereas in SPS fine grains can be easily achieved. Thus SPS is a more convenient option of achieving desired results in the end product in a very short duration [174].

### 2.5.6.2 Parameters affecting SPS

Like every synthesis process, SPS have parameters or operating factors which ultimately affects component properties. Parameters of SPS are the heating rate, the rate of load application and release, maximum applied load/pressure during holding, holding temperature. All these parameters affect the physical and microstructural outcomes of the product [175].

***Temperature***

In SPS heat is produced by the applied current through the powder. Thus, by studying the density of the sample one can detect the effect of sintering temperature for a particular material. Such a change in density by varying sintering temperature was experimentally analyzed by Garay and developed the following equation (2) [44].

$$\rho = s\,(T/T_m) + b \qquad \text{…….. (2)}$$

where

$\rho$ = fractional density

T = sintering temperature

s = slope (can be referred as temperature sensitivity)

$T_m$ = melting point of material

b = intercept of the density axis

From the aforementioned relationship, it is clear that the density of the sample depends on sintering temperature. For materials which have a higher degree of temperature, sensitivity have greater effects of sintering temperature and vice-versa which is primarily for ceramics and carbides.

***Pressure***

Spark plasma sintering is carried out under uniaxial pressure acting on sample and this also has a pronounced effect on the density of the sample. The applied pressure has two advantageous effects 1) it prevents agglomeration by reshuffling of activated particles, and 2) acting as a driving force accelerating the process. Effects of pressure can be given by the following relation (3) [43]:

$$\frac{d\rho}{(1-\rho)dt} = B\left(g\frac{\gamma}{x} + P\right) \qquad \text{..... (3)}$$

where,

ρ = fractional density

t = sintering time

B = term which comprises temperature and diffusion coefficient

γ = surface energy

g = geometrical constant

x = parameter which represents particle size

P = applied external pressure

***Heating rate***

For any sintering method heating rate is a major role-playing parameter as higher heating rate give finer grain size. Also, higher heating rate increases productivity and increased sinterability as a result of higher powder activity by the neck formed during the sintering operation. The difference in temperature which is

measured on the graphite surface of the die has effects on the heating rate and ultimately on the densification [176].

## 2.6. Raman Spectroscopy

Conventionally Raman spectroscopy is used for characterization of carbon-based materials. Raman spectroscopy has the ability to sense very small changes in the carbon materials which makes it a very useful tool for numerous researches, especially which deals with carbon nanostructures. Its speciality lies in the sensitivity for symmetric covalent bonds. Every band of Raman spectrum is directly related to a particular vibrational frequency of bonds in a molecule [177]. This method of characterization is helpful in a wide range of application like identifying the bonding type in molecules or solids and also doping in case of semiconductors. The present state of research in the field of condensed matter physics and material science mainly concentrates on an exploration of new carbon nanomaterials and defining their utilisation in the field of electronics, optoelectronics, plasmonics and life sciences.

There are many prime properties of carbon such as electronic band structure, geometrical structure and phonon structure is found by Raman scattering. Other than this Raman spectroscopy has the capability of differentiating multiple phases of the same material. It is also capable of giving information about crystallite size, clustering of $sp^2$ phase, presence of $sp^2$-$sp^3$ hybridization [178] and the presence of chemical impurities, the magnitude of the mass density, the optical energy gap, elastic constants, doping, defects and other crystal disorder, edge structure, strain, number of graphene layers, nanotube diameter, chirality, curvature, and the metallic vs semiconducting behaviour.

***Diamond***

For diamond first order Raman spectrum is a single line at 1332 $cm^{-1}$, which is known as D band (refer Fig 2.27 (a)). Raman spectra of nanocrystalline diamond have a slightly downshifted $sp^3$ band. The presence of extra band at 1620 $cm^{-1}$ and shoulders on 1620 $cm^{-1}$ and tetrahedral $sp^3$ band, all these points towards $sp^2$ bonded carbon that shows surface defect modes, which might not be of importance for larger diamond crystals. Also, amorphous $sp^3$ bonded carbon is suggested by the presence of wideband around 500 $cm^{-1}$ [178]. Raman spectra shifts towards higher wavenumber ($cm^{-1}$) and broadens when the size of diamond is near around the nano range [179].

***Graphite***

Spectrum of graphite have wavelength of 1582 $cm^{-1}$ (as shown in Fig 2.27(b)). Graphite have $sp^2$ bonded carbon in a planar arrangement where bonding energy of $sp^2$ bonds is greater than that of $sp^3$ bonds of diamond [180]. Vibration frequency is pushed higher with presence of higher energy of $sp^2$ bonds and hence the frequency of the band in Raman spectrum is shifted to higher frequency. The band with wavelength 1582 $cm^{-1}$ of graphite is known as G band. If graphite is ground to smaller crystallites we can observe disorder or D band appearing somewhere near around 1280 and 1400 $cm^{-1}$ based the excitation wavelength.

***Graphene***

Graphite have stacks of graphene sheets with $sp^2$ bonds. The presence of frequency band at 2700 $cm^{-1}$ [181] which is known as the G' band in Raman spectra of graphene is relatively sharper than the G band of graphene compared to graphite (Fig 2.27 (b)).

***Fullerene***

The buckyball $C_{60}$ have $sp^2$ bonded carbon atoms. Spectrum of $C_{60}$ shows line near to 1462 $cm^{-1}$ and is known as pentagonal pinch mode. The sharpness of band is related to the uniformity of the bonds. $C_{60}$ actually have atoms which are identical. In case of $C_{70}$ the Raman spectrum shows multiple bands [182]. This is because of the lack of molecular symmetry the multiple bands Raman is present (shown in Fig. 2.27(c)).

***Nanotubes***

The SWCNT shows similar Raman spectra as that of graphene. This is because SWCNT is a rolled-up graphene sheet. Raman spectra of SWCNT shows a well-defined G and G' bands similar to graphite and graphene. A separate band around 1350 $cm^{-1}$ is also visible which is known as D band. This band represents that there is presence of some variance in the graphene structure and leading to formation of hybridized vibrational mode related to graphene edges. The D band is also in relation with disorder band or defect band with intensity of G band which is frequently used as a measure of quality of nanotubes. Distinct series of bands referred to as Radial Breathing Mode (RBM) bands which are also visible in low-frequency end spectrum [183]. RBM bands are distinct to SWCNTs and corresponds with expansion and shrinkage of tubes. Diameter of SWCNTs is related to the frequency of these bands which provides vital information of their aggregation sate. When the RBM bands shifts towards higher wavenumber it is representative of SWCNTs with diameter less than 1 nm (Fig. 2.27(d)).

MWCNTs don’t show RBM bands because the breathing mode is restricted by the outer tubes. In such case, the D band is more prominent than SWCNTs which is obvious indicative of more disorder in the structure.

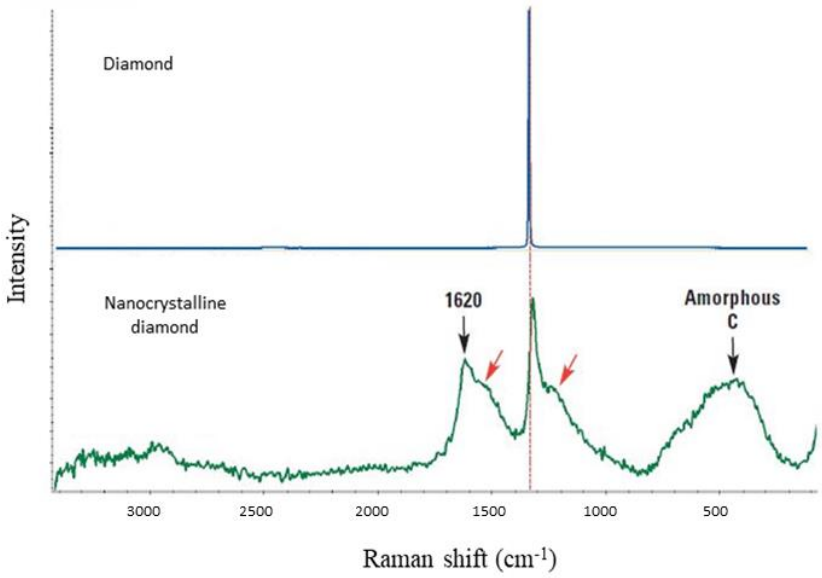
Diamond
Intensity
Nanocrystalline
diamond
1620
Amorphous
C
3000
2500
2000
1500
1000
500
Raman shift (cm-1)

**(a)**

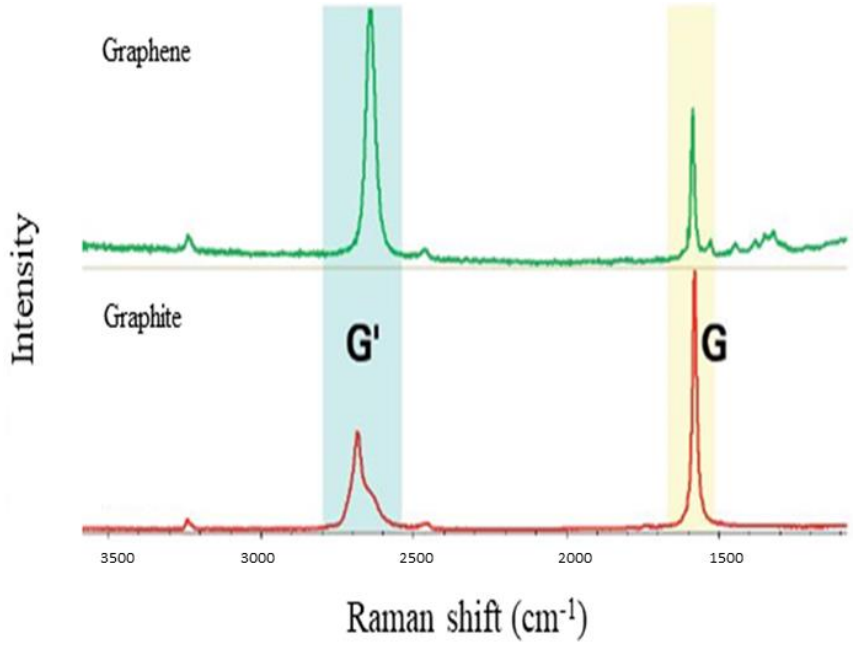
Graphene
Intensity
Graphite
G'
G
3500
3000
2500
2000
1500
Raman shift (cm-1)

**(b)**

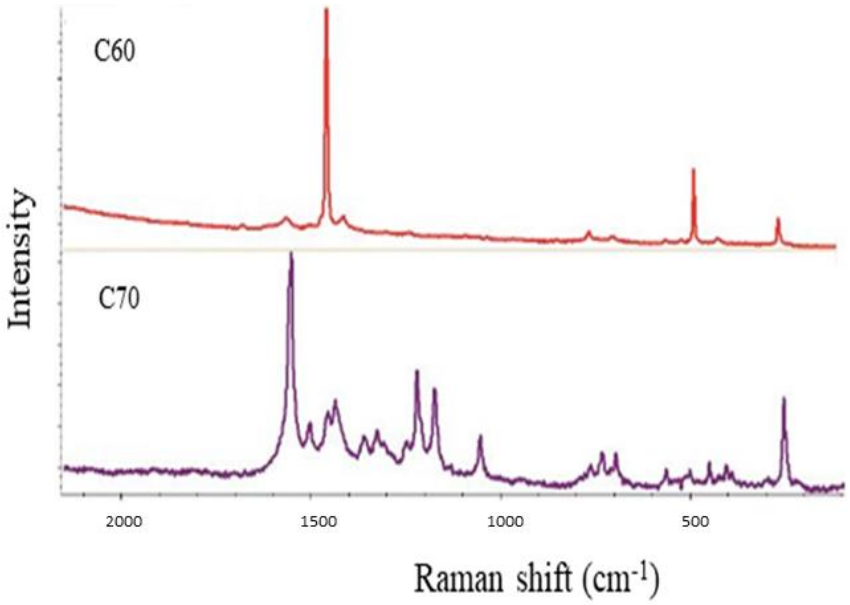


**(c)**

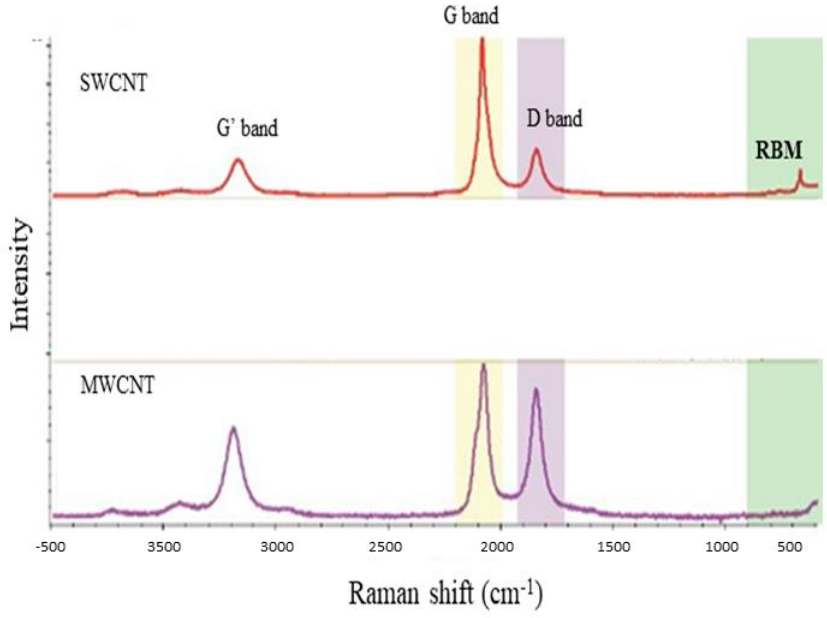


**(d)**

Fig 2.27: Raman spectrum of different carbon materials

# 3. Literature Gap and The Aim

After going through the research that has been undertaken for the formation and growth of diamond particles from the various carbon allotropes with and without the application of a catalyst, it can be concluded that the diamond formation usually requires high temperature and high pressure and expensive machinery.

Having understood the significance of MA and SPS, it was aimed to synthesize diamond via powder metallurgy; accordingly, the following objectives were decided:

(i) Synthesize the **supersaturated solid solution (SSSS)** of graphite in nickel by mechanical alloying, and carry out a detailed study on the associated changes in the nickel lattice, like **crystallite size, lattice strain, lattice parameter**, **dislocation density** which lead to the formation of a supersaturated solid solution.

(ii) Hot press/ SPS the prepared mechanically activated SSSS to **transform the graphite into diamond** at lower pressure and temperature as compared to HPHT process.

(iii) Characterize the synthesized diamond particles obtained.

# 4. Experimental Method

## 4.1. Raw Materials

In this research work, elemental nickel (Ni) and graphite ($C_{gr}$) powders were used as raw materials, details of which are given in Table 4.1. The SEM micrographs of the raw materials are shown in Fig.4.1.

Table 4.1: Details of raw materials

| S.No | Raw Material | Purity | Shape | Size |
|---|---|---|---|---|
| 1 | Graphite powder | 99.20% | Flakes | 10-15 µ |
| 2 | Nickel powder | 99.80% | Spherical | 2-4 µ |
| 3 | Nanodiamonds | 99.9% | Spherical | 50 nm |

*used as seed nuclei

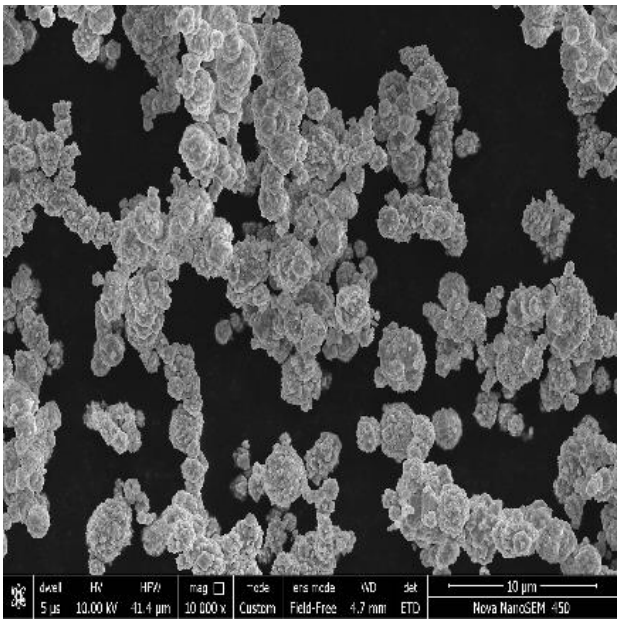


(i) Nickel

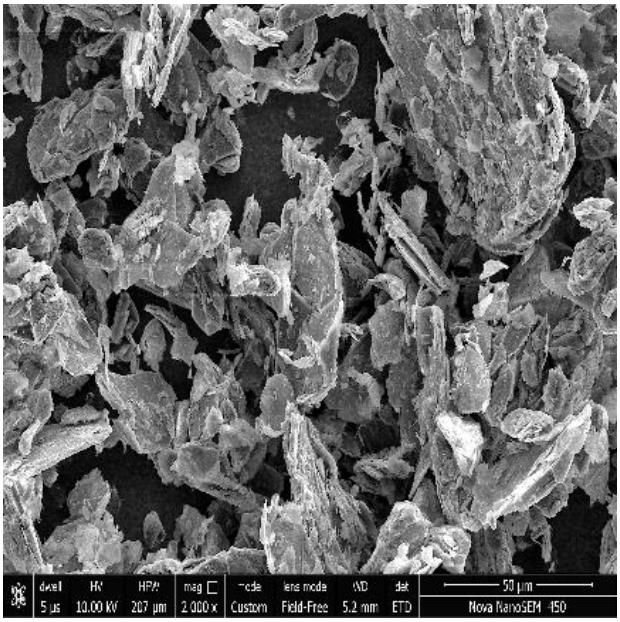


(ii) Graphite

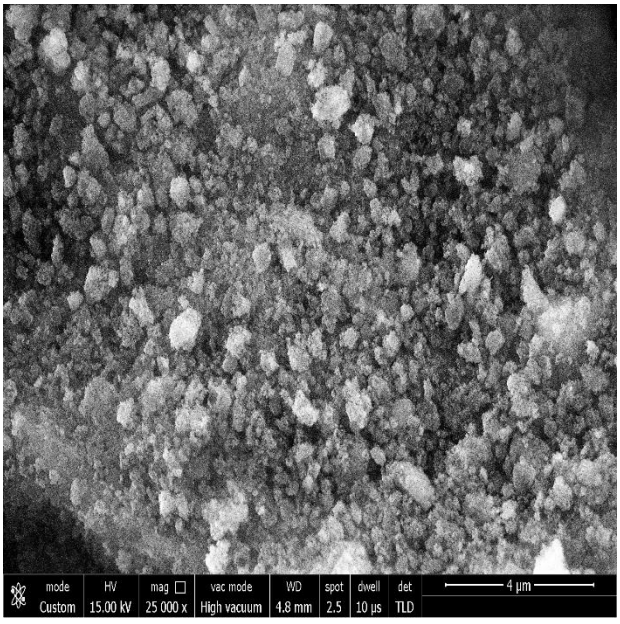


(iii) Nanodiamonds

Fig 4.1: SEM micrographs of as- received powders

## 4.2 Mechanical Alloying

### 4.2.1 Process

Mechanical alloying (MA) of the elemental powders Ni and $C_{gr}$ in the composition of Ni-x wt. % $C_{gr}$ (with and without dopants), where x= 5, 10, 15 wt%, was done in a Szigvari attrition mill (Fig. 4.2). The mill consists of a vial and a stirrer. Around the vial a water jacket is provided for circulation of water to keep the vial cool during the operation. Nanodiamond powder was used as seed crystals, with doping level of 100 ppm.

1 00 g of the elemental powder mixture and hardened steel balls of 10mm dia were loaded into the vial keeping the ball to powder ratio 10:1. MA was done at rpm of 325 in a nitrogen atmosphere to prevent oxidation. No process control agent (PCA) was required as graphite is a self-lubricant which decreases the tendency of cold welding between powder particles, balls and walls of the vial during the milling operation. Milling was performed up to 15 h duration with interruptions after every 2h 30 min, in order to pick up a small quantity of MA powder for characterization.

The details of the mechanical alloying parameters are shown in Table 4.2.

Table 4.2: Mechanical alloying parameters.

| **Parameter** | **Details** |
|---|---|
| RPM | 325 |
| Grinding media | Hardened steel balls (dia - 10 mm) |
| Ball to powder ratio (BPR) | 10:1 |
| Atmosphere | Purified nitrogen |

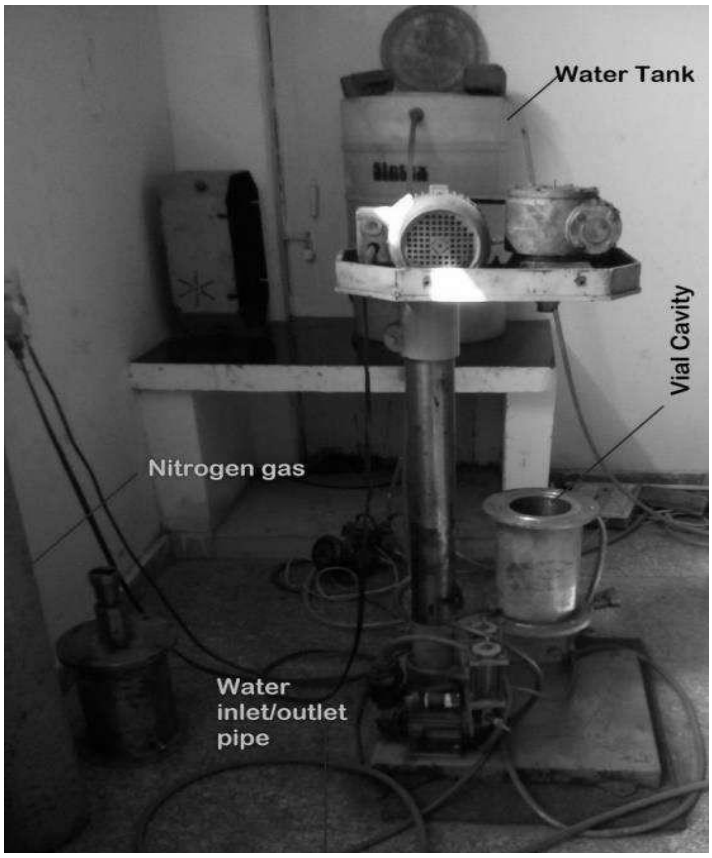


Fig 4.2: Attrition mill.

### 4.2.2 Vacuum degassing

The mechanically alloyed powder was degassed for 2 h in a vacuum of $10^{-2}$ torr at 200 $^{o}$C in a vacuum oven HINDHIVAC Model VO-13. The degassing was done to remove the PCA, adsorbed moisture, entrapped gases, and the volatile impurities.

## 4.3. MA Powder Characterization

### 4.3.1. Morphology

The MA powders prepared were studied using FEI-NOVA NANO SIM-450 SEM to know morphology.

### 4.3.2 XRD studies

The crystallite size and the phases present in the MA powder samples were analyzed using Panalytical X Pert Pro X-ray diffraction unit with Cu Kα radiation (kα =0.1542nm).

### 4.3.3 Transmission electron microscopy

Transmission electron microscopy (TEM), using Tecnai 20, FEI was done to study the microstructural changes in the samples. The MA powder samples were dispersed in ethanol and ultrasonication was done for 1 hr in order to get well dispersion of particles. These dispersed particles were then spread on a copper grid and allowed to dry completely.

### 4.3.4 X-ray photoelectron spectroscopy

X-ray Photoelectron Spectroscopy (XPS) was performed using Omicron nanotechnology X-ray Photoelectron Spectrophotometer. XPS was done to analyse the form in which carbon is getting dissolved in the Ni lattice in order to form SSSS.

## 4.4 Differential Scanning Calorimetry

Differential Scanning Calorimetry (DSC) was performed using NETSZH DSC equipment. About 10 mg of sample was taken in a ceramic crucible and DSC was performed in an argon atmosphere on degassed MA powder to identify graphite-diamond transformation temperature. The heating and cooling rate were 5 $K.min^{-1,}$ and the temperature range was 20°C to 1300°C.

## 4.5. Consolidation of MA Powders

### 4.5.1 Hot-pressing

The MA powder was consolidated by hot pressing at 1000$^{o}$ C under a pressure of 10 MPa. Samples of 10mm (D) X 5mm (H) size were prepared using cylindrical graphite die.

### 4.5.2 Spark plasma sintering

The MA powder was consolidated by spark plasma sintering using Dr Sinter Unit (SPS-625, SPS Syntex Inc., Japan) as shown in Fig. 4.3, under a pressure of 10 MPa at 1000 $^{\circ}$C for 15 min. Samples of 20mm (D) X 5mm (H) were prepared.

Fig 4.3: Dr Sinter spark plasma sintering unit.

## 4.6 Raman Spectroscopy of Consolidated Samples

Raman spectroscopy of consolidated samples was done to know the formation of diamond phase during the consolidation.

Raman spectroscopy of consolidated samples was done withALRIX, STR-500 confocal type Raman spectroscope. For hot pressed, there is no need for sample preparation required.

## 4.7. Extraction of Diamond Powders

The consolidated samples were dissolved in the boiling mixture of sulphuric acid and nitric acid (3:1 ratio). The filtrate mixture obtained was washed with distilled water and dried. Carbonaceous material from the diamond surfaces was removed by heating the powder at 250$^{o}$ C in an oxidative atmosphere.

## 4.8. Characterization of Diamond Powders

The diamond powders thus obtained were characterized for their surface morphology by FE-SEM. Raman Spectroscopy of the powders was carried out. In order to know the particle size and particle size distribution, the powders were also characterized by nanoparticle analyser (Malvern Zetasizer ZSP). The Fourier transform infrared (FTIR) spectra of the MA and diamond powders were determined on KBr pellets.

### 4.8.1. Particle size analysis

In order to know the particle size and size distribution, the extracted diamond powders were also characterized by nanoparticle analyser, Malvern Zetasizer ZSP. The diamond powder particles were first dispersed in ethanol and ultrasonication was done for 15-20 min. The powder sample was then put in the particle size analyser. The laser beam was allowed to fall on the particles and light scattered by them was then collected. The angle of diffraction is proportional to the particle size.

### 4.8.2. Fourier transform infrared spectroscopy

The Fourier transform infrared (FTIR) spectroscopy was done to identify chemical bonds present in the diamond powder by producing an IR spectrum. This

high-resolution spectrum produces a characteristic fingerprint that can be used to screen and scan samples. For performing FTIR spectroscopy Perkin Elmer FT-IR Spectrum 2 was used.

FTIR of the MA and diamond powders were determined on KBr pellets. The sample was ground up with KBr and compressed under vacuum for 2 min, the pellets obtained were scanned from 4000 to 400 $cm^{-1}$ on a Perkin-Elmer FTIR spectrophotometer.

# 5. Results and Discussion

## 5.1. Mechanical Alloying

During the studies, it was observed that 5 wt.% $C_{gr}$ and 10 wt.% $C_{gr}$ formed solid solution with nickel after 4 and 9 hrs respectively (Fig 5. 2 (a)). Then detailed studies were performed on dissolution of 15wt.% $C_{gr}$ in the nickel lattice.

### 5.1.1. Morphology

The progressive changes in the morphology of the powder particles with increasing milling duration are shown in Fig 5.1. During MA, powder particles experience repeated cold welding, deformation and fracture which in turn changes the shape and size of the powder particles. As milling progresses, the nickel powder particles become finer. The graphite particles that are in the flaky form can no longer be seen in SEM micrograph after milling for 15 h indicating submerging of graphite in the nickel lattice resulting in graphite encapsulated irregular shaped whereas received nickel (Fig. 5.1(g)).

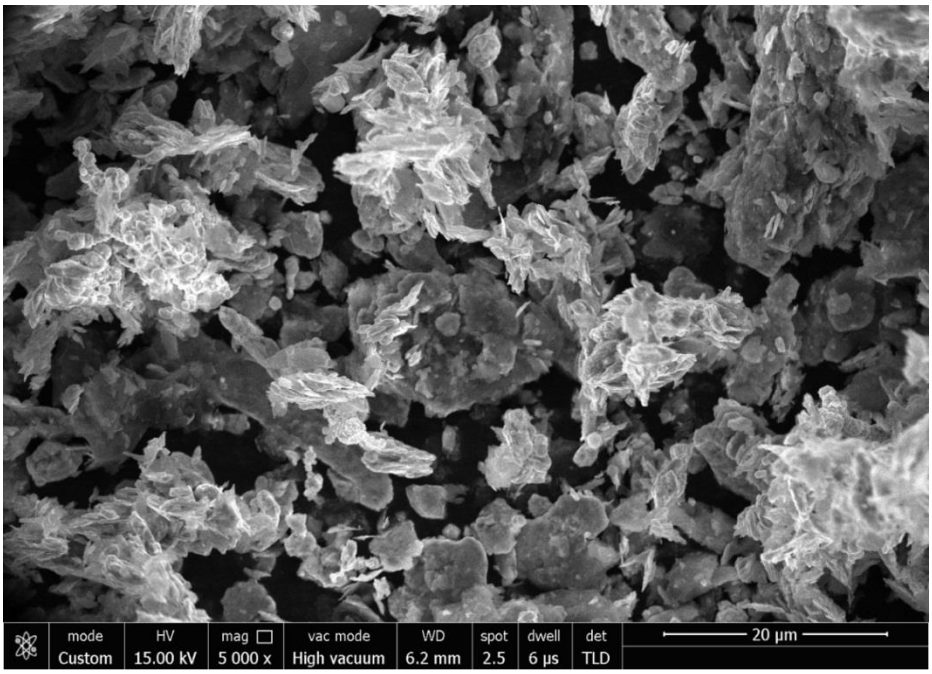
mode
Custom
HV
15.00 kV
mag
5 000 x
vac mode
High vacuum
WD
6.2 mm
spot
2.5
dwell
6 µs
det
TLD
20 µm

(a) 2.5 h

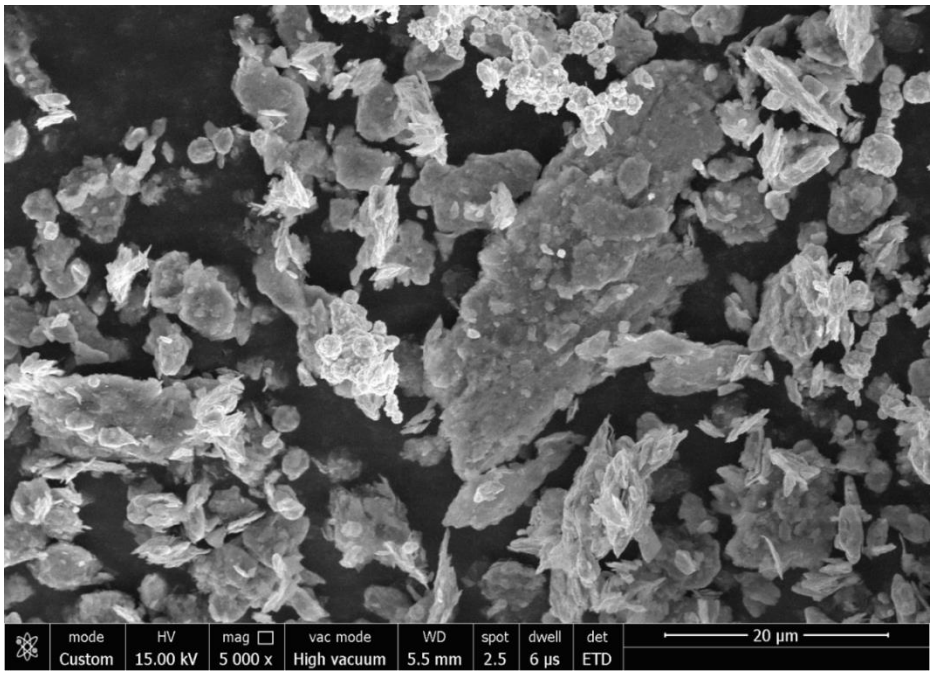
mode
Custom
HV
15.00 kV
mag
5 000 x
vac mode
High vacuum
WD
5.5 mm
spot
2.5
dwell
6 µs
det
ETD
20 µm

(b) 5 h

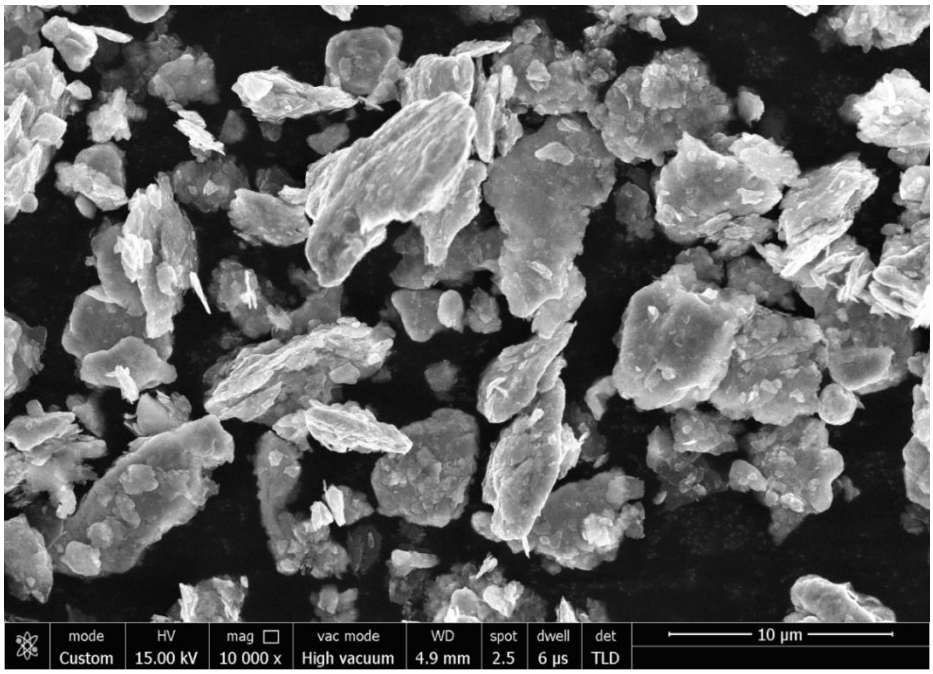
mode
Custom
HV
15.00 kV
mag
10 000 x
vac mode
High vacuum
WD
4.9 mm
spot
2.5
dwell
6 µs
det
TLD
10 µm

(c) 7.5 h

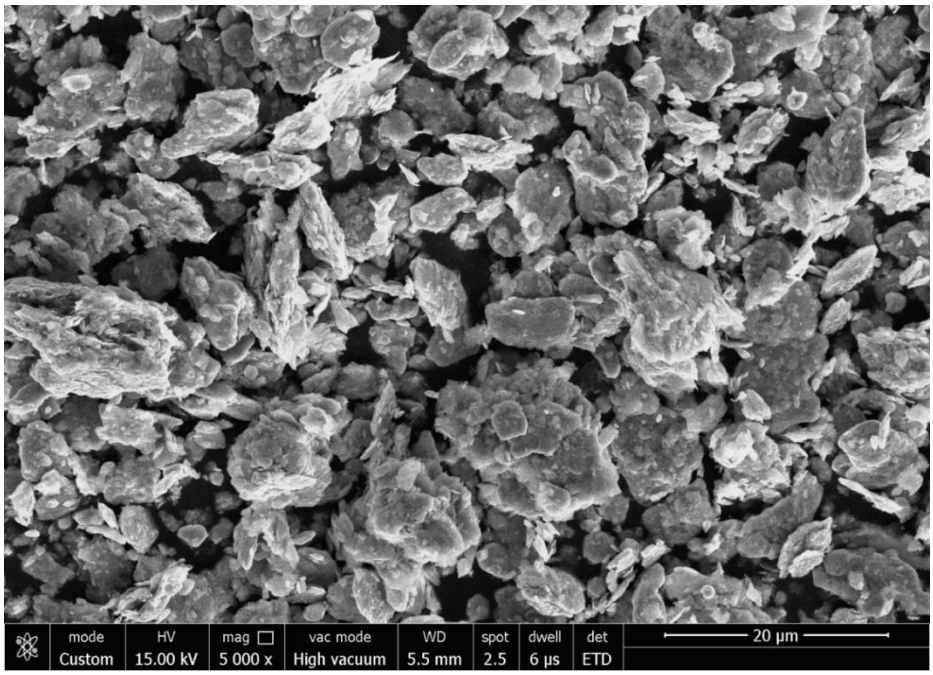
mode
Custom
HV
15.00 kV
mag
5 000 x
vac mode
High vacuum
WD
5.5 mm
spot
2.5
dwell
6 µs
det
ETD
20 µm

(d) 10 h

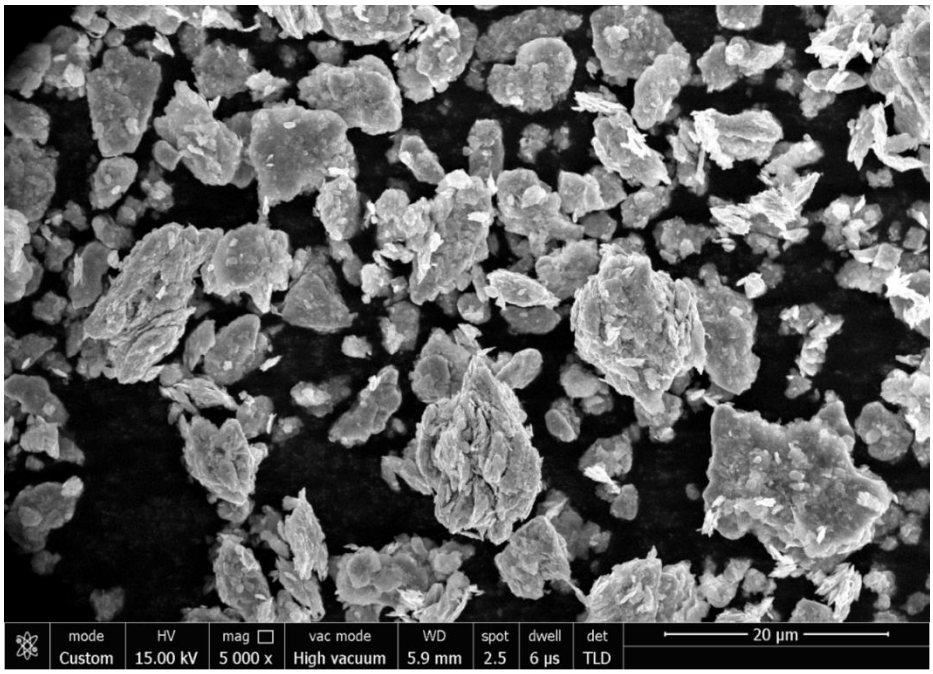


(e) 12.5 h

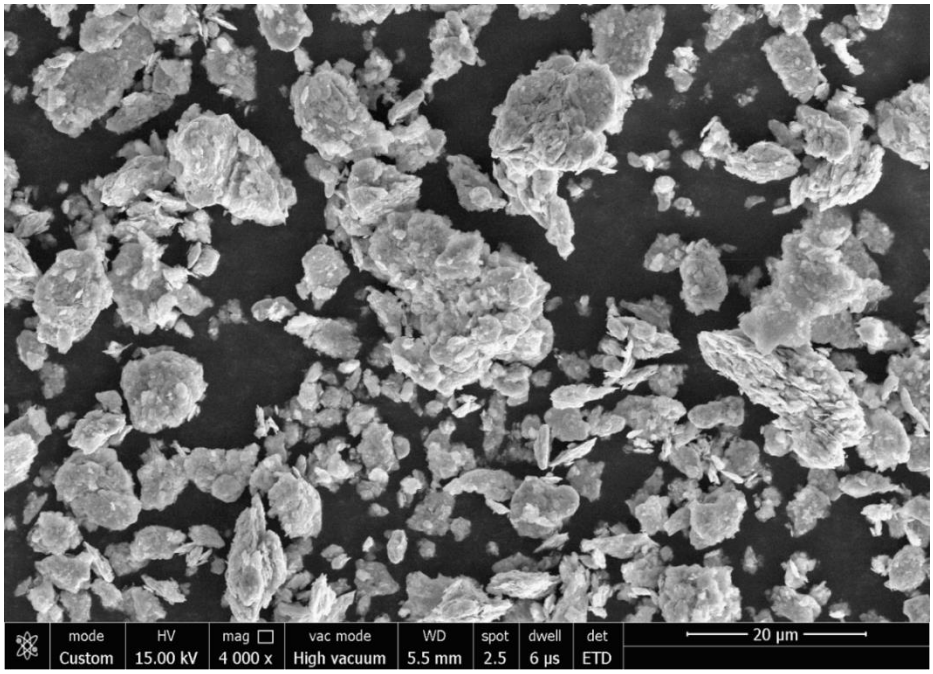


(f) 15 h

Fig 5.1: SEM micrographs of MA powders for different milling duration

### 5.1.2. XRD analysis

XRD patterns of MA powders (Fig. 5.2) confirm the increasing dissolution of graphite flakes within the nickel particle during milling.

Peaks at 44.50°, 51.84° and 76.38° 2θ values represent (111), (200) and (220) planes of nickel, respectively; while the peak at 25.60° 2θ value represents (002) plane of graphite. It can be observed that as the milling proceeds, the peak corresponding to (002) plane of graphite starts disappearing and is no more detectable after 15 h of milling indicating complete dissolution of graphite in the nickel lattice. Shifting of nickel peak (111) towards lower diffraction angle, with milling duration is in confirmation of the progressive dissolution of graphite in nickel. No amorphous broadening is seen in the XRD patterns of MA powders due to high energy processing. Rather, the high energy processing expedites the diffusion of graphite atoms in nickel lattice thus avoiding the problem of amorphization of graphite as in other processes [38]. The carbon content in the solid solution in nickel lattice can be estimated by using the following equation (4) [184];

$$a=0.35240+ 0.00080 (at.\ \%C)\ nm \qquad \ldots\ldots\ldots\ldots\ldots (4)$$

where ‘a’ is lattice parameter.

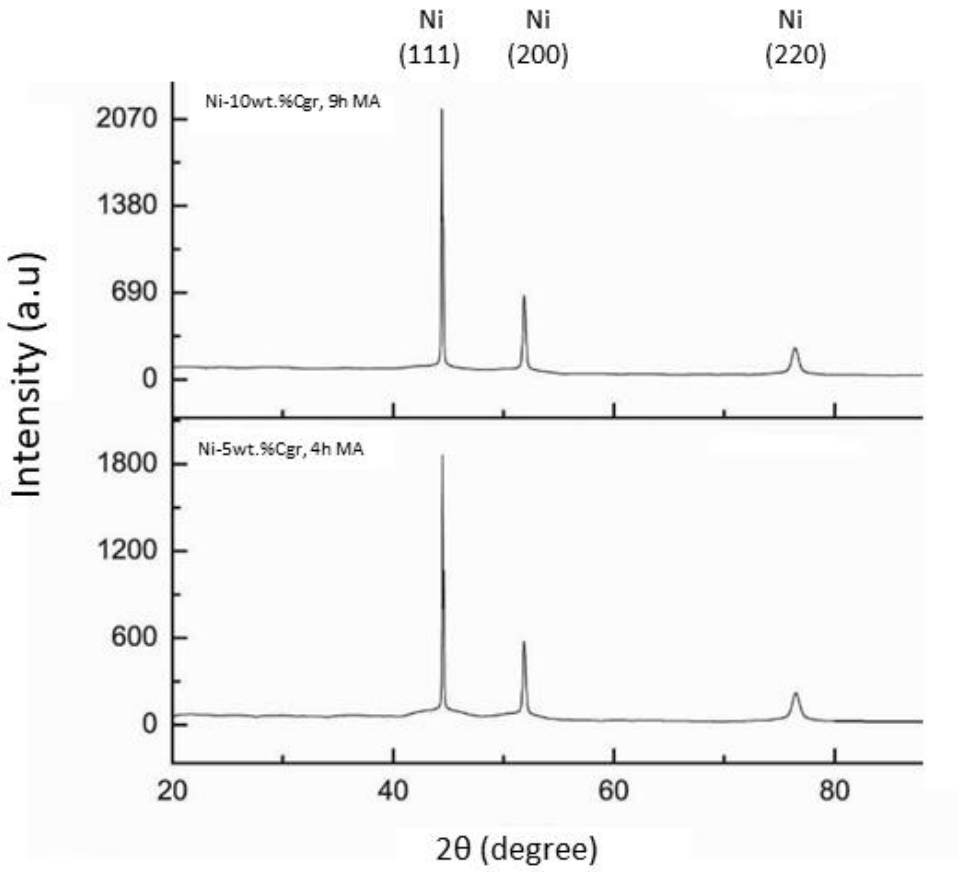
Ni
(111)
Ni
(200)
Ni
(220)
Ni-10wt.%Cgr, 9h MA
2070
1380
690
0
Ni-5wt.%Cgr, 4h MA
1800
1200
600
0
Intensity (a.u)
20
40
60
80
2θ (degree)

(a)

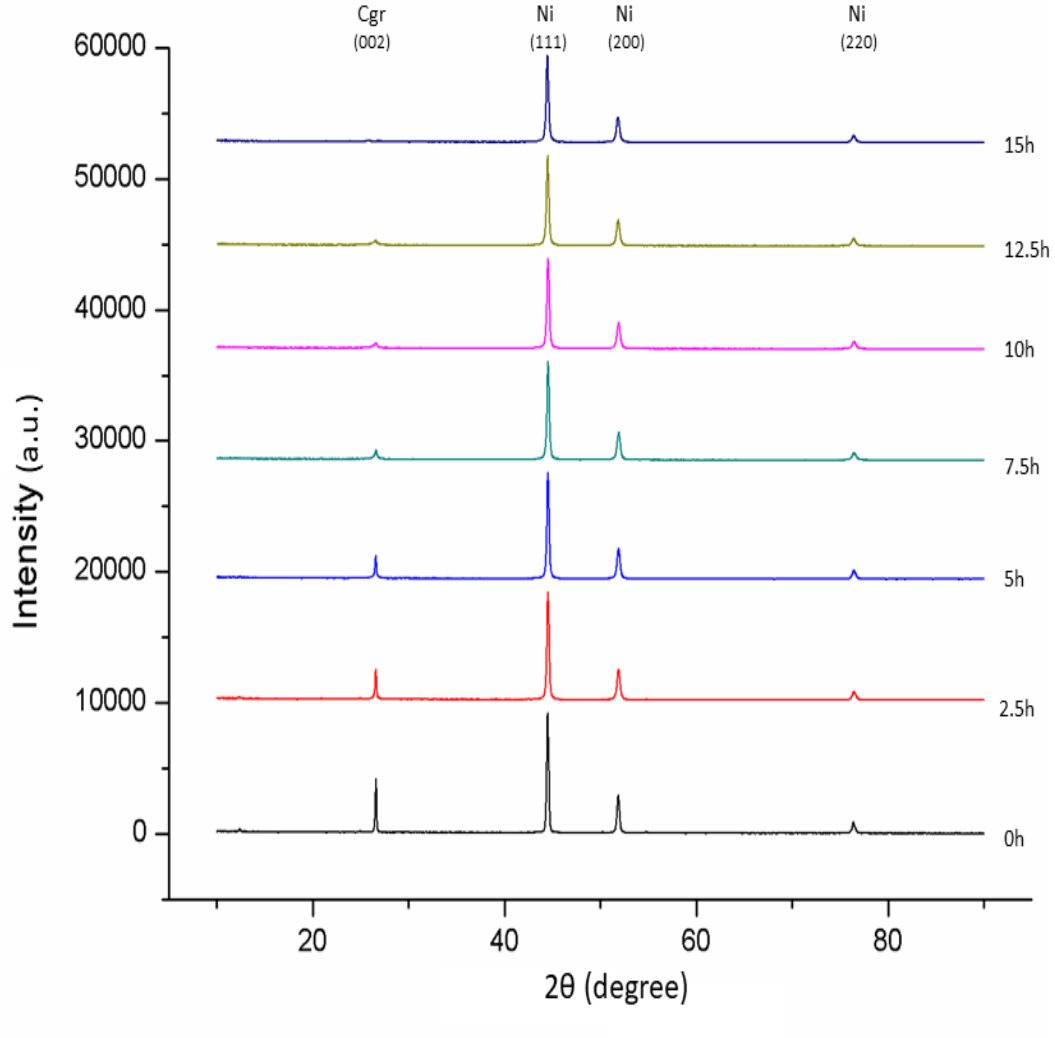


(b)

Fig 5.2: XRD pattern of (a) Ni-x wt.% $C_{gr}$ (x= 5, 10 )milled for 4 h and 9 h, respectively (b) Ni-15wt%$C_{gr}$ milled for different milling duration

The change in lattice parameter with milling duration is shown in Fig.5.5. After 15h MA, the carbon content in solid solution is estimated to be about 1.7wt% (7.8 at.%). This value is about eight times more than the corresponding value (0.21wt.%; 1 at. %) reported in the literature [40]. Also, the formation of $Ni_3C$ phase didn't take place in the present case which impairs the dissolution of graphite in nickel. It is an attribute of high energy milling, which made the kinetics of the diffusion process faster enough not to provide sufficient time for the formation of $Ni_3C$. It should be emphasized that during high energy milling a large number of dislocations are created

in the Ni lattice, resulting in the nanostructured lattice having much more grain boundary area. During milling, the graphite atoms must have diffused to interstitial positions, along with the dislocation edges and at the grain boundary regions. It is also corroborated by the TEM images of the as-milled powder (Fig. 5.6).

***Crystallite size***

Nickel peak broadening can be seen in Fig. 5.2. Broadening in nickel peak results both due to reduced grain size and/or by induced lattice strain. The crystallite size is calculated by Scherrer's equation (5), given as:

$$d = \frac{k\lambda}{\beta\, Cos\theta} \qquad \text{…….. (5)}$$

where d-- average grain size, k-- Scherrer constant (k=0.9), λ-- X-ray wavelength, β-line broadening at half the maximum intensity (FWHM) and θ- Bragg's angle (in degrees) [185].

The variation in nickel crystallite size during milling, as calculated by XRD measurements is shown in Fig. 5.3. The grain size of nickel decreases with increasing milling duration and reduces to a minimum value of about 43 nm after milling for 15h. Powder particles undergo intense plastic deformation during high energy milling. The grain size decreases with increasing milling duration which can be comprehended by the creation of shear bands, which possesses a large number of dislocations, in the nickel lattice during the high energy milling process. At some particular dislocation density because of thermoplastic imbalance, crystal breaks down into the subgrains [186, 187]. Once the grains reach to nano level, further refinement requires very high stresses for dislocation creation and movement. This hinders further plastic deformation and the grain refinement. In the initial stage of the grain refinement (curve AB) nickel particles get impacted at higher strain rate and alloying of the graphite atoms takes place at the surface. Once the nickel surface gets completely alloyed with graphite the deformation process becomes relatively slow as graphite acts as a lubricant (curve BC). Further, during MA processing when the graphite from

surface diffuses deep into the Ni lattice the impact force on Ni surface increases to some extent resulting in little expedite of the crystal fracturing process (curve CD) (The nature of the curves in Fig. 5.4 & 5.5 can also be understood in this light).

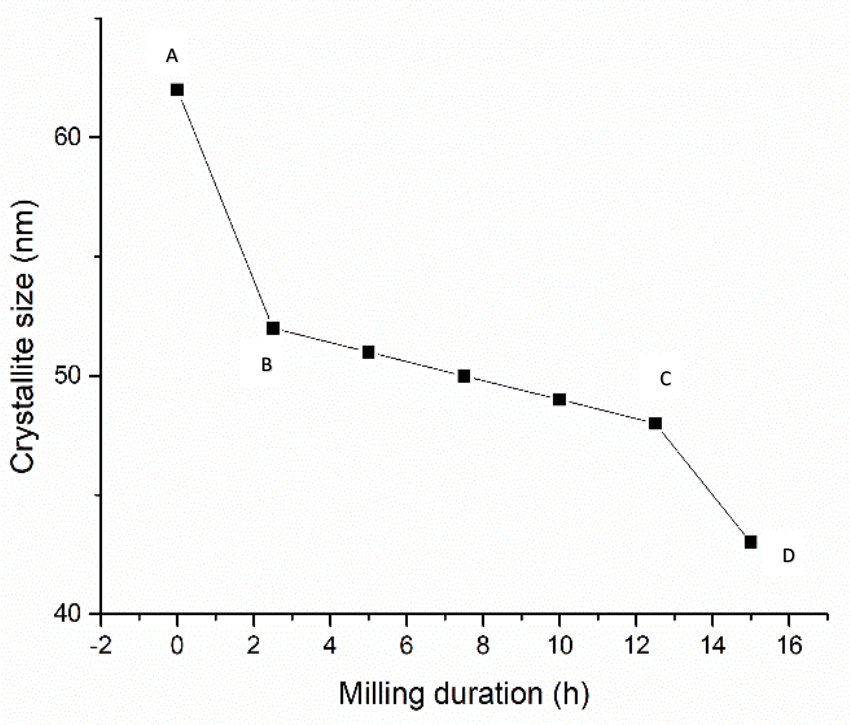


Fig 5.3: Variation in crystallite size with milling duration in Ni-15 wt.% $C_{gr}$ powder

***Lattice strain***

To evaluate lattice strain from XRD data a plot of β Cos θ Vs Sin θ was made, the slope of which corresponds to the contribution of lattice strains [185]. The effect of milling duration on lattice strain is shown in Fig. 5.4. With the increase in milling duration, the lattice strain increases and reaches the level of 0.3%. This increase in lattice strain is due to high plastic deformation and dissolution of graphite in nickel lattice. The extension of the solid solubility limit of graphite in nickel lattice is associated with the production of nanocrystalline structure and these high internal lattice strains.

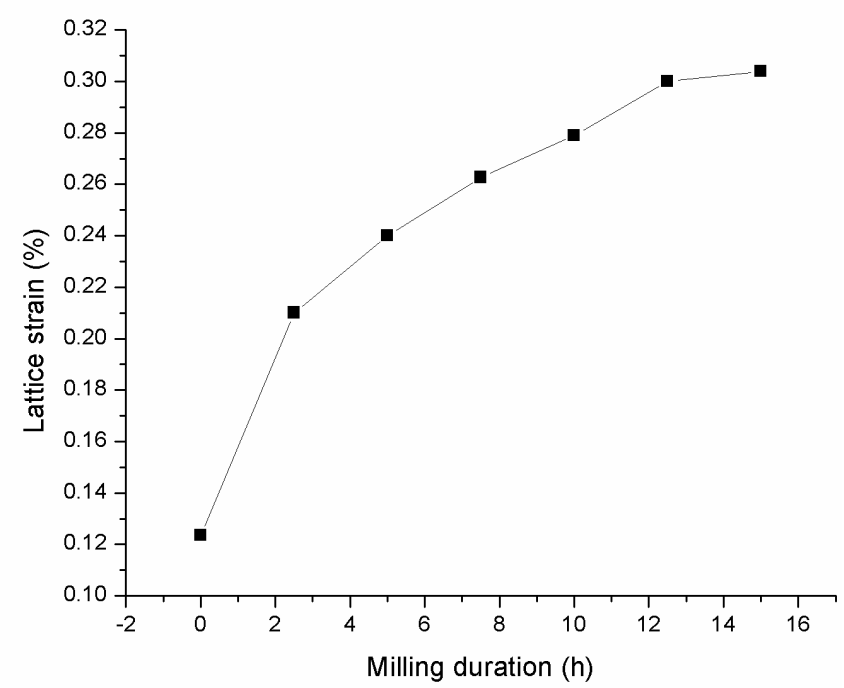


Fig 5.4: Effect of milling duration on the lattice strain in Ni-15 wt.% $C_{gr}$ powder

***Lattice parameter***

Fig 5.5 shows the effect of milling duration on the nickel lattice parameter. The increase in lattice parameter is associated with the dissolution of graphite in nickel lattice and the strains induced within the lattice due to plastic deformation of powder particles under shear force applied by the balls (grinding media). It may be concluded that the solid solubility of graphite in nickel has approached near to its maximum possible limit.

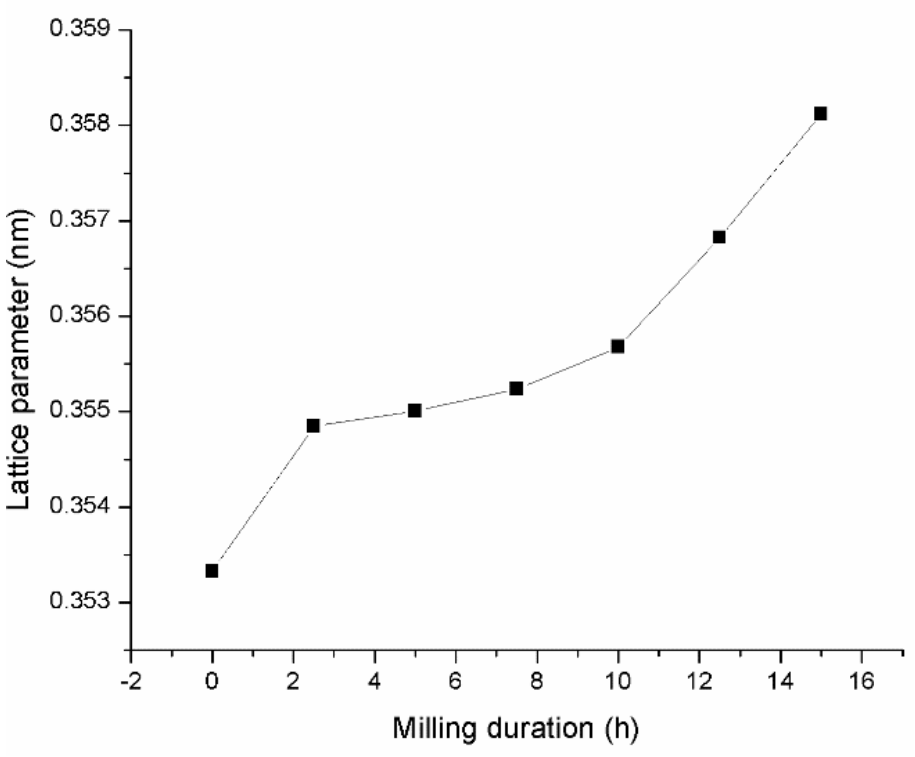


Fig 5.5: Variation of nickel lattice parameter with milling duration in Ni-15 wt.% $C_{gr}$ powder

***Dislocation density***

Fig 5.6 shows the effect of milling on the dislocation density of nickel matrix. The dislocation density in the Ni matrix was calculated by equation (6) [185];

$$\rho_D = 2\sqrt{3}\frac{\langle \varepsilon^2 \rangle^{1/2}}{D \times b}, \qquad \text{..... (6)}$$

where,

$\rho_D$ is dislocation density, ε is lattice strain, D is grain size and b is Burger's vector

During milling, severe plastic deformation imposed by collisions of balls on powder particles results in increased concentration of dislocations which in turn shows increment in the dislocation density from .022 x $10^{16}/m^2$ to 0.057 x $10^{16}/m^2$. As milling proceeds, following the process of relaxation due to restricted movement of the dislocations, larger grain breaks into smaller ones, resulting in massive decrease in dislocation density. After this relaxation, further increase in milling duration increases the dislocation density to 0.0797 x $10^{16}/m^2$.

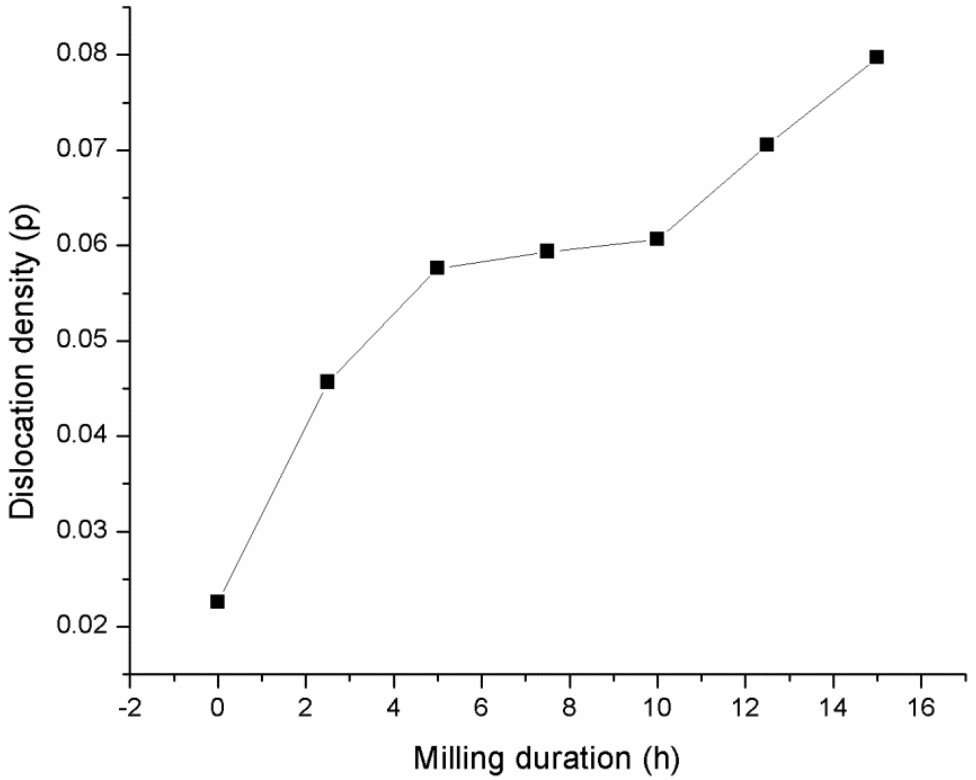


Fig 5.6: Variation of dislocation density with milling duration in Ni-15 wt.% $C_{gr}$ powder

### 5.1.3 TEM studies

Fig 5.7 shows TEM micrographs of as-received and as-milled powder samples. Fig 5.7(a) shows separate nickel and graphite particles along with their SAED patterns showing polycrystalline and monocrystalline phases, respectively. With the increasing milling duration, the graphite atoms start diffusing into nickel lattice which can be seen very clearly in Fig 5.7 (b, c, d). After 15 h of milling (Fig 5.7 (d)) no free

graphite particles were seen. SAED pattern of Fig. 5.7(d) also confirms the absence of free monocrystalline graphite phase.

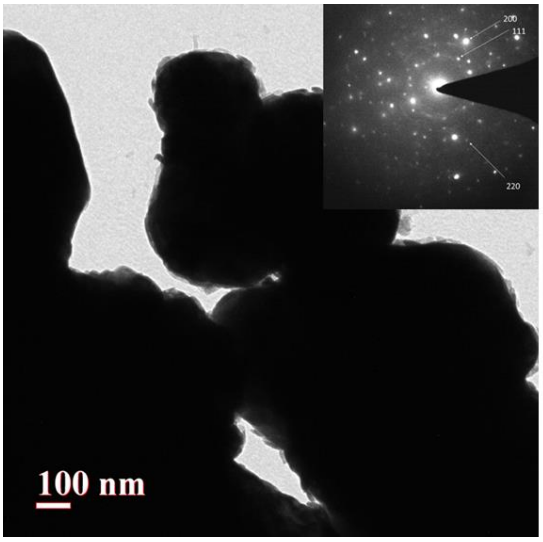


(i) Nickel

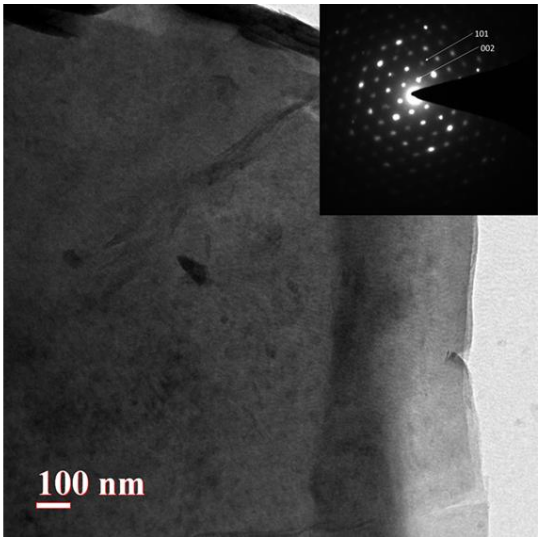


(ii) Graphite

(a) as- received

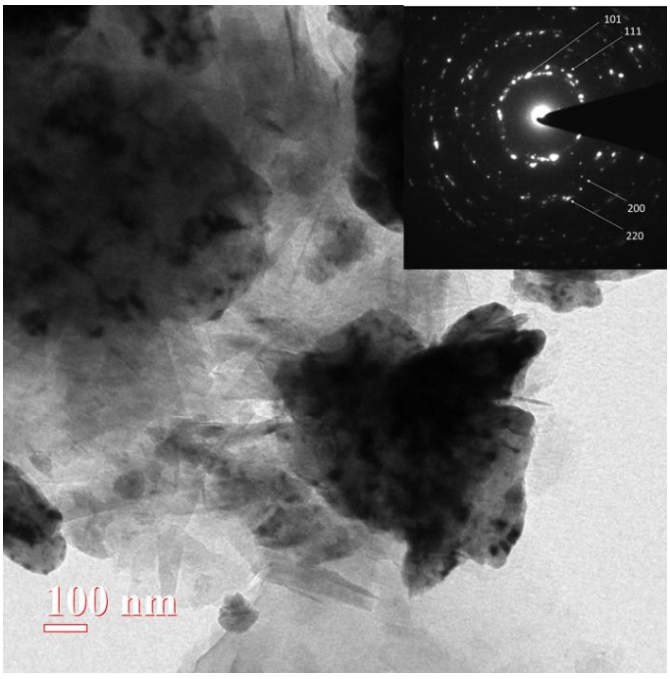


(b) 5h

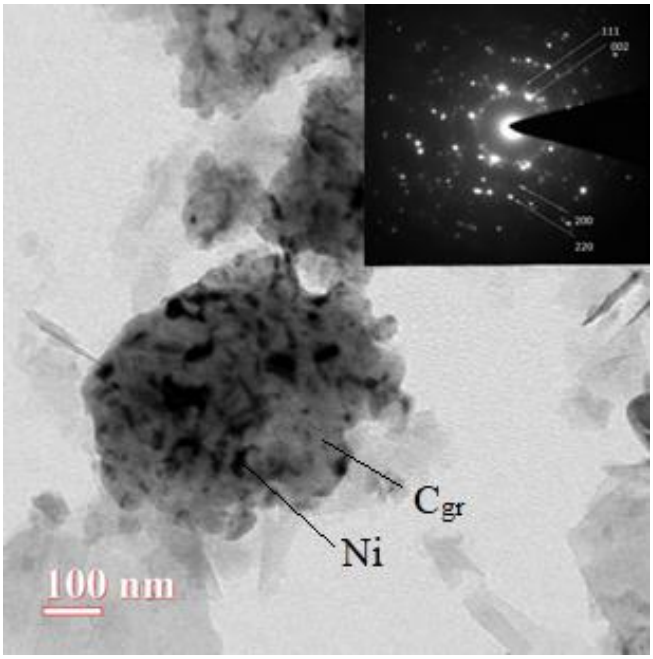


(c) 10h

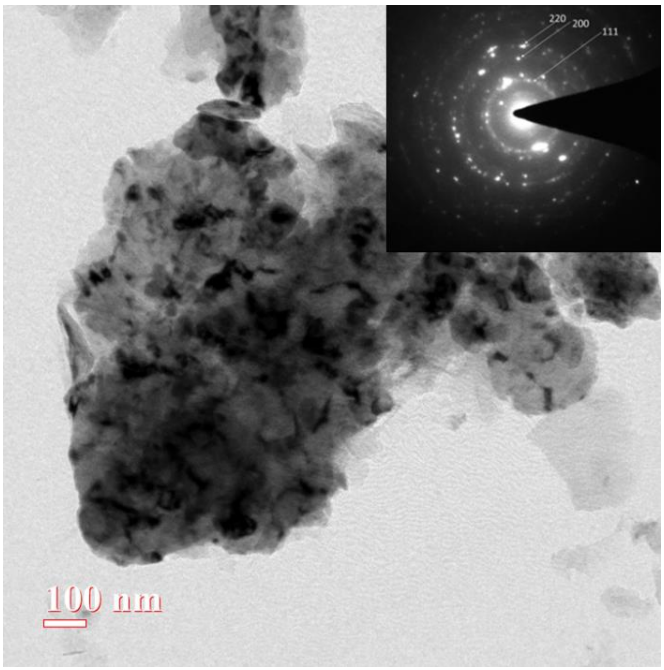


(d) 15 h

Fig. 5.7: TEM micrographs of as-milled powder

The HRTEM image of 15h milled powder (Fig 5.8 (b)) showing the presence of the different coherent planes, also confirms the complete dissolution of graphite in nickel lattice. No overlapped planes are visible in the case of as-received samples (Fig 5.8(a)). These TEM images are well-corroborated with the XRD results.

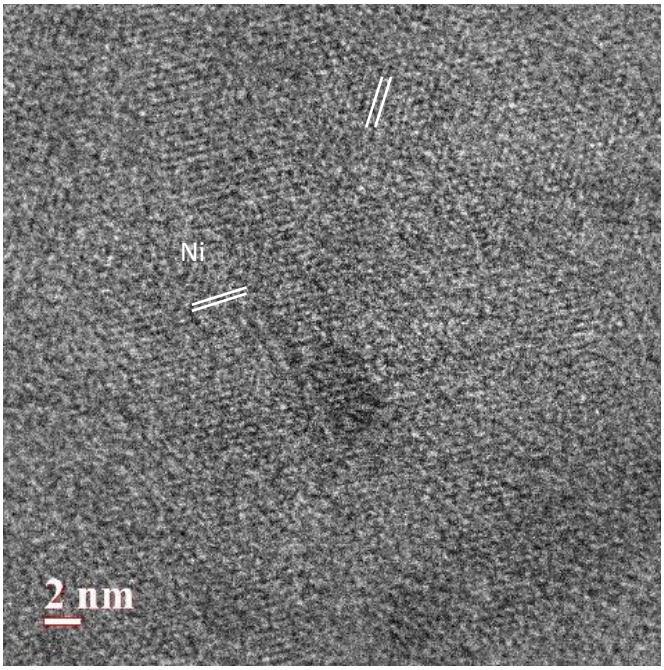


(i) Nickel

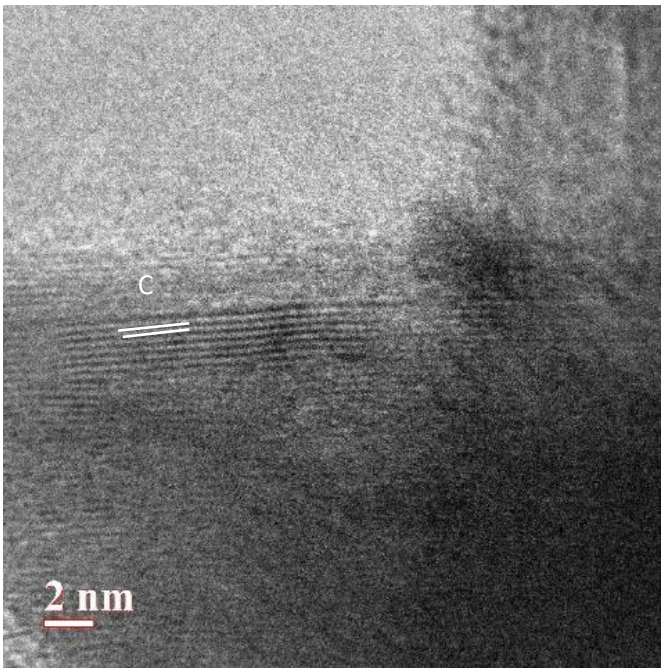


(ii) Graphite

(a) as-received powder

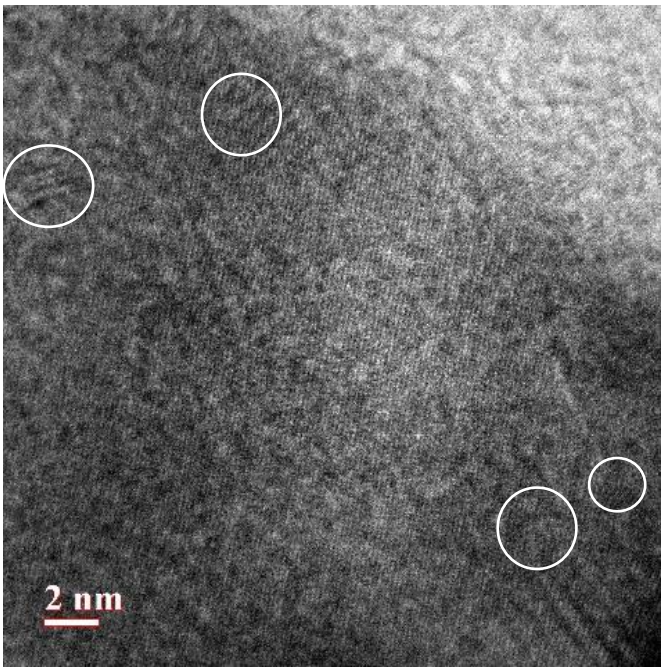


(b) 15 h

Fig 5.8: HRTEM images of (a) as received powders (b) after milling for 15 h

### 5.1.4. X-ray photoelectron spectroscopy

XPS was carried out to know the carbon atomic bindings in 15h-milled Ni-15 wt.% $C_{gr}$ powder. The analysis of the XPS of C1s spectra shows that the carbon peak consists of two peaks as shown in Fig. 5.9. The peak with the highest binding energy, i.e. 286 eV represents the formation of carbon dioxide while the peak with the binding energy 284.4 eV is due to C-C $sp^2$ hybridization [188]. The presence of C-C $sp^2$ peaks suggests the presence of graphite and graphene layers in the sample. It is clear from the spectra that during mechanical alloying graphite that is made up of various graphene layers connected via Van der Waal forces get separated and results in the formation of the SSSS occupying the space within the Ni crystal lattice.

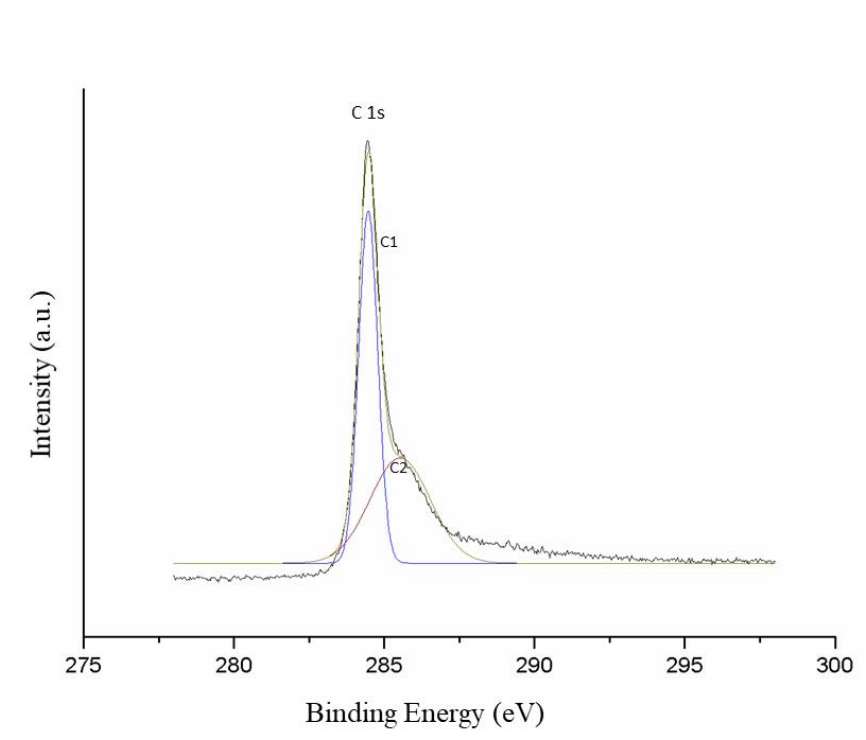


Fig 5.9: XPS spectra of Ni-15 wt.% $C_{gr}$ milled for 15 h

## 5.2. Differential scanning calorimetry

The DSC curve of the supersaturated solid solution is shown in Fig. 5.10. It indicates that milled powder has undergone an exothermic reaction at 1084 ºC. During the DSC analysis, the nickel lattice got annealed by releasing the heat energy and precipitation of excessive graphite dissolved started at this temperature. This could be a good guideline for the selection of hot pressing/ SPS temperature.

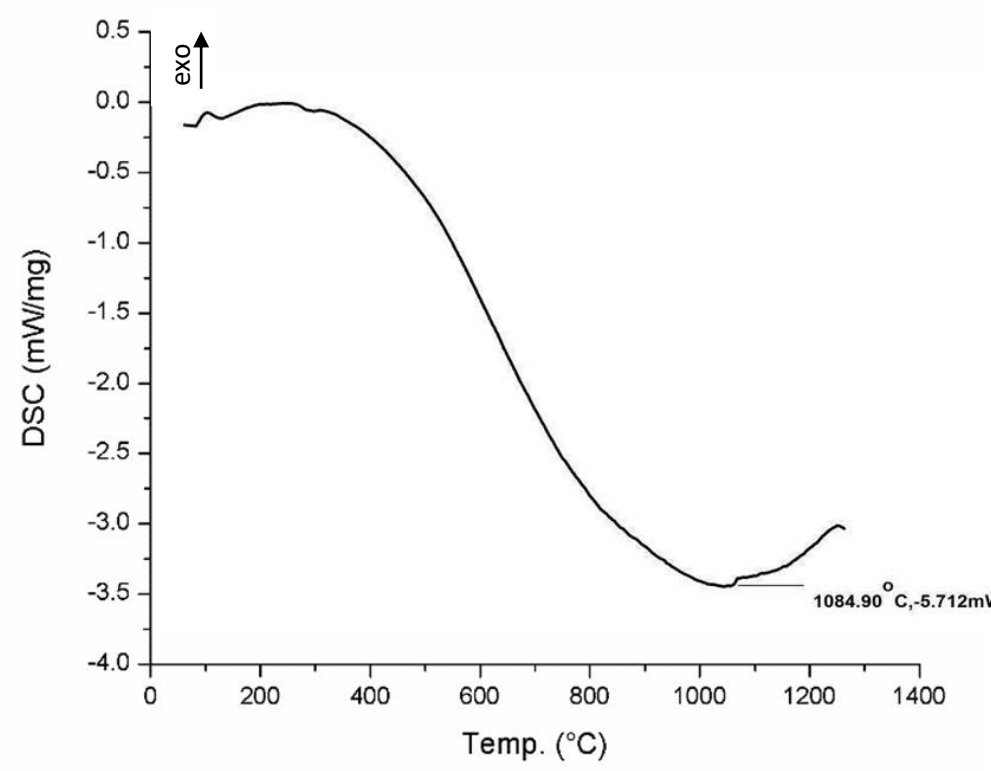


Fig 5.10: DSC curve of 15 h milled powder

## 5.3. Analysis of Consolidated Samples

### 5.3.1. Raman spectroscopy

The formation of diamond in consolidated samples was confirmed by Raman spectra obtained (Fig. 5.11). The peaks at 1334 $cm^{-1}$ and 1333 $cm^{-1}$ obtained confirms the formation of diamond during HP and peaks at 1347 $cm^{-1}$ and 1341 $cm^{-1}$ also confirms the formation of diamond [178]. The peaks in case of SPS have marginally shifted towards the higher wavenumber ($cm^{-1}$), which indicates formation of nanodiamond. This may be due to excessive heat production during plasma heating period, which in turn must have produced large number of diamond nuclei, growth of which took place during the Joule heating period, resulting in nanodiamond formation. The peaks at 1586 $cm^{-1}$corresponds to graphite peaks while the peaks at 2684 $cm^{-1}$ and 2725 $cm^{-1}$ for HP and SPS processes, respectively, corresponds to G' band. The D-peak is more prominent in doped samples due to readily available seed nuclei which facilitated the diamond growth. It is also supported by an increase in the $I_D/I_G$ ratio (Table 5.1).

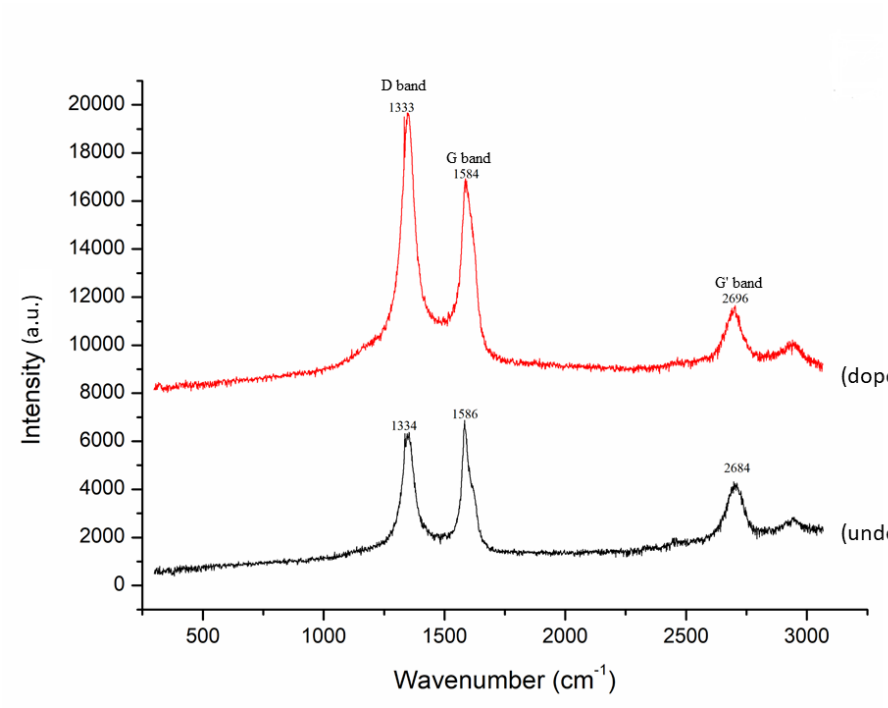


(i) Hot pressed

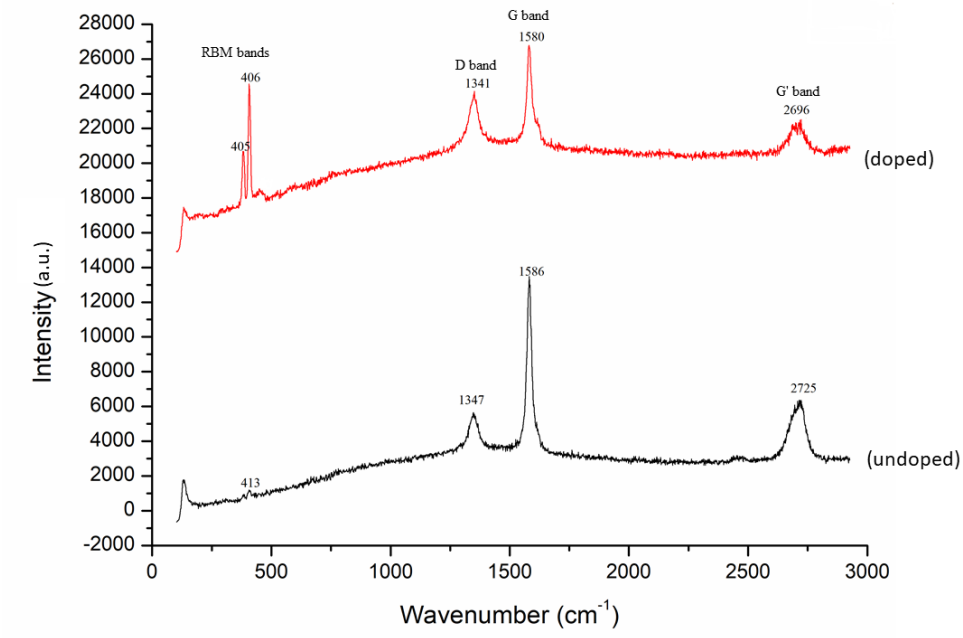


(ii) SPSed

Fig 5.11: Raman spectra of Ni-$C_{gr}$ consolidated samples.

Table 5.1: Comparison of $I_D/I_G$ peak ratio

| S. No | Sample | $I_D/I_G$ | |
|---|---|---|---|
| | | **Hot pressed** | **Spark plasma sintered** |
| 1 | Ni-15wt% $C_{gr}$ | 0.68 | 0.41 |
| 2 | Ni-15wt% $C_{gr}$ (doped) | 0.76 | 0.78 |

High energy milling of Ni-15wt.% $C_{gr}$ resulted in the dissolution of graphite as interstitial, along with the dislocation lines in the form of chains, and at the nano-grain boundaries as discussed in the Section 5.1.2. During high energy milling, high dislocation density and strains were created in the nickel lattice, and also the activation of graphite took place by reducing its particle size. All these factors resulted in an increase in catalytic activity in the system many folds. During hot pressing/ SPS of the SSSS, the applied pressure and the temperature forced the dissolved graphite to squeeze out. During this squeezing, the graphite and the nickel came in intimate contact to the atomic proximity and transformation of hexagonal graphite ($sp^2$) to cubic diamond ($sp^3$) happened. The mechanical activation of the nickel lattice as well as of the graphite made the transformation possible at a lower pressure of 10 MPa and temperature 1000 $^oC$, as compared to the HPHT process.

Also, presence of radial breathing mode (RBM) bands in spectra of SPSed samples (Fig. 5.11 (ii)) indicate the formation of single-walled carbon nanotubes (SWCNTs), which have quite likely formed due to the successful efforts of the graphene sheets to achieve the stable state by lowering the activation energy by joining the edges. The applied pressure and fast heating of SPS must have been a helping factor in this process. The diameter of these SWCNTs appears to be smaller than 1nm as indicated by the shift of RBM bands towards the higher wavenumber ($cm^{-1}$) [189]. The schematic of the graphite transforming into various carbon allotropes is shown in Fig. 5.12.

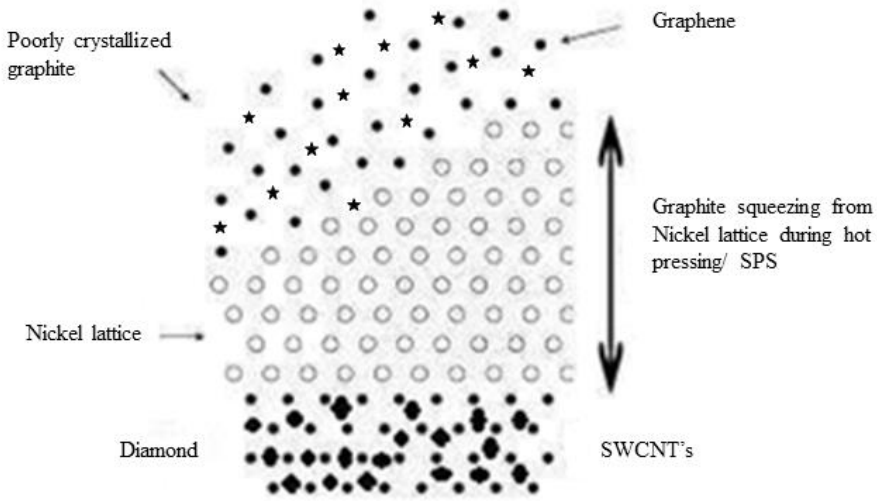


Fig 5.12: Schematic of the graphite squeezing from nickel lattice during hot pressing/ SPS of SSSS

## 5.4. Analysis of Diamond Powder

### 5.4.1. Morphology

SEM micrographs of the extracted diamonds are shown in Fig. 5.13. It can be seen that the diamond particles, in both the cases, are aggregates of irregularly shaped crystallites.

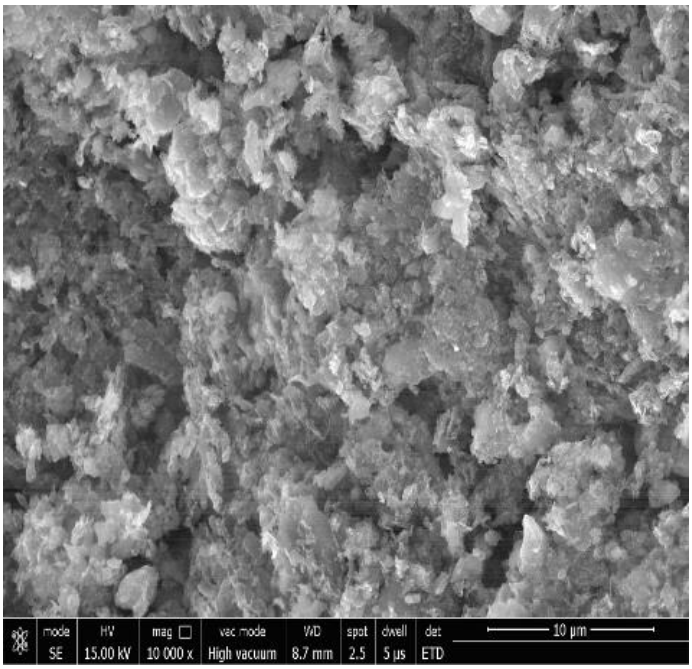


(i) HP

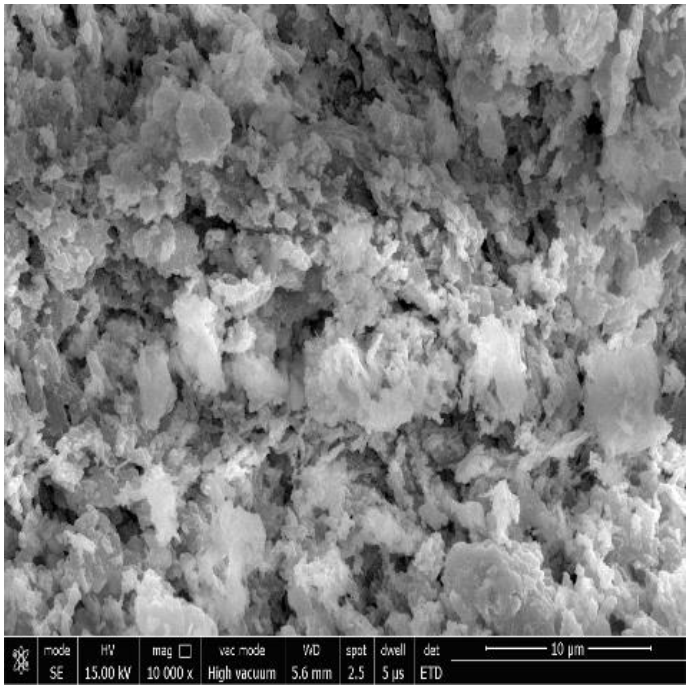


(ii) SPS

Fig 5.13: SEM micrographs of extracted diamond powders

## 5.4.2. Particle size distribution

Particle size distribution curves obtained for diamond powders obtained by HP/ SPS of SSSS are shown in Fig. 5.14. Average particle size in diamond powders obtained from HP and SPS samples are 3.8 µm and 2.0 µm, respectively while in the case of doped SSSS the average particle size is 3.1 µm and 0.81 µm, respectively. This smaller particle size in the cases of doped SSSSs is an attribute of the presence of doped nanodiamond particles which acts as nuclei resulting in smaller diamond particles. In the absence of dopant, first, the nuclei are formed which then grow in all directions thereby forming larger size diamond particles.

It can be also be seen (Table 5.2) that the HP diamond particles are of micron range while those of SPS are of nano range, having a semi-log normal distribution.

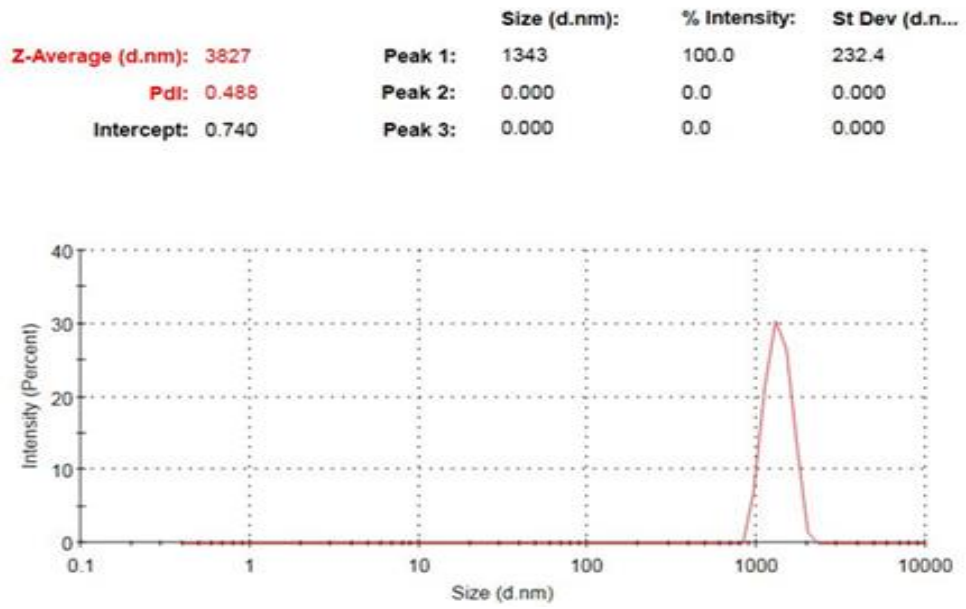


(a) HP undoped

| | | | Size (d.nm): | % Intensity: | St Dev (d.n... |
|---|---|---|---|---|---|
| Z-Average (d.nm): | 3137 | Peak 1: | 1768 | 100.0 | 189.7 |
| PdI: | 0.297 | Peak 2: | 0.000 | 0.0 | 0.000 |
| Intercept: | 0.948 | Peak 3: | 0.000 | 0.0 | 0.000 |

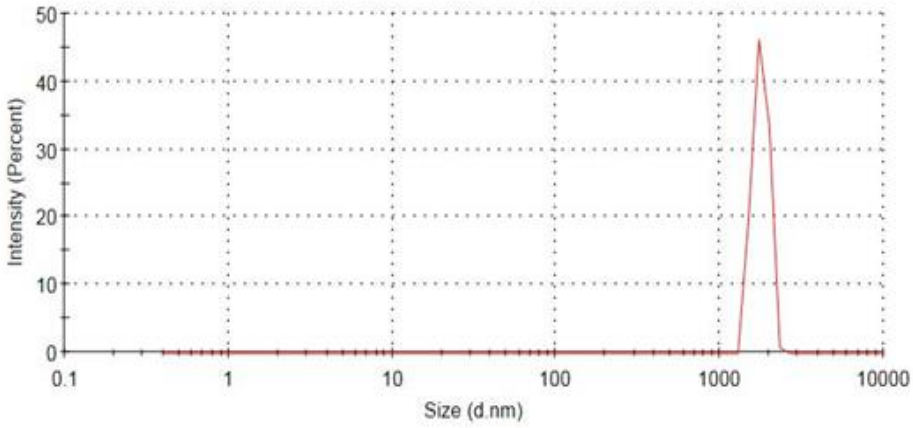


(b) HP doped

| | | | Size (d.nm): | % Intensity: | St Dev (d.n... |
|---|---|---|---|---|---|
| Z-Average (d.nm): | 2063 | Peak 1: | 1601 | 100.0 | 219.5 |
| PdI: | 0.166 | Peak 2: | 0.000 | 0.0 | 0.000 |
| Intercept: | 0.885 | Peak 3: | 0.000 | 0.0 | 0.000 |

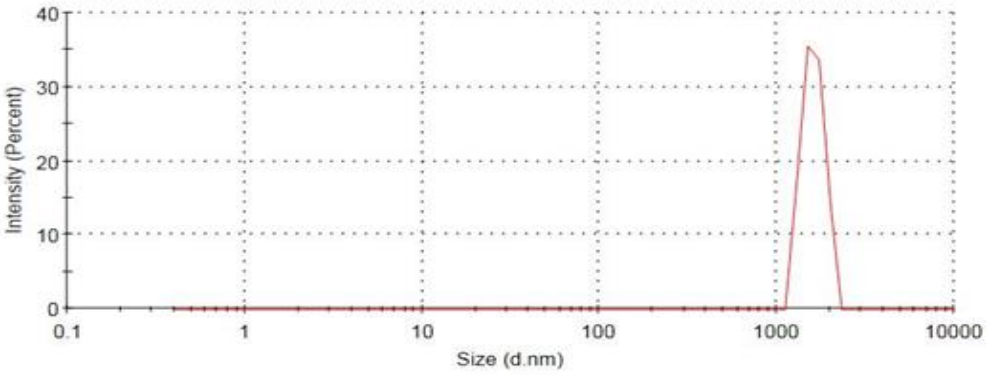


(c) SPS undoped

| | | Size (d.nm): | % Intensity: | St Dev (d.n... |
|---|---|---|---|---|
| Z-Average (d.nm): 813.0 | Peak 1: | 674.0 | 100.0 | 173.0 |
| PdI: 0.367 | Peak 2: | 0.000 | 0.0 | 0.000 |
| Intercept: 0.888 | Peak 3: | 0.000 | 0.0 | 0.000 |

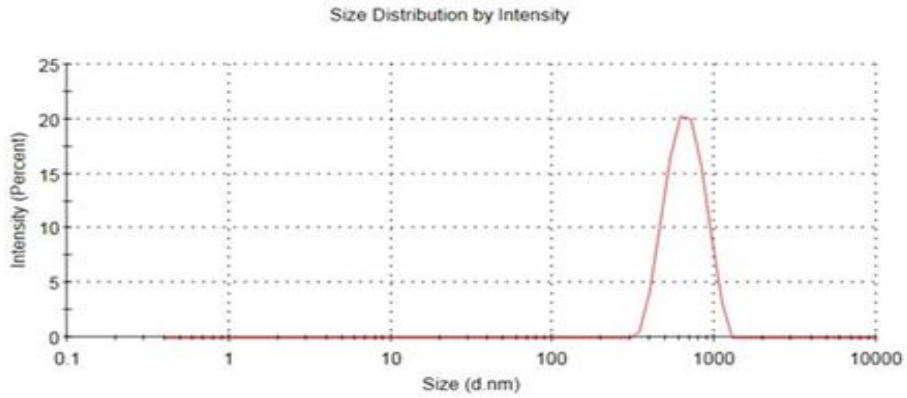


(d) SPS doped

Fig 5.14: Particle size distributions of extracted diamond powders

## 5.4.3. TEM studies

TEM micrographs of the diamond particles prepared by HP/ SPS are shown in Fig 5.15. The insets are the corresponding SAED patterns. It can be seen that the diamond particles formed by HP have sub-micron crystallites while those prepared by SPS are nanocrystalline and ultra nanocrystalline.

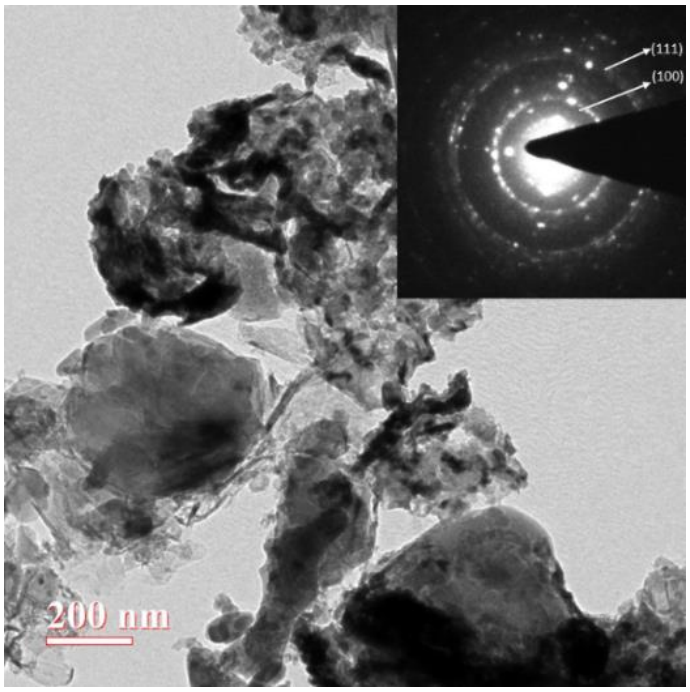


(i) Hot pressed

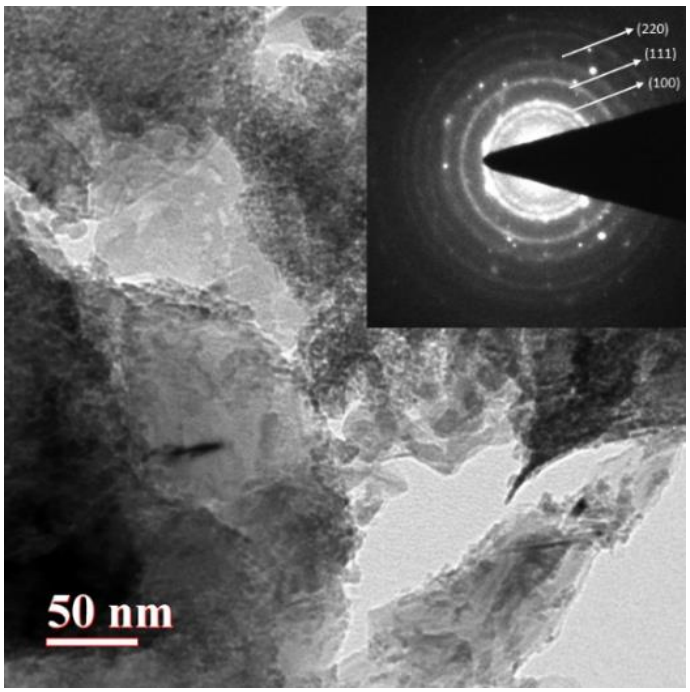


(a) Nanocrystalline diamond

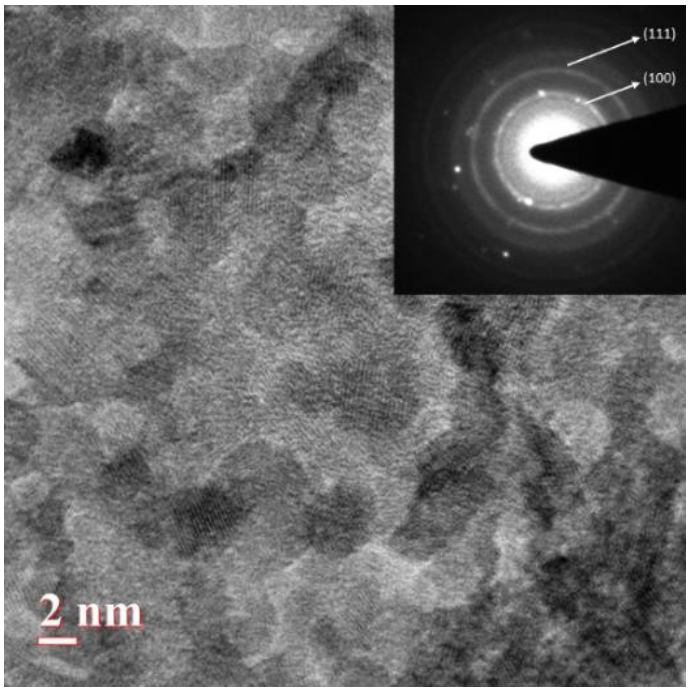


(b) Ultra nanocrystalline diamond

(ii) SPSed

Fig 5.15: TEM micrographs of diamonds synthesized by (i) HP (ii) SPS

## 5.4.4. IR spectroscopy

FTIR spectrums of the prepared SSSSs and the diamond particles obtained by HP and SPS, with and without doping of nanodiamonds are shown in Fig. 5.16 and Fig. 5.17, respectively. The strong peak at around 3436 $cm^{-1}$ is attributed to O-H stretching vibrations of C-OH group and water. The strong band at 1731 $cm^{-1}$ is attributed to stretching vibration modes of C=O in carboxylic acid and carbonyl groups. The peak at 1600 $cm^{-1}$ is assigned to the skeletal vibrations of un-oxidized graphitic domains (this region is related to C=C stretching). The band at 1040 $cm^{-1}$ is assigned to C–O (epoxy) groups while the band at 1210 $cm^{-1}$ is usually attributed to C–OH stretching vibrations (This region is also related to C-H bending vibrations) [190-192]. The peaks at close to 2900 $cm^{-1}$ are associated with C-H stretching peaks.

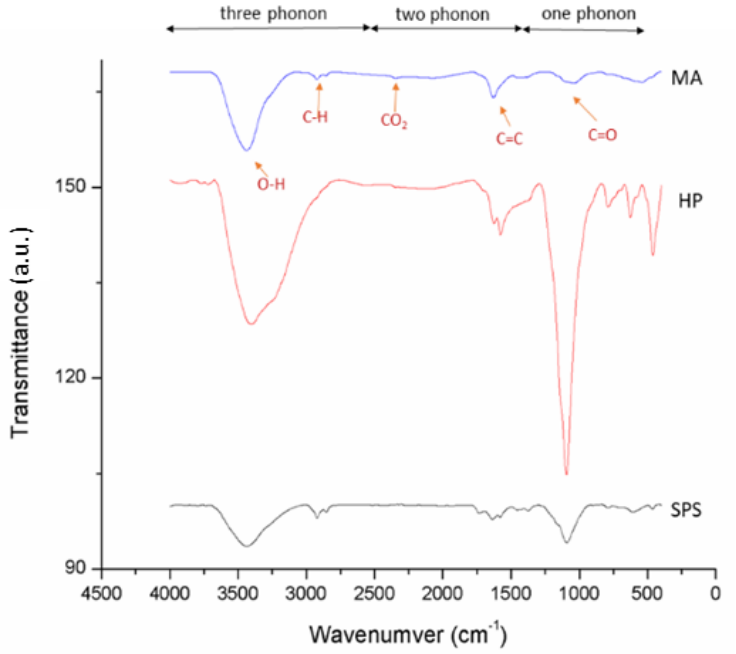


Fig 5.16: FTIR spectrums of SSSS, and the diamond particles (undoped case)

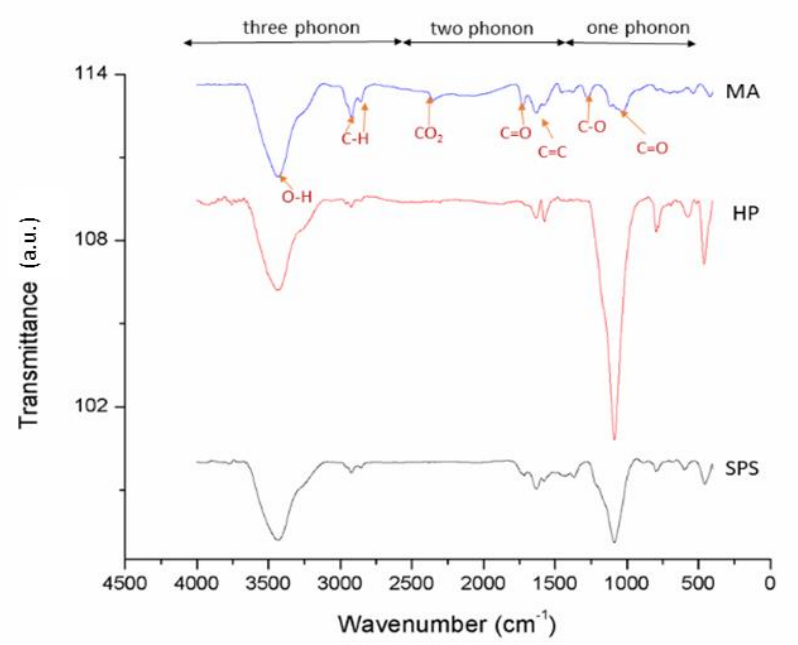


Fig 5.17: FTIR spectrums of SSSS, and the diamond particles (doped case)

From the IR spectra in Fig. 5.16, it can be seen that there are peaks at 1285 $cm^{-1}$ (type IaA diamond) but no peaks were observed at 1185 $cm^{-1}$ (type IaB diamond), and 1130 $cm^{-1}$ and 1344 $cm^{-1}$ (type Ib diamond) for HP diamond whereas in Fig. 5.17 peak at 1344 $cm^{-1}$ (type Ib) was observed for SPS diamond.

# 6. Conclusions

Conclusions of the present studies are summarized as follows:

1) Supersaturated solid solution (SSSS) of graphite up to 15wt.% (46.4 at.%) in nickel was successfully prepared by MA technique.

2) The average crystallite size of Ni in SSSS was found to be 43nm. The variation in crystallite size, lattice strain, lattice parameter and dislocation density were found to be dependent on the three-step graphite dissolution process.

3) The diamond formation was achieved by hot pressing/ spark plasma sintering of the SSSS containing 15wt.% $C_{gr}$ in nickel under a pressure of 10 MPa at 1000 $^{o}$C, which is much lower to pressure and temperature as compared required in HPHT technique.

4) The average size of the diamond particles obtained was found to be **3.8 µm** and **2.5 µm,** in the case of HP/ SPS samples, respectively.

5) Diamond particles having **sub-micron** crystallites were formed when the consolidation was done by hot pressing.

6) Diamond particles having a **nano (<100nm)/ ultra nano (1-10nm) size** crystallites and **SWCNTs,** were formed when consolidation was done by SPS.

7) Type IaA diamonds were formed from HP while type Ib diamonds were formed by SPS.

# Suggestions for future work

Further studies, as mentioned below, may be undertaken:

1) Studies may be undertaken on the consolidation of SSSS by HIP and its effects on the formation of diamond.

2) Tribological studies may be undertaken on the consolidated samples.

3) Studies on optical, electrical, mechanical properties of synthesized diamond may be undertaken.

4) Effect of addition of other impurities, like boron on the synthesized diamond, may be studied

# References


[1] E Bruton, Diamonds, Chilton Book Company, 1971.

[2] R.F. Davis, Diamond Films and Coatings, Noyes Publications, USA, 1993.

[3] O.A. Shenderova and D.M. Gruen, Ultrananocrystalline Diamond: Synthesis, Properties And Applications, William Andrew, 2nd ed., 2012

[4] A.M. Zaitsev, Optical Properties of Diamond: A Data Handbook, Springer Verlag Berlin Heidelberg, New York 2013.

[5] J.E. Field, The Properties of Natural and Synthetic Diamond, Academic Press, 1992.

[6] J.E. Field, The Properties of Diamond, Academic Press, 1979.

[7] https://www.statista.com/statistics/274921/worldwide-production-of-rough-diamonds/

[8] J. Kenda and J. Kopac, "Diamond tools for machining of granite and their wear", Mechanical Journal, 12 (2009) 775.

[9] J.C. Casebeer and C.A. Rae, "Keratorefractive diamond blade and surgical method", U.S. Patent 5, 222, 967 (1993).

[10] R. Davidian and J. Keith, "Universal interface for accessory blades", U.S. Patent D694, 598 (2013).

[11] T. Nakasuji, S. Kodera, S. Hara, H. Matsunaga, N. Ikawa and S. Shimada, "Diamond turning of brittle materials for optical components", CIRP Annals, 39 (1990) 89.

[12] V. F. Dorfman, A. Goel and D.J. Bray, "Erosion resistant diamond-like nanocomposite coatings for optical components", U.S. Patent 5, 718, 976 (1998).

[13] M.C. Costello, D.A. Tossell, D.M. Reece, C.J. Brierley and J.A. Savage, "Diamond protective coatings for optical components", Diamond and Related Materials, 3 (1994) 1137.

[14] C.H. Whitfield, E.M. Brody and W.A. Bassett, "Elastic moduli of NaCl by Brillouin scattering at high pressure in a diamond anvil cell", Review of Scientific Instruments, 47 (1976) 942.

[15] Y. Akahama and H. Kawamura, “High-pressure raman spectroscopy of diamond anvils to 250 GPa: method for pressure determination in the multimegabar pressure range”, Journal of Applied Physics, 96 (2004) 3748.

[16] Y.J. Chen and T.F. Young, “Thermal stress and heat transfer characteristics of a Cu/diamond/Cu heat spreading device”, Diamond and Related Materials, 18 (2009) 283.

[17] https://arstechnica.com/science/2016/01/diamonds-can-be-used-to-date-the-modern-theory-of-plate-tectonics/

[18] J. Sung, “Diamond Nanotechnology: Synthesis and Applications”, Pan Stanford, 2009

[19] J. P. Boudou, P. A. Curmi, F. Jelezko, J. Wrachtrup, P. Aubert, M. Sennour, G. Balasubramanian, R. Reuter, A. Thorel and E. Gaffet, “High yield fabrication of fluorescent nanodiamonds”, Nanotechnology, 20 (2009) 235602.

[20] M. Frenklach, W. Howard, D. Huang, J. Yuan, K. E. Spear and R. Koba, “Induced nucleation of diamond powder”, Applied Physical Letters, 59 (1991) 546.

[21] V. Yu. Dolmatov, A. Vehanen, V. Myllymäki, K. A. Rudometkin, A. N. Panova, K. M. Korolev and T. A. Shpadkovskaya, “Deep purification of detonation nanodiamond material”, Journal of Superhard Materials, 35 (2013) 408.

[22] S. Koizumi, C. E. Nebel and M. Nesladek, Physics and Applications of CVD Diamond, Wiley-VCH Verlag GmbH & Co. KGaA, 2008.

[23] S. Kaciulis, “Spectroscopy of carbon: from diamond to nitride films”, Surface and Interface Analysis, 44 (2012) 1155.

[24] I. M. Afanasov, O. N. Shornikova, V. V. Avdeev, O. I. Lebedev, G. V. Tendeloo and A. T. Matveev, “ Expanded graphite as a support for Ni/carbon composites”, Carbon, 47 (2009) 513.

[25] C. M. Mani, M. Braun, V. Molinari, M. Antonietti and N. Fechler, “A high-throughput composite catalyst based on nickel carbon cubes for the hydrogenation of 5-hydroxymethylfurfural to 2, 5-dimethylfuran”, Chem Cat Chem., 9 (2017) 3388.

[26] M. Mehrabi, P. Parvin, A. Reyhani and S. Z. Mortazavi, “Hydrogen storage in multi-walled carbon nanotubes decorated with palladium

nanoparticles using laser ablation/chemical reduction methods.” Materials Research Express, 4 (2017) 095030.

[27] R. Akbarzadeh and H. Dehghani, “Intensified electrochemical hydrogen storage capacity of multi-walled carbon nanotubes supported with Ni nanoparticles”, Journal of Solid State Electrochemistry, 22 (2017) 395.

[28] N. Chawla and K. K. Chawla, Metal Matrix Composite, Springer Science+ Business Media, Inc., USA, 2013.

[29] C. Suryanarayana, “Mechanical alloying and milling”, Progress in Materials Science, 46 (2001) 1.

[30] P. R. Soni, Mechanical Alloying- Fundamentals & Applications, Cambridge Int Science Publishing, UK, 2000.

[31] C. C. Koch, “The synthesis and structure of nanocrystalline materials produced by mechanical attrition: a review”, Nanostructured Materials, 2 (1993) 109.

[32] K. N. Ishihara, F. Kubo, E. Yamasue and H. Okumura, “Formation of supersaturated Fe-Li solid solution by mechanical alloying”, Review on Advanced Material Science, 18 (2008) 284.

[33] R. Lei, M. Wang, H. Wang and S. Xu, “New insights on the formation of supersaturated Cu-Nb solid solution prepared by mechanical alloying”, Materials Characterization, 118 (2016) 324.

[34] N.T. Rochman, K. Kawamoto, H. Sueyoshi, Y. Nakamura and T. Nishida, T. "Effect of milling temperature and additive elements on an Fe–C system alloy prepared by mechanical alloying", Journal of Materials Processing Technology, 89 (1999) 367.

[35] X. Liu, Y. Liu, X. Ran, J. An and Z. Cao, "Fabrication of the supersaturated solid solution of carbon in copper by mechanical alloying", Materials Characterization, 58 (2007) 504.

[36] N. Q. Wu, J. M. Wu, G-X. Wang and Z. Z. Li, "Amorphization in the Al-C system by mechanical alloying", Journal of Alloys and Compounds, 260 (1997) 121.

[37] Y. Minamino, Y. Koizumi, N. Tsuji, N. Hirohata, K. Mizuuchi and Y. Ohkanda, "Microstructures and mechanical properties of bulk nanocrystalline

Fe–Al–C alloys made by mechanically alloying with subsequent spark plasma sintering", Science and Technology of Advanced Materials, 5 (2004) 133.

[38] B. Bokhonov and M. Korchagin, “The formation of graphite encapsulated metal nanoparticles during mechanical activation and annealing of soot with iron and nickel”, Journal of Alloys and Compounds, 333 (2002) 308.

[39] G. L. Caer, E. B. Grosse, A. Pianelli, E. Bouzy and P. Matteazzi, “Mechanically driven syntheses of carbides and silcides”, Journal of Material Science, 25 (1990) 4726.

[40] T. Tanaka, K. N. Ishihara and P. H. Shingu, “Formation of metastable phases of Ni-C”, Metallurgical Transactions A, 23 (1992) 2431.

[41] B. Ghosh, H. Dutta and S. K. Pradhan, “Microstructure characterization of nanocrystalline $Ni_3C$ synthesized by high-energy ball milling”, Journal of Alloys and Compounds, 479 (2009) 193.

[42] T. Nickchi, M. Ghorbani, A. Alfantazi and Z. Farhat, “Fabrication of low friction bronze–graphite nano-composite coatings”, Materials & Design, 32 (2011) 3548.

[43] E.A. Olevsky, S. Kandukuri and L. Froyen, “Consolidation enhancement in spark-plasma sintering: Impact of high heating rates”, Journal of Applied Physics, 102 (2007) 114913.

[44] Z. A. Munir, U. A. Tamburini and M. Ohyanagi, "The effect of electric field and pressure on the synthesis and consolidation of materials: a review of the spark plasma sintering method", Journal of Materials Science, 41 (2006) 763.

[45] G.W. Nieman, J.R. Weertman, and R.W. Siegel, “Micro-hardness of nanocrystalline palladium and copper produced by inert-gas condensation”, Scripta metallurgica, 23 (1989) 2013.

[46] N.P. Rao, S.L. Girshick, P.H. McMurry, and J.V. Heberlein, “Production of nanostructured materials by hypersonic plasma particle deposition”, U.S. Patent 5, 874, 134, 1999.

[47] L.E. McCandlish, B.H. Kear, and S.J. Bhatia, “Spray conversion process for the production of nanophase composite powders”, U.S. Patent 5, 352, 269. 1994

[48] C. Suryanarayana, “Nanocrystalline materials”, International Materials Reviews, 40 (1995) 41.

[49] C.R. Hammond, The elements, Handbook of Chemistry and Physics, 2000.

[50] http://blog.mbl.edu/?p=2221.

[51] https://sciencenotes.org/carbon-facts/

[52] A. Hirsch, "The era of carbon allotropes", Nature Materials, 9 (2010) 868.

[53] A.H.C. Neto, “The carbon new age”, Materials Today, 13 (2010), 12.

[54] https://www.azom.com/article.aspx?ArticleID=1630

[55] P. Delhaes, Graphite and Precursors, CRC Press, London, 2014.

[56] D. D. L. Chung, "Review graphite", Journal of Materials Science, 37 (2002) 1475.

[57] H.S. Lipson and A. R. Stokes. "The structure of graphite", Proceedings of the Royal Society of London. Series A. Mathematical and Physical Sciences, 181 (1942) 101.

[58] W.G. Wyckoff, Crystal Structures, John Wiley & Sons, London, 1963.

[59] A.D. McNaught, Compendium of Chemical Terminology, Oxford: Blackwell Science, 1997.

[60] S. Shaji and V. Radhakrishnan, "Analysis of process parameters in surface grinding with graphite as lubricant based on the Taguchi method", Journal of Materials Processing Technology, 141 (2003) 51.

[61] P. Ravindran, K. Manisekar, R. Narayanasamy and P. Narayanasamy. "Tribological behaviour of powder metallurgy-processed aluminium hybrid composites with the addition of graphite solid lubricant", Ceramics International, 39 (2013) 1169.

[62] J. Gu, N. Li, L. Tian, Z. Lv and Q. Zhang, "High thermal conductivity graphite nanoplatelet/UHMWPE nanocomposites", RSC Advances, 5 (2015) 36334.

[63] Y. Zhu, S. Murali, W. Cai, X. Li, J.W. Suk, J.R. Potts and R.S. Ruoff, “Graphene and graphene oxide: synthesis, properties, and applications”, Advanced Materials, 22 (2010) 3906.

[64] Y. Cao, V. Fatemi, S. Fang, K. Watanabe, T. Taniguchi, E. Kaxiras and P. Jarillo-Herrero, “Unconventional superconductivity in magic-angle graphene superlattices”, Nature, 556 (2018) 43.

[65] J.R. Manning, “Correlation factors for impurity diffusion. bcc, diamond, and fcc structures”, Physical Review, 136 (1964) A1758.

[66] P. Scharff, “New carbon materials for research and technology”, Carbon, 36 (1998) 481.

[67] J.M. Andersson, N. Anderson and A B Sandvik, “Diamond coated cutting tool insert”, U.S. Patent 6, 051, 079, 2000

[68] D.U. Braga, A.E. Diniz, G.W. Miranda and N.L. Coppini, “Using a minimum quantity of lubricant (MQL) and a diamond coated tool in the drilling of aluminum–silicon alloys”, Journal of Materials Processing Technology, 122 (2002)127.

[69] A.K. Chattopadhyay, L. Chollet and H.E. Hintermann, “On performance of brazed bonded monolayer diamond grinding wheel”, CIRP Annals, 40 (1991) 347.

[70] X.Z.W.X.H. Ruiwei and X. Wei, “Semiconductor wafer slicing with diamond tools”, Diamond & Abrasives Engineering, 1 (2004).

[71] L.L. Glass and S.P. Sharma, “Production of diamonds from graphite using explosive-driven implosions”, AIAA Journal, 14 (1976) 402.

[72] P.A. Bianconi, S.J. Joray, B.L. Aldrich, J. Sumranjit, D.J. Duffy, D.P. Long, J.L. Lazorcik, L. Raboin, J.K. Kearns, S.L. Smulligan and J.M. Babyak, “Diamond and diamond-like carbon from a preceramic polymer”, Journal of the American Chemical Society, 126 (2004) 3191.

[73] R. L. Vander Wal, "Soot Precursor Material: Spatial Location via Simultaneous LIF-LII Imaging and Characterization via TEM", Conference Paper, Central States Section Meeting, NASA Lewis Research Center; Cleveland,OH United States, 1996,.

[74] A. D. McNaught and A. Wilkinson, Diamond-like Carbon Films, IUPAC Compendium of Chemical Terminology 2nd ed., Oxford Blackwell Scientific Publications, 1997.

[75] M. Bendikov, F. Wudl and D.F. Perepichka, “Tetrathiafulvalenes, oligoacenenes, and their buckminsterfullerene derivatives: the brick and mortar of organic electronics” Chemical Reviews, 104 (2004) 4891.

[76] Y.F. Chang, J.P. Zhang, H. Sun, B. Hong, Z. An and R.S. Wang, “Geometry and stability of fullerene cages: C24 to C70”, International Journal of Quantum Chemistry, 105 (2005) 142.

[77] T. Ando, “The electronic properties of graphene and carbon nanotubes”, NPG Asia Mater, 1 (2009) 17.

[78] D.V. Kosynkin, A.L. Higginbotham, A. Sinitskii, J.R. Lomeda, A. Dimiev, B.K. Price and J.M. Tour, “Longitudinal unzipping of carbon nanotubes to form graphene nanoribbons”, Nature, 458 (2009) 872.

[79] B. J. Hinds, N. Chopra, T. Rantell, R. Andrews, V. Gavalas and L.G. Bachas, “Aligned multiwalled carbon nanotube membranes”, Science, 303 (2004).62.

[80] https://www.newworldencyclopedia.org/entry/File:NanoBud.JPG

[81] J.L. Delgado and M. Herranz, “The Nano-Forms of Carbon”, Journal of Materials Chemistry, 18 (2008) 1417.

[82] J. K. McDonough and Y. Gogotsi, “Carbon onions: synthesis and electrochemical applications”, The Electrochemical Society Interface, 22 (2013) 61.

[83] V.L. Kuznetsov, A.L. Chuvilin, Y.V. Butenko, I.Y. Mal'kov and V. M Titov, “Onion-like carbon from ultra-disperse diamond”, Chemical Physics Letters, 222 (1994) 343.

[84] V.L. Kuznetsov, A.L. Chuvilin, E.M. Moroz, V.N. Kolomiichuk, S.K. Shaikhutdinov, Y.V. Butenko and I.Y. Mal’kov, “Effect of explosion conditions on the structure of detonation soots: ultradisperse diamond and onion carbon”, Carbon, 32 (1994) 873.

[85] http://www.nasa.gov/mission_pages/spitzer/multimedia/pia15266.html.

[86] Y.S. Kim, N.H.A. Raston and M.B. Gu, “Aptamer-based nanobiosensors”, Biosensors and Bioelectronics, 76 (2016) 2.

[87] K. Maehashi, T. Katsura, K. Kerman, Y. Takamura, K. Matsumoto and E. Tamiya, “Label-free protein biosensor based on aptamer-modified carbon nanotube field-effect transistors”, Analytical Chemistry, 79 (2007) 782.

[88] R.T. Yang, “Hydrogen storage by alkali-doped carbon nanotubes–revisited”, Carbon, 38 (2000) 623.

[89] X. Zou and Y. Zhang, “Noble metal-free hydrogen evolution catalysts for water splitting”, Chemical Society Reviews, 44 (2015) 5148.

[90] R. H. Baughman, A.A. Zakhidov and W.A. De Heer, “Carbon nanotubes--the route toward applications”, Science, 297 (2002) 787.

[91] P.M. Ajayan and J.M. Tour, “Materials science: nanotube composites”, Nature, 447 (2007) 1066.

[92] E.T. Mombeshora and V.O. Nyamori, “A review on the use of carbon nanostructured materials in electrochemical capacitors”, International Journal of Energy Research, 39 (2015) 1955.

[93] V.N. Mehta, S. Jha, H. Basu, R.K. Singhal and S.K. Kailasa, “One-step hydrothermal approach to fabricate carbon dots from apple juice for imaging of mycobacterium and fungal cells”, Sensors and Actuators B: Chemical, 213 (2015) 434.

[94] F. Yuan, Z. Wang, X. Li, Y. Li, Z.A. Tan, L. Fan and S. Yang, “Bright multicolor bandgap fluorescent carbon quantum dots for electroluminescent light-emitting diodes”, Advanced Materials, 29 (2017) 1604436.

[95] W.M. Zhang, J.S. Hu, Y.G. Guo, S.F. Zheng, L.S. Zhong, W.G. Song and L.J. Wan, “Tin-nanoparticles encapsulated in elastic hollow carbon spheres for high-performance anode material in lithium-Ion batteries”, Advanced Materials, 20 (2008) 1160.

[96] H. Zhang, G. Cao and Y. Yang, “Supercapacitors based on 3D nanostructured electrodes”, Three-Dimensional Nanoarchitectures (2011) 477.

[97] B. Fleming, “Recent advancement in automotive radar systems [Automotive Electronics]”, IEEE Vehicular Technology Magazine, 7 (2012) 4.

[98] T. Maitra, S. Sharma, A. Srivastava, Y.K. Cho, M. Madou and A. Sharma, “Improved graphitization and electrical conductivity of suspended carbon nanofibers derived from carbon nanotube/polyacrylonitrile composites by directed electrospinning”, Carbon, 50 (2012) 1753.

[99] C. Frondel and U. B. Marvin, “Lonsdaleite, a new hexagonal polymorph of diamond”, Nature, 214 (1967) 587.

[100] A.El Goresy, L.S. Dubrovinsky, P. Gillet, S. Mostefaoui, G. Graup, M. Drakopoulos, A.S. Simionovici, V. Swamy, and V.L. Masaitis, “A new natural, super-hard, transparent polymorph of carbon from the Popigai impact crater, Russia”, Comptes Rendus Geoscience, 335 (2003) 889.

[101] J. Singh, Physics of Semiconductors and their Heterostructures, McGraw-Hill, New York, 1993.

[102] K. Kobashi, Diamond Films: Chemical Vapor Deposition for Oriented and Heteroepitaxial Growth, Elsevier Ltd., Great Britain, 2010.

[103] O.P. Hugh, Handbook of Carbon, Graphite, Diamond and Fullerenes: Properties, Processing and Applications, Noyes Publication, USA, 1993.

[104] D. Halliday, R. Resnick and J. Walker, Fundamentals of Physics Extended", John Wiley & Sons, USA, 2010

[105] H. O. Pierson, Handbook of Carbon, Graphite, Diamond and Fullerencs-Properties, Processing and Applications", William Andrew Publishing, 1994.

[106] http://www.ioffe.ru/SVA/NSM/Semicond/Diamond/bandstr.htm

[107] E. Kohn, A. Denisenko, M. Kubovic, T. Zimmermann, O. A. Williams and D. M. Gruen, "A New diamond based heterostructure diode", Semiconductor Science and Technology, 21 (2006) L32

[108] http://www.e6cvd.com/

[109] S. M. Sze, Physics of semiconductor devices, Wiley-Interscience, New York, 1981.

[110] K.E. Spear and J.P. Dismukes, Synthetic Diamond: Emerging CVD Science and Technology, John Wiley & Sons, USA, 1994.

[111] M.M. Choy, K.H. Hellwege and A.M. Hellwege, Elastic, Piezoelectric, Pyroelectric, Piezooptic, Electrooptic Constants, and Nonlinear Dielectric Susceptibilities of Crystal, Springer Verlag, 1979.

[112] S. Logothetidis, J. Petalas, H. M. Polatoglou and D. Fuchs, "Origin and temperature dependence of the first direct gap of diamond", Physical Review B, 46 (1992) 4483.

[113] H. R. Philipp and E. A. Taft, "Optical properties of diamond in the vacuum ultraviolet", Physical Review, 127 (1962) 159.

[114] R. A. Roberts and W. C. Walker, "Optical study of the electronic structure of diamond", Physical Review, 161 (1967) 730.

[115] A. Fujishima, Y. Einaga, T. N. Rao and D. A. Tryk, Diamond Electrochemistry, Elsevier BKC Tokyo, 2005.

[116] C. E. Nebel and J. Ristein, "Thin-film Diamond I: (part of the Semiconductors and Semimetals Series), Elsevier, USA, 2003.

[117] P.W. May, “Diamond thin films: a 21st-century material”, Philosophical Transactions of the Royal Society of London. Series A: Mathematical, Physical and Engineering Sciences, 358 (2000) 473.

[118] http://www.chm.bris.ac.uk/motm/diamond/diamprop.htm .

[119] http://www.diamond-materials.com/downloads/cvd_diamond_booklet.pdf

[120] F. De Weerdt and J. Van Royen, “Defects in coloured natural diamonds”, Diamond and Related Materials, 10 (2001) 474.

[121] W. Kaiser and W.L. Bond, “Nitrogen, a major impurity in common type I diamond”, Physical Review, 115 (1959) 857.

[122] T. Evans, and C. Phaal, “Imperfections in type I and type II diamonds”, Proceedings of the Royal Society of London. Series A. Mathematical and Physical Sciences, 270 (1962) 538.

[123] J. Siebert, F. Guyot and V. Malavergne, “Diamond formation in metal-carbonate interactions”, Earth and Planetary Science Letters, 229 (2005) 205.

[124] A.S. Osipov, S. Nauyoks, T.W. Zerda and O.I. Zaporozhets, “Rapid sintering of nano-diamond compacts”, Diamond and Related Materials, 18 (2009) 1061.

[125] J. C Yung and J. Ji, Diamond Nanotechnology: Syntheses and Applications”, Pan Stanford Publishing Ltd., 2010.

[126] J.C. Angus, Synthetic diamond: emerging CVD science and technology, 1994.

[127] P. Decarli and J. Jamieson, "Formation of diamond by explosive shock", Science, 133 (1961) 1821.

[128] A. Mirzaei, H. Ham, H.G. Na, Y.J. Kwon, S.Y. Kang, M.S. Choi, J.H. Bang, N.H. Park, I. Kang and H.W. Kim, “Surprising synthesis of nanodiamond from single-walled carbon nanotubes by the spark plasma sintering process”, Electronic Materials Letters, 12 (2016) 747.

[129] F. Zhang and E. Burkel, “Synthesis of diamond using spark plasma sintering”, Sintering of Ceramics-New Emerging Techniques, (2012).

[130] X.Z. Zhao, R. Roy, K.A. Cherian and A. Badzian, “Hydrothermal growth of diamond in metal–C–$H_2O$ systems”, Nature, 385 (1997) 513.

[131] H. Nakano, A. Kouchi, M. Arakawa, Y. Kimura, C. Kaito, H. Ohno And T. Hondoh, “Alteration of interstellar organic materials in meteorites' parent bodies”, Proceedings of the Japan Academy B, 78 (2002) 277.

[132] K.E. Spear, A.W. Phelps and W.B. White, “Diamond polytypes and their vibrational spectra”, Journal of Materials Research, 5 (1990) 2277.

[133] F.P. Bundy, W.A. Bassett, M.S. Weathers, R.J. Hemley, H.U. Mao and A.F. Goncharov, “The pressure-temperature phase and transformation diagram for carbon”, Carbon, 34 (1996) 141.

[134] M. Sherif El-Eskandarany, K. Aoki, H. Itoh and K. Suzuki, “Effect of ball-to-powder weight ratio on the amorphization reaction of Al50Ta50 by ball milling”, Journal of the Less common Metals, 169 (1991) 235.

[135] T. Fukunaga, K. Nakamura, K. Suzuki and U. Mizutani, “Amorphization of immiscible Cu-Ta system by mechanical alloying and its structure observation”, Journal of Non-crystalline Solids, 117 (1990) 700.

[136] C. Suryanarayana, “Does a disordered γ-TiAl phase exist in mechanically alloyed TiAl powders?”, Intermetallics., 3 (1995) 153.

[137] K. Sakurai, C.H. Lee, N. Kuroda, T. Fukunaga and U. Mizutani, “Nitrogen effect in mechanical alloying of immiscible Cu-V: Extended x-ray absorption fine structure study”, Journal of Applied Physics, 75 (1994) 7752.

[138] L. Lü and M.O. Lai, Introduction to Mechanical Alloying, Springer, Boston,1998.

[139] L.F. Pease III and R.J. Sansoucy, “Advances in powder metallurgy”, Proceedings of the Powder Metallurgy Conference and Exhibition, Chicago, Metal Powder Industries Federation and American Powder Metallurgy Institute, 1991.

[140] D. Gavrilov, O. Vinogradov and W. Shaw, “Simulation of mechanical alloying in a shaker ball mill with variable size particle”, Proceedings of International Conference on Composite Materials, 1995.

[141] P.S. Gilman and J.S. Benjamin, “Mechanical alloying”, Annual Review on Material Science, 13 (1983) 279.

[142] M. Kis-Varga and D.L. Beke, “Phase transitions in Cu-Sb systems induced by ball milling”, Material Science Forum, 225 (1996) 465.

[143] C. Suryanarayana, G.H. Chen and F.H.S. Froes, “Milling maps for phase identification during mechanical alloying”, Scripta Metallurgica et Materialia, 26 (1992) 1727.

[144] S. Çam, V. Demir, and D. Özyürek, “Wear behaviour of A356/$TiAl_3$ in situ composites produced by mechanical alloying”, Metals, 6 (2016) 34.

[145] P.A. Blenkinsop, W.J. Evans and H.M. Flower, “Titanium’95 Science and Technology”, Institute of Materials London, 1996.

[146] M. Miki, T. Yamasaki and Y. Ogino, “Mechanical alloying of Ti–Al powder mixtures under nitrogen atmosphere”, Materials Transactions, JIM, 34 (1993) 952.

[147] A. Calka and J.S. Williams, “Synthesis of nitrides by mechanical alloying”, Material Science Forum, 88 (1992) 787.

[148] Y. Chen, T. Halstead and J.S. Williams, “Influence of milling temperature and atmosphere on the synthesis of iron nitrides by ball milling”, Materials Science and Engineering: A, 206 (1996) 24.

[149] N. Atsumi, K. Yoshioka, T. Yamasaki and Y. Ogino, “Nitriding of transition metals by mechanical alloying in nitrogen gas”, Journal of the Japan Society of Powder and Powder Metallurgy, 40 (1993) 261.

[150] P.Y. Lee and C.C. Koch, “The formation and thermal stability of amorphous Ni-Nb alloy powder synthesized by mechanical alloying”, Journal of Non-crystalline Solids, 94 (1987) 88.

[151] L.B. Hong, C. Bansal and B. Fultz, “Steady state grain size and thermal stability of nanophase $Ni_3Fe$ and $Fe_3X$ (X= Si, Zn, Sn) synthesized by ball milling at elevated temperatures”, Nanostructured Materials, 4 (1994) 949.

[152] W.E. Frazier and M.J. Koczak, “Mechanical and thermal stability of powder metallurgy aluminum-titanium alloys”, Scripta Metallurgica, 21 (1987) 129.

[153] L.L. Schwab, Synthesis of binary nanocrystalline aluminum alloys through high energy ball milling, PhD diss., The Graduate School, Stony Brook University: Stony Brook, 2016.

[154] P.K. Ivison, N. Cowlam, I. Soletta, G. Cocco, S. Enco and L. Battezzati, “The influence of hydrogen contamination on the amorphization reaction of CuTi alloys”, Material Science and Engineering: A., 134 (1991) 859.

[155] P.K. Ivison, I. Soletta, N. Cowlam, G. Cocco, S. Enzo and L. Battezzati, “Evidence of chemical short-range order in amorphous CuTi alloys produced by mechanical alloying”, Journal of Physics: Condensed Matter, 4 (1992) 1635.

[156] E. Gaffet, M. Harmelin and F. Faudot, “Far-from-equilibrium phase transition induced by mechanical alloying in the Cu-Fe system”, Journal of Alloys and Compdounds, 194 (1993) 23.

[157] D.A. Rigney, “Sliding wear of metals”, Annual Review on Material Science, 18 (1988) 141.

[158] R.B. Schwarz, R.R. Petrich and C.K. Saw, “The synthesis of amorphous Ni-Ti alloy powders by mechanical alloying”, Journal of Non-crystalline Solids, 76 (1985) 281.

[159] T. B. Massalski, Binary Alloy Phase Diagrams, ASM, 1986.

[160] G.B. Schaffer, and P.G. McCormick, “Displacement reactions during mechanical alloying”, Metallurgical Transactions A, 21 (1990) 2789.

[161] M.S. El-Eskandarany, Mechanical alloying: For fabrication of advanced engineering materials. Univ. Press of Mississippi, 2013.

[162] L.M. Rodríguez-Lorenzo, M. Vallet-Regı and J.M.F. Ferreira, “Fabrication of hydroxyapatite bodies by uniaxial pressing from a precipitated powder”, Biomaterials, 22 (2001) 583.

[163] J. Langer, M.J. Hoffmann and O. Guillon, “Direct comparison between hot pressing and electric field-assisted sintering of submicron alumina”, Acta Materialia, 57 (2009) 5454.

[164] H.V. Atkinson and S. Davies, “Fundamental aspects of hot isostatic pressing: an overview”, Metallurgical and Materials Transactions A, 31 (2000) 2981.

[165] S.N. Nasser, W.G. Guo, V.F. Nesterenko, S.S Indrakanti and Y.B. Gu, “Dynamic response of conventional and hot isostatically pressed Ti–6Al–4V alloys: experiments and modelling”, Mechanics of Materials, 33 (2001) 425.

[166] A.J. Gant and M.G. Gee, “Wear of tungsten carbide–cobalt hardmetals and hot isostatically pressed high speed steels under dry abrasive conditions”, Wear, 251 (2001) 908.

[167] H.Y. Bor, C. Hsu, and C.N. Wei, “Influence of hot isostatic pressing on the fracture transitions in the fine grain MAR-M247 superalloys”, Materials Chemistry and Physics, 84 (2004) 284.

[168] W.X. Yuan, J. Mei, V. Samarov, D. Seliverstov, and X. Wu, “Computer modelling and tooling design for near net shaped components using hot isostatic pressing”, Journal of Materials Processing Technology, 182 (2007) 39.

[169] J.J. Sousa, A. Sousa, F. Podczeck, and J.M. Newton, “Factors influencing the physical characteristics of pellets obtained by extrusion-spheronization” International Journal of Pharmaceutics, 232 (2002) 91.

[170] M. A. Rahman and M.N. El-Sheikh, “Workability in forging of powder metallurgy compacts”, Journal of Materials Processing Technology, 54 (1995) 97.

[171] M. Zabihi, M.R. Toroghinejad and A. Shafyei, “Application of powder metallurgy and hot rolling processes for manufacturing aluminum/alumina composite strips”, Materials Science and Engineering: A, 560 (2013) 567.

[172] V. Mamedov, “Spark plasma sintering as advanced PM sintering method”, Powder Metallurgy, 45 (2002) 322.

[173] A.A. Aldoshan, “Spark plasma sintering of titanium aluminide intermetallics and its composites”, PhD diss., Oklahoma State University, 2012.

[174] L. Yongming, P. Wei, L. Shuqin, W. Ruigang and L. Jianqiang, “A novel functionally graded material in the Ti–Si–C system”, Material Science and Enggineering A, 345 (2003) 99.

[175] J.E. Garay, “Current-activated, pressure-assisted densification of materials”, Annual Review on Materials Research, 40 (2010) 445.

[176] M. Eriksson, Z. Shen and M. Nygren, “Fast densification and deformation of titanium powder”, Powder Metallurgy, 48 (2005) 231.

[177] D.W. Ball, “Theory of Raman spectroscopy”, Spectroscopy, 16 (2001) 32.

[178] A.C. Ferrari, and J. Robertson, “Raman spectroscopy of amorphous, nanostructured, diamond–like carbon, and nanodiamond”, Philosophical Transactions of the Royal Society of London. Series A: Mathematical, Physical and Engineering Sciences, 362 (2004.) 2477.

[179] A.C. Ferrari and J. Robertson, “Resonant Raman spectroscopy of disordered, amorphous, and diamond-like carbon”, Physical Review B, 64 (2001) 075414.

[180] S. Reich and C. Thomsen, “Raman spectroscopy of graphite”, Philosophical Transactions of the Royal Society of London. Series A: Mathematical, Physical and Engineering Sciences, 362 (2004) 2271.

[181] L.M. Malard, M.A.A. Pimenta, G. Dresselhaus and M.S. Dresselhaus, “Raman spectroscopy in graphene”, Physics Reports, 473 (2009) 51.

[182] D.S. Bethune, G. Meijer, W.C. Tang and H.J. Rosen, “The vibrational Raman spectra of purified solid films of $C_{60}$ and $C_{70}$”, Chemical Physics Letters, 174 (1990) 219.

[183] S. Costa, E. Borowiak-Palen, M. Kruszynska, A. Bachmatiuk and R.J. Kalenczuk, “Characterization of carbon nanotubes by Raman spectroscopy”, Materials Science-Poland, 26 (2008) 433.

[184] M. C. Cadeville, C. Lerner and J. M. Friedt, “Electronic structure of interstitial carbon in ferromagnetic transition metals prepared by splat-quenching”, Physica B+ C, 86 (1977) 432.

[185] B. D. Cullity and S. R. Stock, Elements of X-ray Diffraction, Prentice Hall, 2001.

[186] E. Botcharova, M. Heilmaier, J. Freudenberger, G. Drew and D. Kudashow, “Supersaturated solid solution of niobium in copper by mechanical alloying”, Journal of Alloys and Compounds, 351 (2003) 119.

[187] A. Goyal and P. R. Soni, “Functionally graded nanocrystalline silicon powders by mechanical alloying”, Materials Letters, 214 (2018) 111.

[188] T. Susi, T. Pichler and P. Ayala, “X-ray photoelectron spectroscopy of graphitic carbon nanomaterials doped with heteroatoms”, Beilstein Journal of Nanotechnology, 6 (2015) 177.

[189] J. Hodkiewicz, “Characterizing carbon materials with Raman spectroscopy”, Thermo Fisher Scientific, 2010.

[190] D. C. Marcano, D. V. Kosynkin, J. M. Berlin, A. Sinitskii, Z. Sun, A. Slesarev, L. B. Alemany, W. Lu and J. M. Tour, “Improved synthesis of graphene oxide”, ACS Nano, 4 (2010) 4806.

[191] Y. Xu, H. Bai, G. Lu, C. Li and G. Shi, “Flexible graphene films via the filtration of water-soluble noncovalent functionalized graphene sheets”, Journal of the American Chemical Society,130 (2008) 5856.

[192] S. Verma, H. P. Mungse, N. Kumar, S. Choudhary, S. L. Jain, B. Sain and O. P. Khatri, “Graphene oxide: An efficient and reusable carbo catalyst for aza-Michael addition of amines to activated alkenes”, Chemical Communications, 47 (2011) 12673.

# List of publications

1) Nitika Kundan, Biswajit Parida, Anup Kumar Keshri and P. R. Soni, "***Synthesis and Characterization of the Nanostructured Solid Solution with Extended Solubility of Graphite in Nickel by Mechanical Alloying***", International Journal of Minerals, Metallurgy and Materials, 26 (2019) 1031-1037.

2) Nitika Kundan, Biswajit Parida, Anup Kumar Keshri and P. R. Soni, "***Synthesis of Sub-micron/Nano Diamond Powder by Hot pressing/ Spark Plasma Sintering of Supersaturated Solid Solution of Ni- $C_{gr}$***", International Conference on Recent Trends in Engineering, Technology, Agriculture, Applied Sciences, Humanities and Business Management for Sustainable Development (ETAHBS-2018), Oct. 22-23, 2018, NIT Srinagar: Journal of Material Science and Mechanical Engineering (Proc. Conf.), 5 (2018) 187.

3) Nitika Kundan, Anup Kumar Keshri and P. R. Soni, "***Characterization of Diamonds Synthesized via Powder Metallurgy Route***", International Conference on Recent Advances in Engineering, Technology and Science, Nov. 11th, 2018, New Delhi, Proceedings of SARC Int. Conf., (2018) 45.

4) Nitika Kundan and P. R. Soni, "***Spark Plasma Sintering- A Novel Technique***", IIM Metal NEWS, 18 (2015) 23.

5) Nitika Kundan, Anup Kumar Keshri and P. R. Soni, "***Synthesis and Characterization of Nanocrystalline Diamond Powder by SPS of Mechanically Alloyed Supersaturated Solid Solution of Ni-$C_{gr}$***" (under preparation).